



**Faculty of Pharmacy**  
**with the Division of Laboratory Medicine**  
Medical University of Białystok

**Dawid Maliszewski**

Synthesis and investigation of biological activities  
of the new 1,3,5-triazine derivatives

Doctoral dissertation in medical and health sciences  
in the discipline of pharmaceutical sciences

Białystok, 2022

Supervisors:

**Dr hab. Danuta Drozdowska,**

Department of Organic Chemistry, Medical University of Białystok, Poland

**Prof. Dr. Rasime Demirel,**

Department of Biology, Eskisehir Technical University, Turkey

## Table of contents

<b>Abbreviations .....</b>	<b>5</b>
<b>I. Introduction.....</b>	<b>9</b>
1.1. Approved and investigated drugs with s-triazine core.....	10
1.1.1. Altretamine .....	10
1.1.2. Decitabine.....	11
1.1.3. Oteracil .....	12
1.1.4. Almitrine.....	13
1.1.5. ZSTK474 .....	14
1.2. Anticancer s-triazine derivatives.....	15
1.3. Antimicrobial s-triazine derivatives.....	16
1.4. Antineurodegenerative s-triazine derivatives .....	20
1.5. Designing of innovative multitarget drugs .....	22
<b>II. Aims and Scopes.....</b>	<b>25</b>
<b>III. Materials and methods .....</b>	<b>27</b>
3.1. Synthesis .....	27
3.2. Antimicrobial activity .....	30
3.2.1. Biological study on selected cell strains of fungi and bacteria.....	30
3.2.2. Relaxation assay of <i>Escherichia coli</i> and <i>Staphylococcus aureus</i> gyrases .....	31
3.2.3. Molecular docking to <i>Escherichia coli</i> and <i>Staphylococcus aureus</i> gyrases .....	31
3.3. Evaluation of anticancer properties .....	33
3.3.1. MCF-7 and MDA-MB-231 cells.....	33
3.3.2. Determination of apoptotic index and cell viability .....	33
3.3.3. Statistical analysis for anticancer evaluation.....	34
3.4. Investigation of antineurodegenerative properties.....	34
3.4.1. Study of the interactions s-triazine derivatives with AChE enzyme.....	34
3.4.2. Study of the interactions s-triazine derivatives with BACE1 enzyme .....	35

<b>IV. Results .....</b>	<b>36</b>
4.1. Synthesis of s-triazine derivatives .....	36
4.2. Antimicrobial activity .....	42
4.3. Anticancer activity .....	50
4.4. Evaluation of AChE and BACE1 inhibition potency of s-triazine derivatives .....	54
<b>V. Discussion.....</b>	<b>55</b>
<b>VI. Conclusion.....</b>	<b>61</b>
<b>VII. Abstract.....</b>	<b>62</b>
<b>VIII. Streszczenie w języku polskim .....</b>	<b>64</b>
<b>IX. References .....</b>	<b>66</b>
<b>X. List of Figures.....</b>	<b>75</b>
<b>XI. List of Schemes .....</b>	<b>76</b>
<b>XII. List of Tables .....</b>	<b>78</b>
<b>XIII. Annex 1.....</b>	<b>79</b>

## Abbreviations

5-FU - 5-Fluorouracil

A2AR - Adenosine A2A receptor

A-549 - Adenocarcinomic human alveolar basal epithelial cells

ABTS - 2,2'-Azino-bis(3-ethylbenzothiazoline-6-sulfonic acid

AChE - Acetylcholinesterase

Aib - 2-Aminoisobutyric acid

AKT - Serine/Threonine-specific protein kinases/ Protein kinase B

Ala - Alanine

AlogP - Octanol-water partition coefficient

AML - Acute Myeloid Leukemia

APP - Amyloid Precursor Protein

AR - Aldose Reductase

ARDS - Acute Respiratory Distress Syndrome

Arg - Arginine

Asp - Aspartic acid

ATP - Adenosino-5'-trifosforan

A $\beta$  - Amyloid beta

BACE1 - Beta-secretase 1

BuChE - Butyrylcholinesterase

Boc - Tert-butyloxycarbonyl protecting group

BSA - Bovine Serum Albumin

CSC - Cancer Stem Cells

CYP51 - Sterol 14 $\alpha$ -demethylase

DABCO - 1,4-Diazabicyclo[2.2.2]octane

DCM - Dichloromethane

DCMT - 2,4-Dichloro-6-methoxy-1,3,5-triazine

DHFR - Dihydrofolate reductase

DILI - Drug-Induced Liver Injury

DMF - Dimethylformamide

DMSO - Dimethyl sulfoxide

DMT/NMM/TosO<sup>-</sup> - 4-(Dimethoxy-s-triazin-2-yl)-4-methylmorpholinium Toluenesulfonate

DNA - Deoxyribonucleic acid

DNMT - DNA Methyltransferase  
DPPH - 2,2-Diphenyl-1-picrylhydrazyl  
DTT - Dithiothreitol  
EDTA - Ethylenediaminetetraacetic acid  
EGFR - Epidermal Growth Factor Receptor  
FDA - Food and Drug Administration  
FiO<sub>2</sub> - The fraction of inspired oxygen  
Fmoc - Fluorenylmethyloxycarbonyl protecting group  
G(0) - Resting phase  
G(1) - Growth 1 phase  
GPX4 - Glutathione peroxidase 4  
GSK-3 - Glycogen synthase kinase 3  
GyrA - Gyrase subunit A  
GyrB - Gyrase subunit B  
hA - Adenosine Receptor  
HCT116 - human colorectal carcinoma  
HepG-2 - human liver cancer cell line  
His - Histidine  
HIV - human immunodeficiency virus  
HT2 - 5-hydroxytryptamine receptors  
HT-22 - Mouse Hippocampal Neuronal Cell Line  
IC<sub>50</sub> - The half maximal inhibitory concentration  
InhA - 2-Trans enoyl-acyl carrier protein reductase  
LBC3 - Glioblastoma multiforme tissue  
LN-18 - Human malignant glioma cell line  
LN-229 - Human brain glioblastoma cell line  
Lys - Lysine  
MCF-7 - Breast cancer cell line  
MDS - Myelodysplastic Syndrome  
MeCN - Acetonitrile  
MeSH - Medical Subject Headings  
MHB - Methylation Haplotype Block  
MIC - Minimum Inhibitory Concentration  
MLK3 - Mixed-Lineage Protein Kinase 3

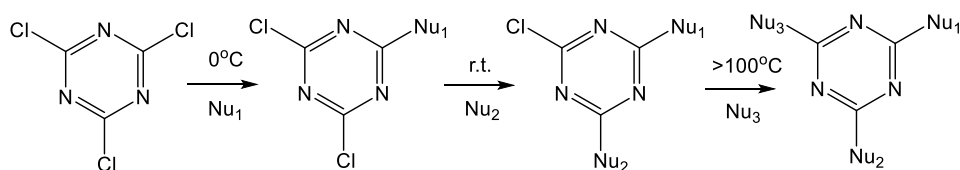
MW - Microwave  
NBP - 4-(4-Nitrobenzyl)pyridine  
NBTI - Novel Bacterial Topoisomerase Inhibitors  
NMM - N-methylmorpholine  
OMe - Methoxy group  
OPRT - Orotate phosphoribosyltransferase  
OtBu - tetr-buthyloxy group  
PaCO<sub>2</sub> - Partial Pressure of Carbon Dioxide  
PaO<sub>2</sub> - Partial Pressure of Oxygen  
PBMC - Peripheral blood mononuclear cell line  
PC-3 - Human prostate cancer cell line  
PDB - Protein Data Bank  
Phe - Phenylalanine  
PI3K - Phosphoinositide 3-kinase  
PSA - Prostate-Specific Antigen  
Rf - Retention Factor  
ROS - Reactive Oxygen Species  
SaO<sub>2</sub> - Arterial oxygen saturation  
SAR - Structure-Activity Relationship  
Ser - Serine  
SGK3 - Serine/threonine-protein kinase  
SH-SY5Y - Neuroblastoma cell line  
TBE - Tris/Borate/EDTA  
TCT - 2,4,6-Trichloro-1,3,5-triazine  
TEAC - Trolox Equivalent Antioxidant Capacity  
THF - Tetrahydrofuran  
TLC - Thin Layer Chromatography  
TOPO IV - Topoisomerase IV  
TosO<sup>-</sup> - Toluenesulfonyl group  
Tris - 2-Amino-2-(hydroxymethyl)-1,3-propanediol  
Trp - Tryptophan  
TrxR - Thioredoxin reductase  
TTC - Triphenyl Tetrazolium Chloride  
U-2932 - B-cell lymphoma

UV - Ultraviolet

WHO - World Health Organization

## I. Introduction

In organic chemistry, heteroatom rings are an integral part of the synthesis of larger structures. Maneuvering in the substituents allows to manipulate the physicochemical properties to obtain the desired properties. More importantly, combinatorial synthesis allows to obtain a wide spectrum of chemical compounds with an equally wide range of biological activities. One such representative is 1,3,5-triazine - a 6 membered aromatic ring with alternating carbon and nitrogen atoms, conventionally known as s-triazine. These names for editorial reasons will be used alternately in the text. According to ChemSpaider, there are about 114 million chemical compounds in the results of its database, of which about 13,000 are currently used as drugs. This represents about 0.01% of the total population. Among these compounds, there are more than 113,000 s-triazine derivatives, 15 of which are approved as drugs and 60 in trials, according to DrugBank [1]. The basis for the synthesis most of the above is the commercially available 2,4,6-trichloro-1,3,5-triazine (TCT), which is ideally suited for the nucleophilic substitution of a chlorine atom. Each substitution of chlorine atoms increasing the activation energies of the next stage of the reaction according to Scheme 1 [2].



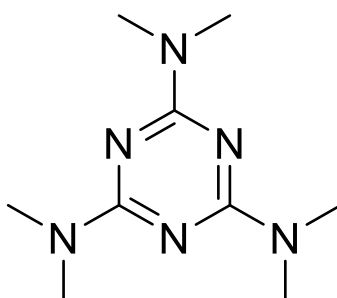
Scheme 1. Three stages of nucleophilic substitution of TCT.

Among the known biological activities of s-triazine and its derivatives are such as antibacterial, fungicidal, antimalarial, anticancer, antiviral, antimicrobial, anti-inflammatory, and antitumor activities. In the following subsections, current examples of tested s-triazine derivatives showing therapeutic potential in three disciplines: cancer, microbiology and neurodegenerative diseases will be presented.

## 1.1. Approved and investigated drugs with s-triazine core

### 1.1.1. Altretamine

Altretamine (Scheme 2), an antineoplastic agent, is a small molecule with the same three dimethylamine substituents. There are many ways to receive it. Two methods are based on the trimerization of dimethyl cyanamide in the presence of bis(trimethylsilyl) methyl lithium in hexane [3], another with N-methylformamide at elevated temperature and pressure [4]. However, the much simpler and highly efficient reactions include the substitution of TCT with dimethylamine in water at 180°C [5] or with bis-(dimethylamino)methane at 120°C [6].



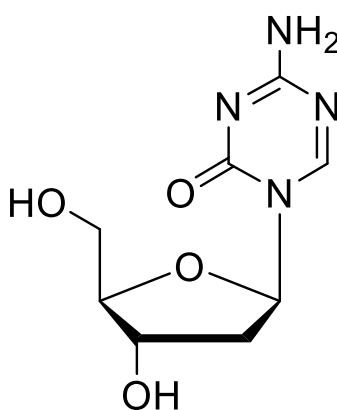
Scheme 2. Structure of Altretamine.

Altretamine, also known as hexalene or hexamethylmelamine, was approved in 1990 by the U.S. FDA. The exact mechanism of the drug is unknown. It is recognized as an alkylating anticancer agent by MeSH [7]. It is used separately [8] in oral palliative treatment of ovarian cancer [9] and in recurrent ovarian cancer [10]. Altretamine exhibits low toxicity, its half-life ranges from 4.7 to 10.2 hours, during which time it is metabolized to hydroxylmelamine as the main active form and cytotoxic to cancer [8]. Metabolism occurs in the liver by oxidative N-demethylation. The DILIrank dataset describes Altretamine as ambiguous DILI-concern with adverse reactions [11]. In 2020 drug-induced liver injury severity and toxicity (DILIST) dataset classified Altretamine as not inducing liver injury [12].

Another form of cell death, such as apoptosis and necrosis, is ferroptosis. A metal-dependent process based on the metabolism of three components: iron, thiols and lipids [8]. The GPX4 enzyme has a preventive function against the negative effects of peroxide lipids inducing cell death. Altretamine turned out to be an inhibitor of GPX4 in an assay on U-2932 cells [13].

### 1.1.2. Decitabine

Myelodysplastic syndromes (MDS) are a group of various diseases, the most notable feature of which is a reduced number of blood cells in the peripheral blood (red blood cells, white blood cells and/or platelets) due to their abnormal formation in the marrow [14]. The second disease is acute myeloid leukemia. AML are malignant neoplasms derived from bone marrow cells that have become independent of regulatory mechanisms and have the ability to multiply uncontrolled. These cells dominate the bone marrow and blood, and can form infiltrates in various organs and impair their function [15]. They are treated with Decitabine (Scheme 3), a pyrimidine nucleoside derivative, approved by the FDA for treatment in 2006.



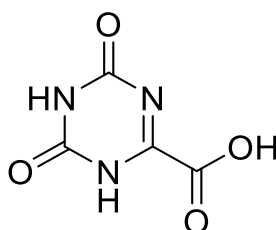
Scheme 3. Structure of Decitabine.

The method to obtain the described drug is a two-step synthesis. The first step involves the preparation of the complex by reacting 1-chloro-2-deoxy-D-ribofuranose with cobalt (II) nitrate and 1,1'-bi-2-naphthol in N, N-dimethyl-formamide at 60°C in an inert gas atmosphere. In the second step, the addition is carried out with 2-(trimethylsilylamino)-4-(trimethylsilyloxy)-s-triazine in triethylamine at 40°C. During the last step, substitution takes place at the 4-position of the s-triazine ring, with removal of the trimethylsilyl groups. The reaction yield was reported to be 89% [16].

Decitabine has DNA hypomethylating properties, due to its inhibition of DNA methyltransferase activity. The mechanism of action is based on the formation of irreversible covalent connection with DNA methyltransferase, which appears much more often in neoplastic cells that also replicate with an increased frequency. Capturing DNMT leads to hypomethylation, double strand damage, and cell death [17, 18].

### 1.1.3. Oteracil

Gastric cancer is the third most common malignant neoplasm in the world, with differences amongst geographic areas. The incidence of stomach cancer increases with age. A factor predisposing to the disease is infection with *Helicobacter pylori*, a diet low in antioxidants, smoking or genetic predisposition. Stomach cancer is usually diagnosed at an advanced stage. The disease begins with scanty, non-specific symptoms, such as abdominal pain or weight loss. Treatment of advanced gastric cancer begins with considering surgery, followed by chemotherapy or radiation therapy. The interest in the subject suggests combining new therapeutics with known anticancer drugs and direct administration to the peritoneum [19]. Teysuno has been available since 2011 in the European Union countries. The active substances in Teysuno are Tegafur, Gimeracil and Oteracil (Scheme 4). Teysuno is an anti-cancer medicine. It belongs to a group of cancer drugs called fluoropyrimidines and is used together with cisplatin, another cancer medicine, to treat advanced stomach cancer. It is also used to treat metastatic colorectal cancer (cancer of the colon and rectum that has spread to other parts of the body) in patients who, due to unacceptable side effects, cannot be further treated with other fluoropyrimidines. For this purpose, the drug can be used as monotherapy or in combination with anticancer drugs (oxaliplatin or irinotecan), including in combination with another drug, bevacizumab [20]. The role of Oteracil is to block OPRT involved in the production of 5-FU in the normal gastrointestinal mucosa and thereby stimulate the amount of 5-FU in healthy tissue. This translates into the possibility of using lower doses of the anti-cancer drug [21].

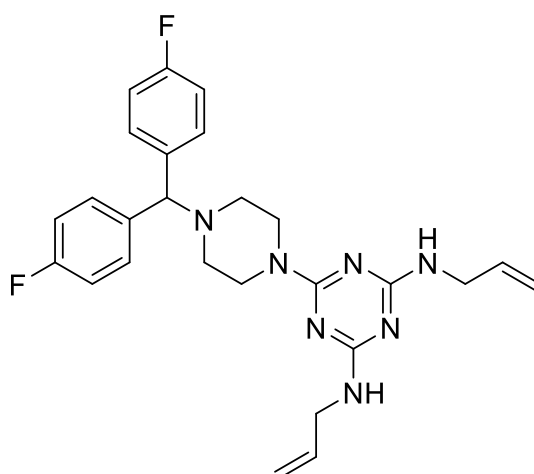


Scheme 4. Structure of Oteracil.

Oteracil is the one which based on 1,3,5-triazine ring. The product is obtained with 95% efficiency during intramolecular cyclization. 2-Carbamido-2-oxoacetic acid, urea and p-toluenesulfonic acid in ethanol are used for the reaction. By mixing all ingredients at room temperature and heating to 50 °C. Upon alkalization with potassium hydroxide, a product in the form of salt is precipitated from the solution [22].

#### 1.1.4. Almitrine

Almitrine (Scheme 5) is an organic chemical, a respiratory stimulant drug used to treat chronic obstructive pulmonary disease. Almitrine stimulates the peripheral chemoreceptors of the aorta and cervical glomerulus, as a result of which  $\text{SaO}_2$  and  $\text{PaO}_2$  increase, and  $\text{PaCO}_2$  is decreased [23]. The direct effect of stimulation of these receptors is the improvement of blood oxygenation, which is associated with improved alveolar ventilation and an increase in the ventilation-perfusion ratio [24]. At the recommended daily doses (50 or 100 mg), Almitrine does not affect the functional parameters of the lungs, i.e. respiratory capacity, respiratory rate, oxygen consumption. Moreover, it improves the condition of patients with hypoxemia [25]. In 2012, Almitrine was withdrawn from use due to numerous reports of nerve damage to the hands and feet, as well as weight loss [26]. In 2019, as the race to find a way to save people suffering from COVID-19 and/or ARDS began, a bright light fell on Almitrine again. Accelerated attempts to stimulate and improve the breathing process began. The drug contributed to an increase in the  $\text{PaO}_2/\text{FiO}_2$  ratio, however, patients required further and other rescue methods or they died. This could be due to the intervention of Almitrine in an excessively advanced stage of the disease [27]. The correct use of the therapeutic in the early stages of the disease will be considered [28].

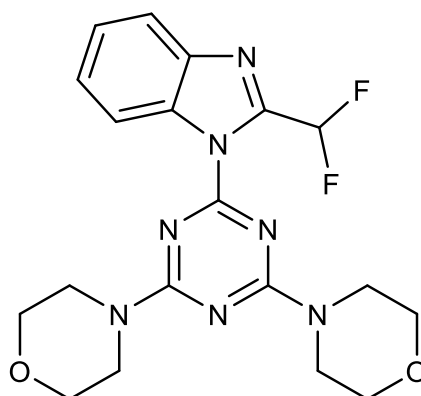


Scheme 5. Structure of Almitrine.

TCT is used to synthesize Almitrine. In the first stage, there are two substitutions of the chlorine atom with an allylamino group in a slightly basic environment. The second step is a third chlorine substitution by 1-(bis(4-fluorophenyl)methyl)piperazine reagent in butan-1-ol by heating to reflux [29].

### 1.1.5. ZSTK474

ZSTK474 (2-(2-difluoromethylbenzimidazol-1-yl)-4,6-dimorpholino-1,3,5-triazine) (Scheme 6) is organic compound belonging to benzimidazole derivatives. Orally available s-triazine derivative, an ATP-competitive inhibitor of phosphatidylinositol 3-kinase (PI3K) with potential anti-tumor activity. The PI3K inhibitor ZSTK474 inhibits all four PI3K isoforms (16, 44, 4.6 and 49 nM for PI3K $\alpha$ , PI3K $\beta$ , PI3K $\delta$  and PI3K $\gamma$ , respectively) [30]. Inhibition of activation of the PI3K/AKT (or protein kinase B) signaling pathway results in inhibition of tumor cell growth and survival in susceptible tumor cell populations. Deregulated PI3K signaling may contribute to tumor resistance to various anticancer agents. This agent does not induce apoptosis, but rather induces a strong G(0)/G(1) arrest, which may contribute to its beneficial efficacy in cancer cells. ZSTK474 was tested *in vivo* in Athymic nude mice. Tumor reduction was noted with ZSTK474 treatment, as well as SGK3 activation and expansion of liver CSCs were observed during the experiment. Inhibition of proliferation contributing to the apoptosis of non-stem cells may be the cause of the anti-cancer effect of ZSTK474 [31,32].



Scheme 6. Structure of ZSTK474.

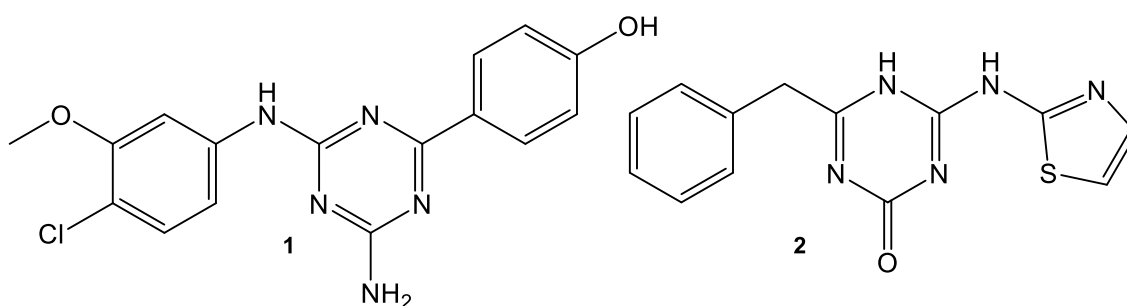
In the first step, the synthesis of ZSTK474 took place in DCM and NaHCO<sub>3</sub> at 0°C between TCT and morpholine in 1:2 molar ratio [33]. This stage occurred almost completely. The product of the first part of the synthesis (6-chloro-2,4-dimorpholine-s-triazine) was mixed with 2-(difluoromethyl)-1H-benzo[d]imidazoles and potassium carbonate in DMSO. The mixture was stirred for 3 hours while heating to 130°C. The yield was equal 84% [34].

## 1.2. Anticancer s-triazine derivatives

A review covering literature reports from the beginning of this century to 2016 summarizes 106 different reports on the synthesis, anticancer activity and mechanisms of action of 1,3,5-triazine derivatives. Many of them have shown remarkable activity, and some of them have entered clinical trials [35].

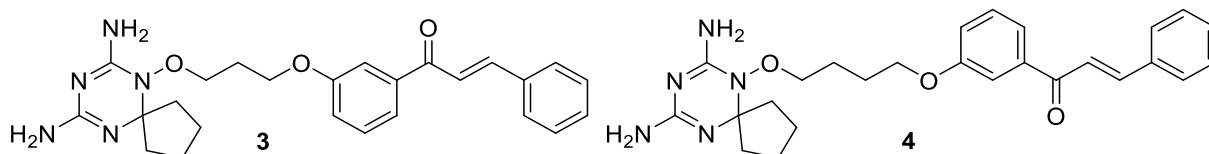
Other active derivatives are still being described. Park et al. designed and synthesized a triazine derivative **1** (Scheme 7) with an amine, chloromethoxyphenyl and p-hydroxyphenyl groups. The first substitution was made in THF at -15°C. The amino group at room temperature was substituted successively. The last step was performed in the presence of (4-hydroxyphenyl)boronic acid and (triphenylphosphine) palladium in microwave (120°C). The developed compound showed an ARs antagonistic and cytotoxic effect for lung cancer cells through increased expression of ROS and its accumulation in the mitochondrial membrane, which leads to the dysfunction of the mentioned organelle. Molecular modeling confirmed the antagonistic nature of the derivative towards hA1 and hA3 receptors [36].

Another method of obtaining an s-triazine ring is intramolecular cyclization. The reaction of 2-phenyl-N-(thiazol-2-ylcarbamothioyl) acetamide with urea in DMF under the influence of MW at 130°C resulted in the formation of a triazole ring as the desired product **2**. The compound **2** (Scheme 7) showed antitumor properties against the lines HepG-2 ( $IC_{50}=29.75\mu M$ ), PC-3 ( $IC_{50}=17.90\mu M$ ), MCF-7 ( $IC_{50}=4.65\mu M$ ), A-549 ( $IC_{50}=7.43\mu M$ ), PBMC ( $IC_{50}=165\mu M$ ) and these values are slightly greater than the reference compound erlotinib. Further *in vitro* and *in silico* studies showed a strong complexing potential against EGFR<sup>WT</sup> and EGFR<sup>T790M</sup> ( $IC_{50}=0.22\mu M$ ;  $IC_{50}=0.18\mu M$ ), the receptor responsible for the regulation of cell proliferation [37].



Scheme 7. Anticancer s-triazine derivatives **1** and **2**.

Ng et al. used synthesized hybrid derivatives of 4,6-diamino-1,2-dihydro-1,3,5-triazine and chalcone for research on cancer cells. Among the 15 newly synthesized s-triazine derivatives, two with the strongest anti-cancer effect were distinguished: **3** and **4** (Scheme 8). Both acted cytotoxic against HCT116 (human colorectal carcinoma) ( $GI_{50}=0.026\mu\text{M}$ ;  $GI_{50}=0.116\mu\text{M}$ ) and MCF-7 ( $GI_{50}=0.080\mu\text{M}$ ;  $GI_{50}=0.127\mu\text{M}$ ) cancer cell lines. In addition, studies have shown strong *in vitro* inhibitory activities against recombinant human DHFR ( $IC_{50}=0.0061\mu\text{M}$ ;  $IC_{50}=0.0026\mu\text{M}$ ) and rat TrxR ( $IC_{50}=4.6\mu\text{M}$ ;  $IC_{50}=5.9\mu\text{M}$ ) enzymes [38].



Scheme 8. Anticancer 4,6-diamino-1,2-dihydro-s-triazine s-triazine derivatives **3** and **4**.

Detailed overview of the literature on synthesis and anticancer activity of 1,3,5-triazine derivatives under study after 2016 are presented in the review of Maliszewski D. and Drozdowska D. [39] (Annex 1). The study presented in this paper focuses on the inhibitory effects of the compounds against enzymes involved in tumorigenesis. In addition, the above work describes the current state of knowledge on the structure-activity relationship of various s-triazine derivatives. Conclusions are presented on how the introduction of new substituents and structure modification leads to the acquisition of activity that inhibits cell proliferation and/or induces apoptosis.

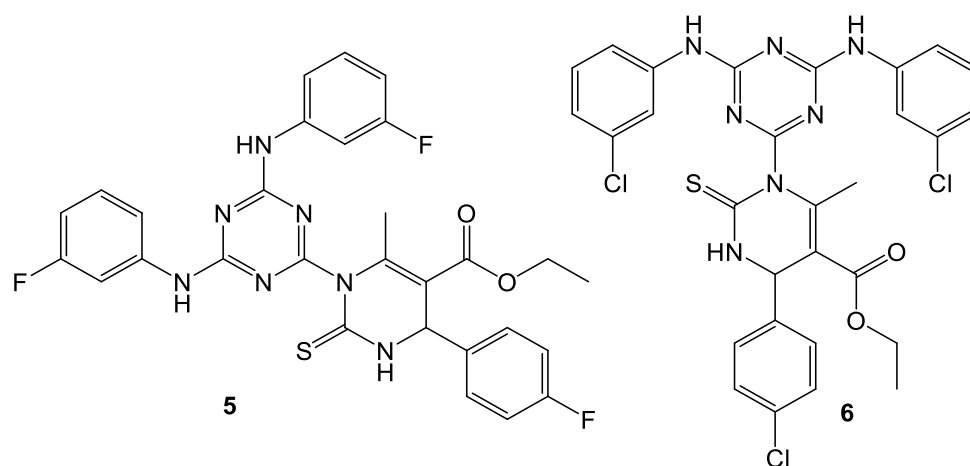
### 1.3. Antimicrobial s-triazine derivatives

Bacterial, viral and fungal infections are still a major problem, and antibiotic resistance, or the ability of microorganisms to resist the effects of a drug, is a threat to global health. Old antibiotics are quickly proving ineffective, and new antibiotics are still scarce, so triazine derivatives have great potential in this area of research. Most of biological active compounds are constructed of heterocyclic rings, e.g. pyrrole, imidazole, thiazole, pyrimidine and triazine. As latest research shown 1,3,5-triazine scaffold is constantly used to obtaining high potency bioactive derivatives. These compounds found application in fight against bacteria, fungi or tumor tissues. This trend is pushing scientists to expand the group of compounds and their applications. In the recent decades due to numerous antimicrobial resistant infections, modern medicine like cancer chemotherapy, invasive surgeries and organ transplantations deliveries can only be performed without the risk because of access to effective antimicrobial treatments. Approximately 35,000 deaths/year in United States and 33,000 deaths/year in Europe and were

induced by antibiotic resistant in Europe [40]. Eukaryotic DHFR is a great target in treatment cancer and also bacterial infections by blocking DNA precursor synthesis. Diamino-1,3,5-triazine and their family derivatives possess significant inhibitory potential regard to *EcDHFR*. NSC120927 is the best example of diamino-s-triazine chemical class ( $IC_{50}=1.15 \pm 0.37\mu\text{M}$  against *Escherichia coli*) [41].

DNA gyrase is a subject of extensive studies as a target for antimicrobial agents, since it is present in bacteria, but is lacking in humans [42]. WHO published a list of priority pathogens for which new antibiotics are essential [43,44], including *E. coli* and *S. Aureus*, for which priority was established as critical and high, respectively. DNA gyrase is inhibited by fluoroquinolones, aminocoumarin and NBTI (Novel Bacterial Topoisomerase Inhibitors) antibiotics, as well as by simocyclinone, which is an antibiotic comprising of an aminocoumarin and a polyketide groups [45]. The fluoroquinolones are example of broad-spectrum antibacterial drugs targeting DNA-gyrase, but because of the increasing bacterial resistance to these agents, there is a need to seek new compounds and new modes of inhibition of this enzyme. Aminocoumarins are competitive inhibitors of DNA gyrase and act by binding into the ATP site within GyrB subunit [46]. Although simocyclinone has aminocoumarin moiety in its structure it does not inhibit the ATPase activity of DNA gyrase, but rather binds to the N-terminal domain of GyrA and prevents DNA binding [47]. The mechanism of inhibition by fluoroquinolones is that they stabilize the cleaved form of the DNA, preventing the relaxed form of DNA to religate [48]. Lastly, NBTIs have a similar mechanism of action to fluoroquinolones, although they are composed of the “left-hand side”– which intercalates the DNA strands and the “right-hand side”, which binds into the pocket in the center of the enzyme, between two GyrA subunits [49], (50).

Anup Masih et al. show antimicrobial potency using s-triazine derivative combined with dihyddropyrimidine scaffold. Antibacterial properties were showed against gram-positive, viz. *Staphylococcus aureus*, *Bacillus subtilis*, *Bacillus cereus* and three gram-negative bacterial strains viz. *Pseudomonas aeruginosa*, *Escherichia coli* and *Proteus vulgaris* using Minimum Inhibitory Concentration (MIC) test by **5** (Scheme 9). Results are in the range from 3 to 13  $\mu\text{g/ml}$ . Authors explain efficiency as inhibition of DNA gyrase supercoiling activity ( $IC_{50} = 3.71 \mu\text{g/ml}$ ). Another analog **6** (Scheme 9) show great antifungal properties against *Candida albicans*, *Candida glabrata*, *Cryptococcus neoformans* and *Aspergillus niger* (range of minimum inhibitory concentration from 1,25 to 5  $\mu\text{g/ml}$  [51].



Scheme 9. Antibacterial s-triazine derivatives **5** and **6**.

Younis et al. conducted the anti-bacterial research based on the thiazolo[3,2-a][1,3,5]triazine moiety. The three-stage synthesis of the designed compound began with the preparation of a thiourea thiazole ring, which in the next stage is functionalized with furfural. The last step involves an amino group from aminoacetophenone, two formaldehyde molecules and a thiazole ring with a primary imine group, generating a triazine ring (DMF, 100°C, 6h). The obtained derivative contains substituents on the triazine ring nitrogen, which eliminates the effect of delocalized electrons. Antimicrobial activity was confirmed by studies on *Mycobacterium tuberculosis* lines differing in drug resistance (MIC values for drug sensitive strain 2.49  $\mu\text{M}$ , multi-drug resistant strain 9.91  $\mu\text{M}$ , extensively drug resistant strain 39.72  $\mu\text{M}$ ). Compound **7** (Scheme 10) inhibited 2-trans-enyl carrier protein reductase (InhA), reaching an  $\text{IC}_{50}$  value of 3.9  $\mu\text{M}$ . Molecular docking confirmed the activity of this derivative against the tested enzyme. This triazine derivative proved to be not only an antitubercular but an antimicrobial potential drug in general, and with non-toxic properties against human cells [52].

Patil et al. presented a group of 15 1,3,5-triazine derivatives synthesized in a one-step reaction by mixing 2-cyanoguanidine, potassium hydroxide and 4-cyanothiazole. Compound **8** (Scheme 10) showed the best antibacterial (*E. coli*, *K. pneumonia*, *A. Baumannii*) and antifungal (*C. Neoformans*) properties at a concentration of 32 mg/mL. Molecular modeling showed the generation of hydrogen bonds between **8** and *E. coli* DNA gyrase [53].

The new  $\text{N}^2$ -(tetrazol-5-yl)-6-substituted-5,6-dihydro-1,3,5-triazine-2,4-diamines compounds were synthesized in a one-step multi-component reaction (5-amino-1,2,3,4-tetrazoles, cyanamide and aromatic aldehydes). The derivative **9** (Scheme 10) turned out to be the most noteworthy, it obtained a strong inhibitory effect on DHFR ( $\text{IC}_{50}$ =2.658  $\mu\text{g/ml}$ ), DNA

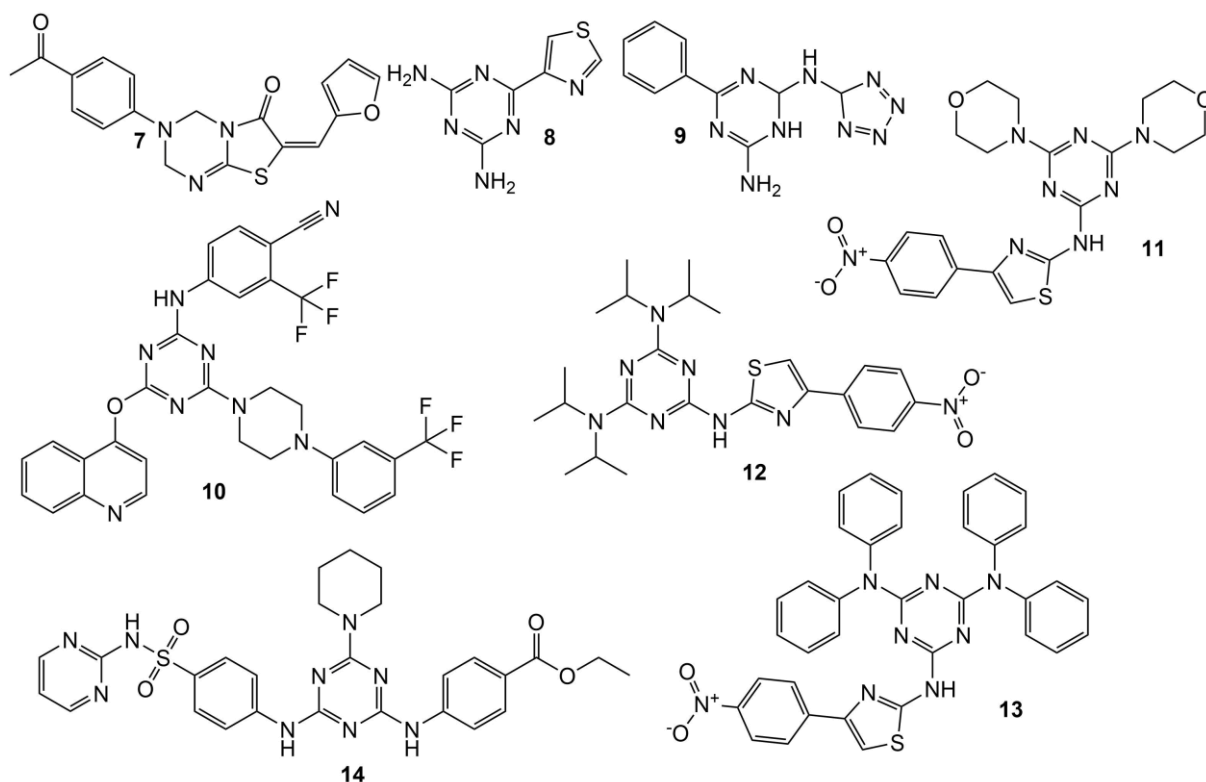
gyrase ( $IC_{50} = 7.536 \mu\text{g/ml}$ ) and *E. coli* TOPO IV ( $IC_{50} = 1.629 \mu\text{g/ml}$ ). Compound **9** stopped the growth of *E. coli* and *P. aeruginosa* with MIC values of  $2.4 \times 10^{-18}$  and  $7.12 \times 10^{-9} \mu\text{g/ml}$ , respectively. Additionally, it was observed an inhibitory effect on the CYP51 protein ( $IC_{50} = 7.451 \mu\text{g/ml}$ ), which explains its antifungal activity (*C. albicans* MIC =  $1.475 \times 10^{-8} \mu\text{g/ml}$ ) [54].

Patel et al. also demonstrated cytotoxic activity of s-triazine analog **10** (Scheme 10) on bacterial cell lines. The obtained MIC values were at the level of 6.25 - 12.5  $\mu\text{g/ml}$ , and the inhibition zone was 25 - 28 mm. The microbiological properties were due to the presence of a strongly electronegative trifluoromethyl group [55].

Gahrotri et al. presented derivatives containing a phenylthiazole group. The tests were carried out on gram negative (*S. typhi*, *E. coli*, and *K. aerogenes*) and gram positive (*B. subtilis*, *B. cereus*, and *S. aureus*) bacteria cell lines. The results showed that compounds **11**, **12** and **13** (Scheme 10) achieved excellent MIC values in the range of 4-8  $\mu\text{g/ml}$  [56].

Desei et al. designed and synthesized fifteen s-triazine derivatives containing piperazine and benzenesulfamide moieties. Derivative **14** (Scheme 10) showed significant activity against *P. aeruginosa* (MIC=25  $\mu\text{g/ml}$ ). Research has shown that the electron withdrawing group at the phenyl group increased activity of investigated compounds [57].

Liu et al. presented and compared numerous examples of potential antimicrobial compounds. Their SAR analysis of substituents and biological properties confirmed the great potential of compounds with an s-triazine ring in the field of finding new drugs with antibacterial and antifungal activity [58].



Scheme 10. Antimicrobial s-triazine derivatives **7-14**.

#### 1.4. Antineurodegenerative s-triazine derivatives

S-triazine derivatives have also proven to be active in the search for new therapeutics in Alzheimer's disease of the target. For example, derivative **15** (Scheme 11) obtained by combining N-methylcyclohexylamine and imidazole through the piperazine ring with 1,3,5-triazine has been shown to be a potential inhibitor of Alzheimer's disease progression. The  $IC_{50}$  value against acetylcholinesterase obtained by **15** ( $0.044 \mu\text{M}$ ) was lower than that for donepezil ( $0.052 \mu\text{M}$ ). At the same time, this compound had a low affinity for BuChE [59].

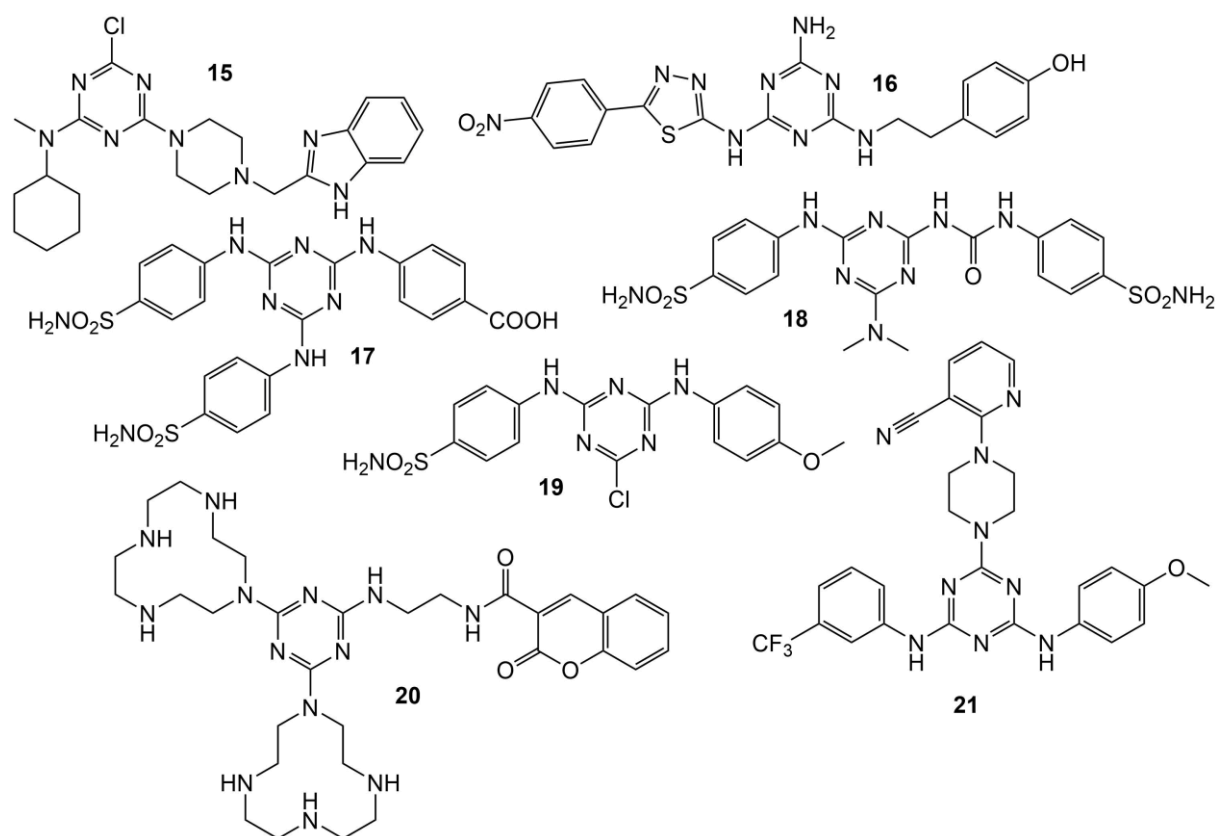
Some studies also confirmed the therapeutic potential of s-triazine derivatives in others neurodegenerative diseases. One of the therapeutic targets in Parkinson's disease are A2A adenosine receptors (A2ARs), and their antagonists increase dopamine transmission. Masih et al. obtained compound **16** (Scheme 11) by 3-step nucleophilic substitution to TCT. The results of the radioligand binding assay of **16** confirmed its high potency to A2ARs ( $K_i=32.1 \text{ nM}$ ) and ten times weaker interaction with A1ARs ( $K_i=322.3 \text{ nM}$ ) [60].

Lolak et al. presented a bis-sulfonamide derivative of s-triazine **17** (Scheme 11) characterized by AChE inhibition ( $IC_{50}=0.39 \mu\text{M}$ ;  $K_i=0.33 \mu\text{M}$ ) [61]. Compound **18** (Scheme 11) with the ureido benzenesulfonamide moieties on the s-triazine ring showed Fe-complexing

( $IC_{50}$ =125.64  $\mu$ M) and BuChE inhibiting activity equal 93.7 %, with simultaneous a low affinity for AChE. Additionally, **18** showed significant antioxidant capacity compared to the ABTS ( $IC_{50}$ =13.16  $\mu$ M) and DPPH ( $IC_{50}$ =297.4  $\mu$ M) assays [62]. In biological studies of s-triazine derivative **19** (Scheme 11) with an aromatic amine, Lorak et al. emphasized the significant inhibitory effect on AChE (96.3 %) [63]. The remaining properties were comparable to **18**.

Gonzalez et al. presented a s-triazine derivative with two heterocycle rings. Researches have shown that compounds **20** (Scheme 11) protects neuronal cells HT-22 from  $A\beta$ + $Cu^{2+}$  induced death by copper chelation [64].

Maqbool et al. designed and synthesized derivative **20** (Scheme 11). Evaluation of **21** found a very good inhibitory effect on AChE ( $IC_{50}$ =0.08  $\mu$ M) and BChE ( $IC_{50}$ =2.01  $\mu$ M). It is promising to reduce the lethal effect of  $H_2O_2$  on the SH-SY5Y neuronal cells. The antioxidant properties are shown in the TEAC assay ( $IC_{50}$ =3.46 $\mu$ M) [65].

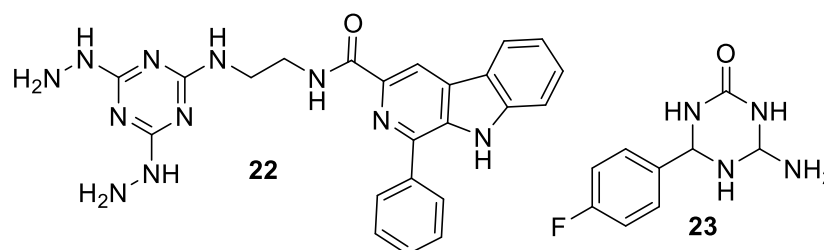


Scheme 11. Antineurodegenerative s-triazazine derivatives **15 -21**.

The compound **22** (N-(2-((4,6-dihydrazineyl-1,3,5-triazin-2-yl)amino)ethyl)-1-phenyl-9H-pyrido[3,4-b]indole-3-carboxamide) (Scheme 12) adheres to  $\beta$ -carboline-1,3,5-triazine derivatives. Baréa et al. obtained **22** by reacting the prepared  $\beta$ -carboline intermediate with 1,3-

dihydrazine-s-triazine in an alkaline environment at 0°C in MeCN/THF. The trisubstituted-s-triazine was converted into the hydrochloride salt. An *in vitro* study against AchE and BuChE indicated a special affinity for the second enzyme (demonstrated strong selective action against BuChE (C=10µM; 82.7% inhibition) compare to AChE (C=10µM; 7.6% inhibition)). An *in silico* study introducing **22** into the BuChE binding side confirmed a strong interaction at the site where butyrylthiocholine binds [66].

Triazinon **23** (Scheme 12) showed well-balanced *in vitro* potency against two enzymes BACE-1 (IC<sub>50</sub>=18.03 µM) and GSK-3 (IC<sub>50</sub>=14.67 µM). The cellular research has confirmed the ability of the compound **23** to protect neuronal cells and neurogenic activity and the absence of neurotoxicity [67,68].



Scheme 12. Antineurodegenerative s-triazine derivatives **22** and **23**.

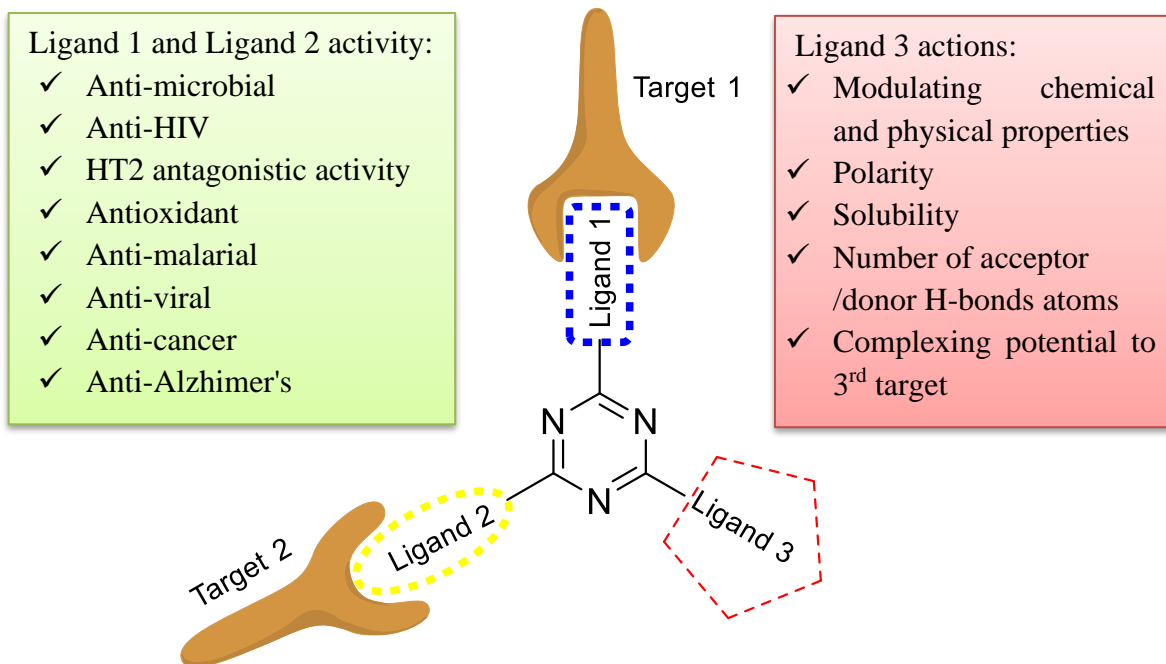
### 1.5. Designing of innovative multitarget drugs

In the world of science, the amount of developed chemicals is constantly growing. The increasing amount does not go hand in hand with the number of drugs being introduced. Most drugs on the market today target at a single biologic substance, like a protein or enzyme. In contrast, multi-target drugs hit several aims, which is often necessary to do in order to yield a therapeutic effect in complex diseases. While single-target drugs were once viewed as desirable largely because of the concern that “off-target” effects could have harmful consequences, multi-target drugs may actually possess a safer profile because of their ability to modify the outcome of a disease. While it’s true that multiple targets mean more chances for off-target effects, if the therapeutic benefit of a multi-target drug outweighs possible side effects that don’t ultimately influence the patient’s ability to return to a healthy state, then it’s likely worth the associated risk. Most diseases — cancer, those caused by chronic inflammation, and neurological and neurodegenerative diseases such as schizophrenia and Alzheimer’s disease — are often caused by multiple genetic and/or environmental factors. One drug taking aim at one target is unlikely to actually modify the outcome of these diseases due to the body’s compensatory mechanisms and redundant functions. Multi-target drugs hold promise for the

treatment of complex conditions that so far cannot be treated by single-target drugs. Unfortunately, multi-target drugs are often ignored because research to develop them is inherently more complex than it is for single-target drugs [69].

University of Rochester Medical Center has been developing a compound called URM-099, which is not a s-triazine derivative. It was originally synthesized as a small molecule therapy to reverse the neurological problems associated with HIV. It is supposed to do this by inhibiting enzymes called kinases (such as mixed lineage kinase type 3, or MLK3), which respond to inflammatory stressors inside and outside cells. These inflammatory signals arise after infection with viruses like HIV, the accumulation of disease-causing proteins like beta-amyloid, oxidative stress from diets high in fat and sugar, and many other insults. This destructive response to inflammation is present in most (if not all) organ systems, suggesting that a drug, which can restore the equilibrium between innate immune cells and target cells might be broadly applicable to a wide variety of diseases. URM-099, through its influence on MLK3 and other kinases, restores the balance of signaling in both cell cultures and animal models of various diseases: Alzheimer's disease, HIV-associated neurocognitive disorders, Parkinson's disease, multiple sclerosis, perioperative cognitive disorders (formerly postoperative cognitive dysfunction), and nonalcoholic steatohepatitis [70–72].

Another multi-target drug candidate, ENMD-2076 from CASI Pharmaceuticals, has shown promise against some of the toughest-to-treat cancers, including ovarian, liver, and triple-negative breast cancer. ENMD-2076 has several mechanisms of action against processes that are essential for tumor growth and development, including the formation of new blood vessels (angiogenesis), cell proliferation, and the cell cycle [73,74].



Scheme 13. Structure-activity relationship of three substituted s-triazine.

## II. Aims and Scopes

A consequence of the overuse and incorrect use of antibiotics and chemotherapeutic agents is the rapid spread of drug-resistant bacteria. This situation is a global problem that affects bacteria both in the community and in the hospital environment. This phenomenon is one of the most serious problems of modern medicine. The search for and synthesis of new compounds that act on bacteria is an urgent necessity of modern science.

Neurodegenerative diseases, a set of diseases that damage neurons in the human brain, are a very significant problem. Such diseases as Alzheimer's and Parkinson's are still incurable, and the development of effective drugs would be a breakthrough in their treatment. Compounds designed on the basis of the s-triazine breast may prove to be very helpful in solving these global problems.

Although advances in cancer biology have led to the development of targeted molecular therapies, chemotherapy remains the most important standard for treating many types of cancer. Chemotherapeutic agents such as cisplatin work by intercalating and cross-linking the DNA of rapidly dividing cancer cells to induce apoptosis. Chemotherapy has numerous side effects, creating a need for new drugs. This is where the need to obtain new chemical compounds appears. Candidates to cure cancer have to find to be a promising anti-cancer drug. It has to have interesting physical and chemical properties that can be targeted to specific molecules or cells using ligands.

The theoretical introduction showed that s-triazine and its derivatives have a diverse profile of biological activity so wide application possibilities. Some compounds whose structure is based on the s-triazine ring, for example Altretamine and Almitrine, are already in use in the medical field [75]. 1,3,5-Triazine ring is present both in compounds with anti-inflammatory, anti-cancer, antibacterial and inhibitory properties of neurodegenerative diseases. Among the many different newly synthesized compounds, several combinatorial libraries based on 1,3,5-triazine and peptide fragments were obtained, and compounds exhibiting high antimicrobial activity and low haemolytic activity were identified [76, 77].

In earlier studies conducted in the Department of Organic Chemistry, triazine derivatives with attached peptide fragments were shown to have anticancer activity. Good activity was observed against the glioblastoma LBC3, LN-18 and LN-229 cell lines [78] as well as DLD and Ht-29 human colon cancer cell lines [79]. Frączyk et al. presented the influence of

the type and number of substituents on the properties of s-triazine derivatives. The study compiled compounds containing one or two groups of 1-(2-chloroethyl)piperazine group as well as aromatic, primary and secondary amines and amino acids as substituents. The derivatives with the amino acids have shown promising results and this subgroup of derivatives is desirable to develop [80].

Taking into account the knowledge and previous studies, it was planned to synthesize a new group of 1,3,5-triazine derivatives. The aim of the planned research was to design and obtain new hybrid structures containing various substituents: dipeptide fragment and the structure responsible for the potential possibility of binding with the molecular target. It was foreseen to test the new derivatives for their effects on the growth and development of bacteria, yeast and fungi, as well as their inhibitory properties on the activity of cancer cells. Moreover, it was planned to test them to confirm their inhibitory activity on enzymes responsible for neurodegenerative processes in Alzheimer's disease. Theoretical calculations were aimed at verifying the strength of binding and stability of binding to selected enzymes.

In summary, main aims and scopes of presented doctoral dissertation were as follows:

- I. Synthesis of new s-triazine derivatives.
- II. Spectral analysis.
- III. Microbiological study on selected cell strains of fungi and bacteria.
- IV. Investigation of the effect on *E. coli* and *S. aureus* DNA gyrases on the relaxation of plasmid DNA in the presence of selected compounds.
- V. Molecular docking.
- VI. Evaluation of anticancer properties.
- VII. Study of the new compounds interactions with AChE and BACE1 enzymes.

### III. Materials and methods

#### 3.1. Synthesis

##### General information

Thin layer chromatography experiments (TLC) were carried out on silica gel (Merck; 60 Å F254). Spots were located with UV light (254 and 366 nm) and 1% ethanolic 4-(4-nitrobenzyl) pyridine (NBP). Analytical RP-HPLC was performed on a Waters 600S HPLC system (Waters 2489 UV/VIS detector, Waters 616 pump, Waters 717 plus autosampler, HPLC manager software from Chromax) using a Vydac C18 column (25 cm × 4.6 mm, 5 mm; Sigma). HPLC was performed with a gradient of 0.1% TFA in H<sub>2</sub>O (A) and 0.08% TFA in MeCN (B), at a flow rate of 1 ml/min with UV detection at 220 nm,  $t_R$  in min.

MS analysis was performed on an MS Bruker micrOTOFQIII.

<sup>1</sup>H-NMR and <sup>13</sup>C-NMR, spectra were recorded on a Bruker Avance DPX 250 (250 MHz) spectrometer and Varian (300 MHz). Chemical shifts (ppm) were relative to TMS, used as an internal standard. Multiplicities are marked as s = singlet, d = doublet, t = triplet, q = quartet, qu = quintet, m= multiplet.

##### General procedure of amino acids condensation

Protected amino acid (2 mmol) and NMM (0.110 ml, 1 mmol) were added to a vigorously stirred solution of DMT/NMM/TosO<sup>-</sup> (0.826 g, 2 mmol) in CH<sub>2</sub>Cl<sub>2</sub> (10 ml) cooled to 0°C. Stirring was continued until the condensing reagent disappeared (TLC analysis, staining with 0.5% solution of NBP) (1 h), after which HCl\*Ala-OMe (0.278 g, 2 mmol) and NMM (0.220 ml, 2 mmol) were added. The mixture was stirred for an additional 2 h at 0 °C and left overnight at room temperature. The mixture was diluted with CH<sub>2</sub>Cl<sub>2</sub> (10 ml), then the solution was washed successively with water, 0.5 M aqueous NaHSO<sub>4</sub>, water, 0.5 M aqueous NaHCO<sub>3</sub> and water again. The organic layer was dried with Na<sub>2</sub>SO<sub>4</sub>, filtered and concentrated to dryness. The residue was dried under a vacuum with P<sub>2</sub>O<sub>5</sub> and KOH to constant weight, to obtain the neutral peptide.

### General procedure of Fmoc group (Pg<sub>a</sub>) deprotection

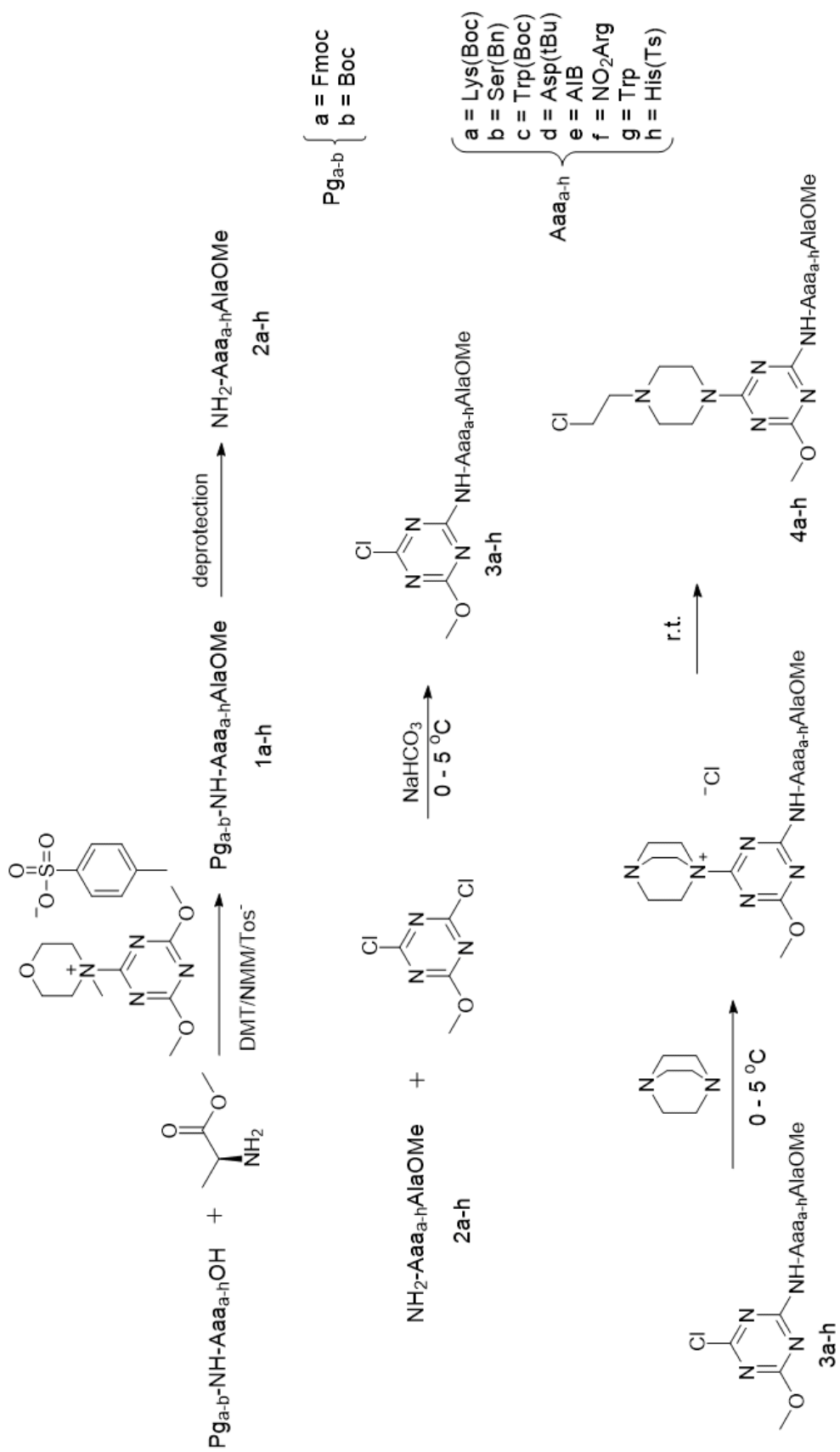
A Fmoc-protected dipeptide solution (1 mmol) dissolved in DCM (5 ml) was cooled in a water-ice bath with vigorously stirring and a 25% piperidine solution in DCM (10 ml) was added. Stirring was continued for 15 min. The solution was then removed in a vacuum evaporator and MeOH (20 ml) was added to the residue. The solvent was removed again using a vacuum evaporator. Stirring was continued for 5 min. The solvent was removed using a vacuum evaporator. To the residue was added 10 ml of DCM and the solvent was removed again in a vacuum evaporator. This procedure was repeated three times more. The solid residue was dried under a vacuum to constant weight. The HCl\*NH<sub>2</sub>-Lys(Boc)-AlaOMe, HCl\*NH<sub>2</sub>-Asp(OtBu)-AlaOMe, HCl\*NH<sub>2</sub>-Trp(Boc)-AlaOMe, HCl\*NH<sub>2</sub>-Arg(NO<sub>2</sub>)-AlaOMe and HCl\*NH<sub>2</sub>-Trp-AlaOMe were obtained in quantitative yield. The derivatives obtained were used in the subsequent reaction steps without additional purification procedures.

### General procedure of Boc group (Pg<sub>b</sub>) deprotection

A solution of Boc-protected dipeptide derivative (1 mmol) dissolved in DCM (5 ml) was cooled in a water-ice bath with intensive stirring and a 4 M solution of HCl in 1,4-dioxane (5 ml) was added. Stirring was continued for 4 h, then 1,4-dioxane (10 ml) was added to the solution. This procedure was repeated three times more. The residue was dried in a vacuum desiccator to constant weight. The NH<sub>2</sub>-Ser(Bn)-AlaOMe, NH<sub>2</sub>-Aib-AlaOMe, and NH<sub>2</sub>-Ser-AlaOMe were obtained in quantitative yield. The derivatives obtained were used immediately in subsequent reaction steps, without additional purification procedures.

### General procedure of synthesis of **3a-f** from DCMT and dipeptides

To vigorously stirred DCM (3 ml), dry NaHCO<sub>3</sub> (0.42 g, 5 mmol) was added portionwise. The resulting suspension was cooled to 0 ° C without ceasing dynamic stirring. Then a solution of DCMT (0.270 g, 1.5 mmol) in DCM (3 ml) was added and a solution of the dipeptide (1.5 mmol) was added dropwise. The reaction was stopped at the disappearance of DCMT as monitored by TLC using a 0.5% NBP solution in ethanol. The reaction mixture was filtered, the filtrate was evaporated under reduced pressure and the obtained precipitate was dried with P<sub>2</sub>O<sub>5</sub> and KOH to constant weight.



Scheme 14. Total synthesis pathway of 2-dipeptide-[4-(2-chloroethyl)piperin-1-yl]-6-methoxy-s-triazine derivatives.

## General procedure of synthesis of 2-[4-(2-chloroethyl)piperazin-1-yl]-4-methoxy-6-(di-peptide)-s-triazines **4a-h**

To a vigorously stirred solution of 2-chloro-4-methoxy-6-(di-peptide)-s-triazine (**3a-h**) (1 mmol) in DCM (10 ml) cooled to 0°C in an ice-water bath was added DABCO (0.112 g, 1mmol). Stirring at 0°C was continued until complete consumption of **3a-h**, as shown by TLC analysis ( $R_f = 0.45$ , DCM; staining with 0.5% solution of NBP in ethanol). The cooling bath was removed and stirring was continued at room temperature until all salt was consumed, as shown by TLC analysis ( $R_f = 0.00$ , pure DCM, colored with 0.5% solution of NBP in ethanol). The solvent was removed by evaporation and the residue was dried under a vacuum with  $P_2O_5$  and KOH to constant. All steps of the synthesis are shown in Scheme 14.

### 3.2. Antimicrobial activity

#### 3.2.1. Biological study on selected cell strains of fungi and bacteria

Testing of the compounds to evaluate their antimicrobial activity was performed in the Department of Biology of Eskisehir Technical University (Turkey). The antimicrobial activities of compounds were performed by using MIC according to CLSI M27-A2 [81] for bacteria, CLSI M07-A10 [82] and CLSI M38-A20 for yeasts and filamentous fungi, respectively, together with some modifications. Tested microorganisms were some members of bacteria, yeast and filamentous fungi as *Bacillus subtilis* (NRS-744), *Escherichia coli* (ATCC-25922), *Staphylococcus aureus* (NRRL B-767), *Candida albicans* (ATCC-90028), *Aspergillus flavus* (NRRL-980), *Aspergillus fumigatus* (NRRL 163), *Fusarium solani* (NRRL-13414), *Penicillium citrinum* (NRRL 1841), respectively. Microbroth dilution susceptibility assay was used for antimicrobial evaluation of the compounds. Stock solutions of the samples were prepared in dimethyl sulfoxide (DMSO). Dilution series using sterile distilled water were prepared from 4 mg/ml to 0.0039 mg/ml in micro-test tubes that were transferred to 96-well microtiter plates. Overnight-grown bacteria and *C. albicans* suspensions in double-strength Mueller–Hinton broth were standardized to  $10^8$  CFU/ml by using McFarland No: 0.5 standard solutions and  $10^5$  cell/ml spore/ml suspension in 1% Tween 80 for yeasts in double-strength MHB and filamentous fungi in double-strength Potato Dextrose Broth, respectively. Then, 100  $\mu$ l of each microorganism suspension was added into the wells. The last well-chain without microorganism was used as a negative control. Sterile distilled water and the medium served as a positive growth control. After incubation for 24 h at 37°C for bacteria and yeasts, and for 25°C at 72 h for filamentous fungi, minimum inhibitory concentration was detected by spraying

of 0.5% TTC (triphenyl tetrazolium chloride, Merck) aqueous solution for bacteria and yeasts, and by investigation of mycelia growing under a stereomicroscope for filamentous fungi. Streptomycin, Nystatin and Ketoconazole were used as control antibiotic agents.

### 3.2.2. Relaxation assay of *Escherichia coli* and *Staphylococcus aureus* gyrases

Kinetoplast DNA (kDNA) (0.20  $\mu$ g) was incubated with 1 U of *S. aureus* gyrase (reaction mixtures for the gyrase supercoiling assays contained: 35 mM Tris-HCl (pH 7.5), 24 mM KCl, 700 mM K-Glu, 4 mM MgCl<sub>2</sub>, 2 mM DTT, 1.8 mM spermidine, 1 mM ATP, 6.5% (w/v) glycerol and 0.1 mg/ml albumin) or 1 U of *E. coli* gyrase (reaction mixtures for the gyrase supercoiling assays contained: 40 mM Tris pH 7.5, 6 mM MgCl<sub>2</sub>, 10 mM DTT, 100 mM potassium glutamate, 50 mg/ml acetylated BSA, 1 mM ATP) in the absence or presence of varying concentrations of the test compounds and **ciprofloxacin** as positive control (100 and 300 nM). Enzyme activity was detected by incubation for 45 min at 37°C in a total reaction volume of 10  $\mu$ l and the reaction was terminated by addition of 2  $\mu$ l of 10% SDS. The reaction mixture was subjected to electrophoresis (2 h, 110 V) through a 1.0% agarose gel in TBE buffer (90mM Tris-borate and 2 mM EDTA). The gels were stained for 30 min with EtBr solution (0.5  $\mu$ g/ml). The DNA was visualized using 312 nm wavelength transilluminator and photographed under UV light. For the quantitative determination of topoisomerase activity, area representing supercoiled DNA, migrating as a single band at the bottom of gel was measured using InGenius gel documentation and analysis system (TK Biotech). The concentrations of the compounds that converted 50% of the supercoiled DNA (IC<sub>50</sub> values) were determined by averaging the data from at least three experiments.

### 3.2.3. Molecular docking to *Escherichia coli* and *Staphylococcus aureus* gyrases

To gain better insight into the interactions of synthesized inhibitors with DNA gyrase we have conducted a molecular docking study with two receptor enzymes from *E. coli* (PDB: 6RKW) and *S. aureus* (PDB: 7MVS). For the ligands, we decided to use three compounds, which showed the most potent inhibitory activity in experiment, namely **4c**, **4d** and **7b**. Since inhibitors do not possess a common moiety characteristic for typical DNA Gyrase inhibitors, like fluoroquinolones, aminocoumarins or NBTI, we started our research with determining the binding site of our molecules. For this purpose, we performed the molecular docking calculations within the presumed area of inhibitor's binding site. This area was chosen, so that it would include the binding sites of simocyclinone and NBTIs, which bind at the interface of the DNA duplex and GyrA subunit. Fluoroquinolones bind into the DNA and since our

inhibitors are analogous to the minor-groove binding agents such as netropsin or distamycin, the DNA duplex was also taken into the area of potential inhibitor binding site. The GyrB ATP/aminocoumarin binding site was also examined for potential binding modes. Unless specified otherwise, all results for both *E. coli* and *S. Aureus* DNA gyrase refer to the binding site at the GyrA subunit [83].

Molecular docking calculations require user to define the search space, which is explored to find the best possible ligand binding conformation. A too small search space may result in insufficient number of conformations. On the other hand, a grid-box that is too big may lead to excessive irrelevant binding poses. In each case the results may lack some of the binding modes with great affinity. Therefore, the definition of search space dimensions is not a straightforward task. Figure 3 shows the potential inhibitor binding area as a black rectangle. It has dimensions of 25 x 90 x 25 Å and is considered too large for a single docking calculation. Therefore, we divided this area into a series of overlapping grid-boxes. Starting from one end of the rectangle, we created a cube with dimensions of 25 x 25 x 25 Å. Then, we moved this cube by 5 Å along y axis of the rectangle. This was done until the putative binding area was divided into 14 identical overlapping grid-boxes. This scan was performed for each inhibitor as a ligand with both *E. coli* and *S. aureus* DNA gyrases as a receptor. After scanning the whole area, grid-box of smaller dimensions (20x20x20 Å) was placed in the location of binding mode with the lowest binding energy and molecular docking calculations were performed several times to further explore the search space of the binding site.

There is a number of available bacterial DNA gyrase structures that can be found in the Protein Data Bank. Recently, the complete structure of *E. coli* DNA gyrase was elucidated using cryo-EM technique [49], providing a solid foundation for drug discovery. The structures of *E. coli* (PDB: 6RKW) as well as *S. aureus* (PDB: 7MVS) [84] DNA gyrases were obtained from Protein Data Bank. In each case the enzyme was prepared for calculations by removing water molecules and co-crystallized ligand as well as adding polar hydrogen atoms. The software used for molecular docking was AutoDock Vina v.1.2.0 [85]. The BIOVIA Discovery Studio software was used to search for residues and nucleotides involved in binding of the studied ligands. To validate our method, we used Blind Docking Server [86], available at: <http://bio-hpc.eu/software/blind-docking-server/>, which performs an exhaustive series of docking calculations across the whole protein surface.

Binding energies, inhibition constants and ligand efficiencies were calculated for each ligand enzyme complex. Binding energy is a value that represents affinity of a ligand binding to the receptor and is calculated using Autodock Vina scoring function. The inhibition constant ( $K_i$ ) was calculated from the binding energy ( $\Delta G$ ) using the formula:  $K_i = \exp(\Delta G/RT)$ , where  $R$  is the universal gas constant ( $1.985 \times 10^{-3} \text{ kcal mol}^{-1} \text{ K}^{-1}$ ) and  $T$  (298.15 K). Ligand efficiency is the binding energy  $\Delta G$  divided by the number of non-hydrogen atoms [87].

### 3.3. Evaluation of anticancer properties

#### 3.3.1. MCF-7 and MDA-MB-231 cells

Studies on cancer cells were done in cooperation with the Department of Pharmaceutical and Biopharmaceutical Analysis and the Department of Hematology Diagnostics of the Medical University of Bialystok. Stock cultures of human MCF-7 and MDA-MB-231 breast cancer cells (purchased from the American Type Culture Collection, Rockville, MD) were maintained in continuously exponential growth by weekly passage in Dulbecco's Modified Eagle's Medium (Sigma) supplemented with 10% FBS(Sigma), 50  $\mu\text{g/ml}$  Streptomycin, 100 U/ml penicillin at 37  $^{\circ}\text{C}$  in a humid atmosphere containing 5%  $\text{CO}_2$ . Cells were cultivated in Costar flasks and subconfluently detached with 0.05% trypsin and 0.02% EDTA in a calcium-free phosphate buffered saline. The study was carried out using cells from passages 3 to 7, growing as monolayer in 6-well plates (Nunc) ( $5 \times 10^5$  cells per well and preincubated 24 hours without phenol red.

#### 3.3.2. Determination of apoptotic index and cell viability

The compounds were dissolved in sterile water and used at concentrations of 1, 5, 10, 50 and 100  $\mu\text{M}$ . Microscopic observations of cell monolayers were performed with a Nikon Optiphot microscope. Wright-Giemsa staining was performed using the Fisher Leuko Stat Kit. Adherent MCF-7 cells grown in 6-well plates were stained after induction of apoptosis with a dye mixture (10  $\mu\text{M}$  acridine orange and 10  $\mu\text{M}$  ethidium bromide, prepared in phosphate buffered saline). At the end of each experimental time point, all of the media was removed and cells were harvested by incubation with 0.05% trypsin and 0.02% EDTA for 1 min and washed with the medium. Then, 250  $\mu\text{l}$  of cell suspension was mixed with 10  $\mu\text{l}$  of the dye mix and 200 cells per sample were examined by fluorescence microscopy, according to the following criteria:

- viable cells with normal nuclei (a fine reticular pattern stained green in the nucleus and red-orange granules in the cytoplasm);
- viable cells with apoptotic nuclei (green chromatin which is highly condensed or fragmented and uniformly stained by the acridine orange);
- nonviable cells with normal nuclei (bright orange chromatin with organized structure);
- nonviable cells with apoptotic nuclei (bright orange chromatin which is highly condensed or fragmented).

### 3.3.3. Statistical analysis for anticancer evaluation

The results were submitted to statistical analysis using the method using a function in Excel developed by Dr. Rajmund Stasiewicz of Bialystok University of Technology. The IC<sub>50</sub> data are presented in Table 6.

## 3.4. Investigation of antineurodegenerative properties

### 3.4.1. Study of the interactions s-triazine derivatives with AChE enzyme

The inhibitory activity of the target compounds on AChE was assessed using the spectroscopic method of Ellman et al. [88]. The Acetylcholinesterase Inhibitor Screening Kit (Catalog Number MAK324), Purified AChE (Catalog Number C3389), and Donepezil were purchased from Sigma Aldrich. Enzyme solutions were prepared by dissolving lyophilized powder in double-distilled water. The compounds were dissolved in DMSO and diluted using 0.1 M KH<sub>2</sub>PO<sub>4</sub>/K<sub>2</sub>HPO<sub>4</sub> phosphate buffer (pH 7.5) at room temperature to yield the corresponding test concentrations 1-100 mM. Measurements were done using a clear 96-well flat-bottom plate. The absorbance was read on an Infinite M200 fluorescence spectrophotometer (TECAN, Männedorf, Switzerland) (ex. 412 nm) in duplicate experiments with two control wells: (No Enzyme) well and one well containing AChE Reference Enzyme (No Inhibitor Control). The experimental procedures for AChE activity assays were performed according to the technical bulletins of the acetylcholinesterase activity assay kit (MAK324; Sigma-Aldrich). Purified AChE was prepared to a concentration of 400 units/l. A reaction mix for each well of reaction was prepared by mixing into a clean tube: 154 µl of Assay Buffer (Catalog Number MAK324A) 1 µl of Substrate (100mM, Catalog Number MAK324B) and 0.5 µl of DNTB (Catalog Number MAK324C). The reaction was initiated by the addition of 45 µl assay buffer, 5 µl of the enzyme and the investigated compounds I-IX (5 µl) to the wells to obtain final concentrations of 1,10, 20, 50, and 100 mM. A positive control of Donepezil was used in the

same range of concentrations. The plate was incubated for 15 min. Then, the reaction mixture 150 ( $\mu$ l) was added to each sample, the control (No Enzyme), and the No Inhibitor Control wells. The plate was tapped to mix. Absorbance was measured at 412 nm at 0 minutes and at 10 minutes. Acetylcholinesterase activity was calculated as % inhibition. Results are reported as  $IC_{50}$ . All samples were assayed in triplicate.

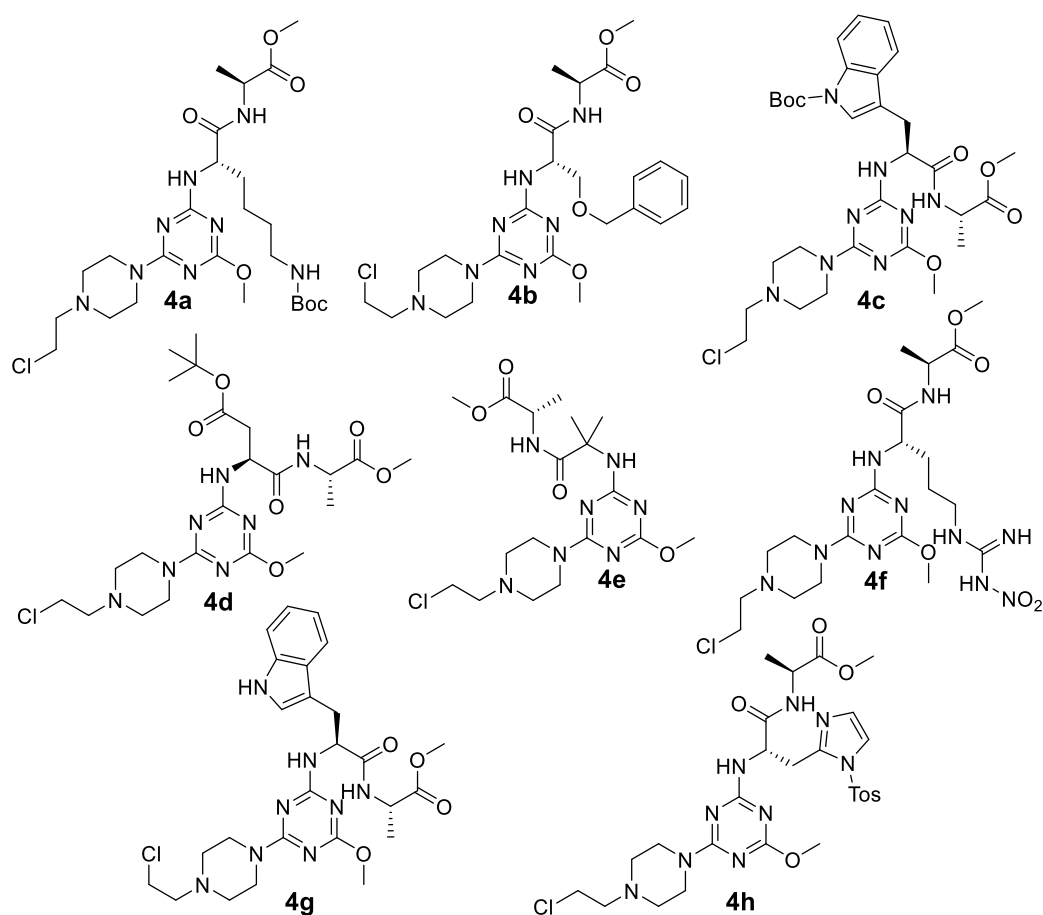
### 3.4.2. Study of the interactions s-triazine derivatives with BACE1 enzyme

The  $\beta$ -Secretase (BACE1) activity detection kit was purchased from Sigma Aldrich (Catalog number CS0010) and the assay was done according to the technical bulletins of the  $\beta$ -secretase activity assay kit [89]. The assay is based on a convenient method of fluorescence resonance energy transfer (FRET), in which fluorescence signal enhancement is observed after the substrate is cleaved by BACE1. Measurements were done using a 96-well flat-bottom plate for fluorescence assay. Stock solutions of all derivatives were prepared in DMSO. Each sample was further diluted in an assay buffer to prepare the appropriate concentrations of the test compounds I-IX (1, 10, 20, 50, and 100Mm). 20 $\mu$ l of BACE1 substrate was added to 1-10 $\mu$ l of each test compound in separate wells of a black 96-well microplate and mixed by gentle pipetting 10 $\mu$ l of BACE1 enzyme solution (dilute 10-fold with Fluorescent Assay Buffer (Catalog Number F8303) to  $\sim$ 0.3 unit/ $\mu$ l) was added just before reading. Fluorescence was measured in “time zero,” immediately after adding the enzyme and after incubation (37°C; 2h). Finally, the fluorescence was read on an Infinite M200 fluorescence spectrophotometer (TECAN, Männedorf, Switzerland) (ex.320 nm; em.405nm) in triplicate experiments with a negative control (no enzyme) and a positive control (supplied enzyme activity). BACE1 activity was calculated as  $IC_{50}$  (the mean half maximal inhibitory concentration of inhibition of BACE1 enzymatic activity were calculated as  $IC_{50}$  ( $\mu$ M)).

## IV. Results

### 4.1. Synthesis of s-triazine derivatives

The synthesised compounds, obtained by the multi-step DCMT substitution method illustrated in Scheme 14, contained a dipeptide sequence include an Ala-OMe fragment substituent on the 1,3,5-triazine ring and a 2-chloroethylamine fragment attached through the piperazine ring. In the first step, the amino acid or dipeptides prepared in advance were used to substitute chlorine. The amino acid substrate solution was added dropwise to a solution of DCMT, sodium bicarbonate in DCM at zero temperature. The reaction was carried out until the DCMT was consumed. After the product (**3a-3h**, Table 1) was purified and dried, the next step was to react with DABCO in DCM. The mixture initially cooled to 0°C was stirred until the starting materials were added. The reaction was then run at room temperature until the product of the first stage was consumed. The obtained products were purified, dried and weighed. The final compounds **4a-4h** and analysis details are presented in Scheme 15 and Table 1.



Scheme 15. Structures of s-triazine derivatives **4a-4h**.

Table 1. Characterization of s-triazine derivatives

Symbol and chemical name	Structure	Results
<b>3a</b> 2-chloro-4-methoxy-6-(NH-Lys(Boc)-Ala-OMe)-1,3,5-triazine		yield = 96.2% as colorless oil. <sup>1</sup> H NMR (700 MHz, CDCl <sub>3</sub> ): δ 1.27 (quint, 2H, J = 4.48 Hz, CH <sub>2</sub> -CH <sub>2</sub> -CH <sub>2</sub> ); 1.41 (d, 3H, J = 5.18 Hz, CH <sub>3</sub> -CH-); 1.43 (s, 9H, (CH <sub>3</sub> ) <sub>3</sub> -C); 1.57 (quint, 2H, J = 4.28 Hz, -CH <sub>2</sub> -); 1.93 (dt, 2H, J <sub>1</sub> = 5.25 Hz, J <sub>2</sub> = 7.52 Hz, -CH-CH <sub>2</sub> -); 3.22 (t, 2H, J = 5.81 Hz, NH-CH <sub>2</sub> -); 3.71 (s, 3H, CH <sub>3</sub> OCO); 4.01 (s, 3H, CH <sub>3</sub> O-); 4.33 (t, 1H, J = 5.52 Hz, NH-CH <sub>2</sub> -); 4.36 (q, 1H, J = 5.18 Hz, CH <sub>3</sub> -CH-) [ppm]. <sup>13</sup> C NMR (176 MHz, CDCl <sub>3</sub> ): δ 17.7, 21.4, 28.2, 29.3, 29.4, 40.5, 47.8, 52.3, 53.6, 54.6, 80.5, 162.2, 156.3, 163.4, 171.7, 172.5, 172.9 [ppm].
<b>3b</b> 2-chloro-4-methoxy-6-(NH-Ser(Bn)-Ala-OMe)-1,3,5-triazine		yield = 98.1%, colorless oil. <sup>1</sup> H NMR (700 MHz, CDCl <sub>3</sub> ): δ 1.41 (d, 3H, J = 5.18 Hz, CH <sub>3</sub> -CH-); 3.72 (s, 3H, CH <sub>3</sub> OCO); 3.84 (d, 2H, J = 6.78 Hz, CH-CH <sub>2</sub> -); 4.01 (s, 3H, CH <sub>3</sub> O-); 4.36 (q, 1H, J = 5.18 Hz, CH <sub>3</sub> -CH-); 4.481 (t, 1H, J = 6.78 Hz, CH-CH <sub>2</sub> -); 4.55 (s, 2H, CH <sub>2</sub> -O-Ar); 7.37-7.44 (m, 5H, Ar) [ppm]. <sup>13</sup> C NMR (176 MHz, CDCl <sub>3</sub> ): δ 17.7, 38.3, 47.8, 52.3, 54.6, 69.3, 72.8, 127.9, 128.5, 128.9, 138.0, 162.2, 163.4, 171.3, 171.7, 172.9 [ppm].
<b>3c</b> 2-chloro-4-methoxy-6-(NH-Trip(Boc)-Ala-OMe)-1,3,5-triazine		yield = 98.1%, colorless oil. <sup>1</sup> H NMR (700 MHz, CDCl <sub>3</sub> ): δ 1.41 (d, 3H, J = 5.18 Hz, CH <sub>3</sub> -CH-); 1.42 (s, 9H, (CH <sub>3</sub> ) <sub>3</sub> C); 3.05 (d, 2H, J = 6.82 Hz, CH-CH <sub>2</sub> -); 3.72 (s, 3H, CH <sub>3</sub> OCO); 4.02 (s, 3H, CH <sub>3</sub> O-); 4.36 (q, 1H, J = 5.18 Hz, CH <sub>3</sub> -CH-); 4.80 (t, 1H, J = 6.82 Hz, CH-CH <sub>2</sub> -); 6.98-7.62 (m, 5H, Ar) [ppm]. <sup>13</sup> C NMR (176 MHz, CDCl <sub>3</sub> ): δ 17.8, 27.6, 28.2, 47.8, 52.3, 53.6, 54.6, 81.4, 115.2, 117.1, 118.8, 120.2, 122.9, 123.7, 129.8, 135.3, 149.2, 162.2, 163.4, 171.7, 172.5, 172.9 [ppm].

Table 1. Characterization of s-triazine derivatives

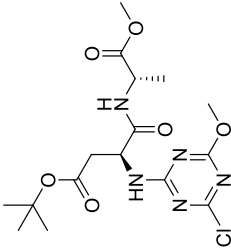
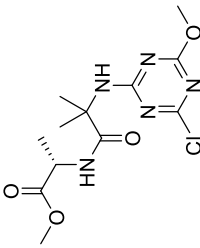
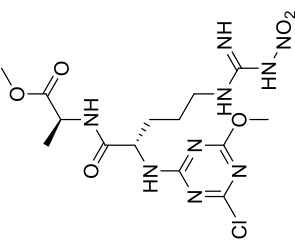
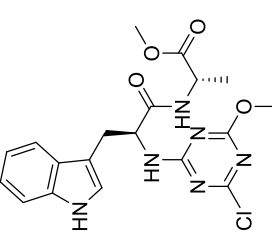
<p><b>3d</b> 2-chloro-4-methoxy-6-(NH-Asp(OtBu)-Ala-OMe)-1,3,5-triazine</p>		<p>yield = 97.6%, colorless oil.  <sup>1</sup>H NMR (700 MHz, CDCl<sub>3</sub>): δ 1.37 (s, 9H, (CH<sub>3</sub>)<sub>3</sub>C); 1.41 (d, 3H, J = 5.18 Hz, CH<sub>3</sub>-CH-); 3.01 (d, 3H, J = 6.23 Hz, CH-CH<sub>2</sub>-); 3.72 (s, 3H, CH<sub>3</sub>OCO); 4.01 (s, 3H, CH<sub>3</sub>O-); 4.36 (q, 1H, J = 5.18 Hz, CH<sub>3</sub>-CH-); 5.03 (t, 1H, J = 6.23 Hz, CH-CH<sub>2</sub>-) [ppm].  <sup>13</sup>C NMR (176 MHz, CDCl<sub>3</sub>): δ 17.7, 28.1, 37.9, 47.8, 52.3, 53.6, 54.6, 81.4, 162.2, 163.4, 171.7, 172.3, 172.5, 172.9 [ppm]</p>
<p><b>3e</b> 2-chloro-4-methoxy-6-(NH-Aib-Ala-OMe)-1,3,5-triazine</p>		<p>yield = 95.8 %, colorless oil.  <sup>1</sup>H NMR (700 MHz, CDCl<sub>3</sub>): δ 1.36 (s, 6H, (CH<sub>3</sub>)<sub>2</sub>C-); 1.41 (d, 3H, J = 5.18 Hz, CH<sub>3</sub>-CH-); 3.72 (s, 3H, CH<sub>3</sub>OCO); 4.01 (s, 3H, CH<sub>3</sub>O-); 4.36 (q, 1H, J = 5.18 Hz, CH<sub>3</sub>-CH-) [ppm].  <sup>13</sup>C NMR (176 MHz, CDCl<sub>3</sub>): δ 17.8, 27.1, 48.1, 54.6, 52.3, 58.1, 163.4, 167.9, 171.7, 172.9, 175.6 [ppm].</p>
<p><b>3f</b> 2-chloro-4-methoxy-6-(NH-Arg(NO<sub>2</sub>)-Ala-OMe)-1,3,5-triazine</p>		<p>yield = 96.7%, colorless oil.  <sup>1</sup>H NMR (700 MHz, CDCl<sub>3</sub>): δ 1.41 (d, 3H, J = 5.18 Hz, CH<sub>3</sub>-CH-); 1.59 (quint, 2H, J = 4.72 Hz, CH<sub>2</sub>-CH<sub>2</sub>); 1.94 (q, 2H, J = 6.47 Hz, -CH-CH<sub>2</sub>); 3.12 (t, 2H, J = 6.25 Hz, CH<sub>2</sub>-CH<sub>2</sub>); 3.72 (s, 3H, CH<sub>3</sub>OCO); 4.01 (s, 3H, CH<sub>3</sub>O-); 4.33 (t, 1H, J = 6.55 Hz, CH-CH<sub>2</sub>); 4.36 (q, 1H, J = 5.18 Hz, CH<sub>3</sub>-CH-) [ppm].  <sup>13</sup>C NMR (176 MHz, CDCl<sub>3</sub>): δ 17.7, 25.7, 30.7, 41.0, 47.8, 52.3, 53.6, 54.6, 154.7, 162.2, 163.4, 171.7, 172.5, 172.9 [ppm].</p>
<p><b>3g</b> 2-chloro-4-methoxy-6-(NH-Trp-Ala-OMe)-1,3,5-triazine</p>		<p>yield = 97.5 %, colorless oil.  <sup>1</sup>H NMR (700 MHz, CDCl<sub>3</sub>): δ 1.41 (d, 3H, J = 5.18 Hz, CH<sub>3</sub>-CH-); 3.05 (d, 2H, J = 6.82 Hz, CH-CH<sub>2</sub>); 3.72 (s, 3H, CH<sub>3</sub>OCO); 4.02 (s, 3H, CH<sub>3</sub>O-); 4.36 (q, 1H, J = 5.18 Hz, CH<sub>3</sub>-CH-); 4.80 (t, 1H, J = 6.82 Hz, CH-CH<sub>2</sub>); 6.98-7.62 (m, 5H, Ar) [ppm].  <sup>13</sup>C NMR (176 MHz, CDCl<sub>3</sub>): δ 17.8, 27.7, 47.8, 52.3, 53.6, 54.6, 109.9, 111.6, 118.7, 120.2, 122.3, 124.4, 127.7, 136.4, 162.2, 163.4, 171.7, 172.5, 172.9 [ppm].</p>

Table 1. Characterization of s-triazine derivatives

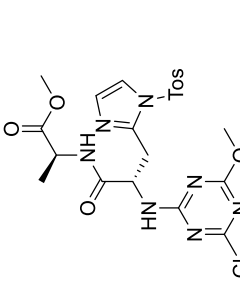
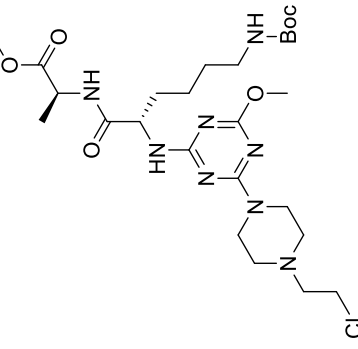
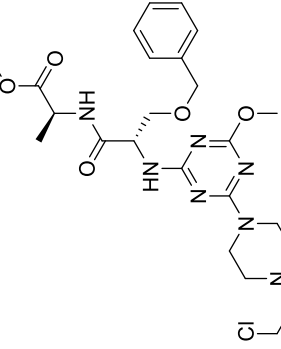
<p><b>3h</b> 2-chloro-4-methoxy-6-(NH-His(Ts)-Ala-OMe)-1,3,5-triazine</p>		<p>yield = 98.8 %, colorless oil.  <sup>1</sup>H NMR (700 MHz, CDCl<sub>3</sub>): δ 1.41 (d, 3H, J = 5.18 Hz, CH<sub>3</sub>-CH-); 2.47 (s, 3H, CH<sub>3</sub>); 3.45 (d, 2H, J = 6.38 Hz, CH-CH<sub>2</sub>); 3.71 (s, 3H, CH<sub>3</sub>OCO); 4.02 (s, 3H, CH<sub>3</sub>O-); 4.36 (q, 1H, J = 5.18 Hz, CH<sub>3</sub>-CH-); 5.03 (t, 1H, J = 6.38 Hz, CH-CH<sub>2</sub>); 7.28-7.79 (m, 6H, Ar) [ppm].  <sup>13</sup>C NMR (176 MHz, CDCl<sub>3</sub>): δ 17.8, 21.3, 30.5, 47.8, 52.3, 127.5, 129.7, 128.8, 135.1, 162.2, 163.4, 171.7, 172.5, 172.9 [ppm]</p>
<p><b>4a</b> 2-[4-(2-chloroethyl)piperazin-1-yl]-4-methoxy-6-(NH-Lys(Boc)-Ala-OMe)-1,3,5-triazine</p>		<p>yield = 98.8%; colorless oil.  <sup>1</sup>H NMR (700 MHz, CDCl<sub>3</sub>): δ 1.27 (quint, 2H, J = 4.48 Hz, CH<sub>2</sub>-CH<sub>2</sub>-CH<sub>2</sub>); 1.41 (d, 3H, J = 5.18 Hz, CH<sub>3</sub>-CH-); 1.43 (s, 9H, (CH<sub>3</sub>)<sub>3</sub>-C); 1.57 (quint, 2H, J = 4.28 Hz, -CH<sub>2</sub>-); 1.93 (dt, 2H, J<sub>1</sub> = 5.25 Hz, J<sub>2</sub> = 7.52 Hz, -CH-CH<sub>2</sub>-); 2.66 (t, 2 x 2H, J = 6.32 Hz, N-CH<sub>2</sub>-CH<sub>2</sub>-N); 2.85 (t, 2H, J = 6.24 Hz, N-CH<sub>2</sub>-CH<sub>2</sub>); 3.22 (t, 2H, J = 5.81 Hz, NH-CH<sub>2</sub>); 3.58 (t, 2 x 2H, J = 6.31 Hz, N-CH<sub>2</sub>-CH<sub>2</sub>-N); 3.86 (t, 2H, J = 6.24 Hz, Cl-CH<sub>2</sub>); 3.71 (s, 3H, CH<sub>3</sub>OCO); 4.01 (s, 3H, CH<sub>3</sub>O-); 4.33 (t, 1H, J = 5.52 Hz, NH-CH<sub>2</sub>CH<sub>2</sub>); 4.36 (q, 1H, J = 5.18 Hz, CH<sub>3</sub>-CH-) [ppm].  <sup>13</sup>C NMR (176 MHz, CDCl<sub>3</sub>): δ 17.7, 21.4, 28.2, 29.3, 29.4, 40.5, 41.2, 44.0, 47.8, 51.8, 52.3, 53.0, 53.6, 54.6, 80.5, 162.2, 156.3, 163.4, 171.7, 172.5, 172.9 [ppm].  HRMS: 588.2994, ([M+H]<sup>+</sup>, C<sub>25</sub>H<sub>44</sub>ClN<sub>8</sub>O<sub>6</sub><sup>+</sup>; calc. 588.11192).</p>
<p><b>4b</b> 2-[4-(2-chloroethyl)piperazin-1-yl]-4-methoxy-6-(NH-Ser(Bn)-Ala-OMe)-1,3,5-triazine</p>		<p>yield = 99.0 %, colorless oil.  <sup>1</sup>H NMR (700 MHz, CDCl<sub>3</sub>): δ 1.41 (d, 3H, J = 5.18 Hz, CH<sub>3</sub>-CH-); 2.66 (t, 2 x 2H, J = 6.32 Hz, N-CH<sub>2</sub>-CH<sub>2</sub>-N); 2.85 (t, 2H, J = 6.24 Hz, N-CH<sub>2</sub>-CH<sub>2</sub>); 3.58 (t, 2 x 2H, J = 6.31 Hz, N-CH<sub>2</sub>-CH<sub>2</sub>-N); 3.72 (s, 3H, CH<sub>3</sub>OCO); 3.84 (d, 2H, J = 6.78 Hz, CH-CH<sub>2</sub>); 3.86 (t, 2H, J = 6.24 Hz, Cl-CH<sub>2</sub>); 4.01 (s, 3H, CH<sub>3</sub>O-); 4.36 (q, 1H, J = 5.18 Hz, CH<sub>3</sub>-CH-); 4.481 (t, 1H, J = 6.78 Hz, CH-CH<sub>2</sub>); 4.55 (s, 2H, CH<sub>2</sub>-O-Ar); 7.37-7.44 (m, 5H, Ar) [ppm].  <sup>13</sup>C NMR (176 MHz, CDCl<sub>3</sub>): δ 17.7, 38.3, 41.2, 44.1, 47.8, 51.8, 52.3, 53.0, 54.6, 69.3, 72.8, 127.9, 128.9, 138.0, 162.2, 163.4, 171.3, 171.7, 172.9 [ppm].  HRMS: 537.3677, ([M+H]<sup>+</sup>, C<sub>24</sub>H<sub>35</sub>ClN<sub>7</sub>O<sub>5</sub><sup>+</sup>; calc. 537.0237).</p>

Table 1. Characterization of s-triazine derivatives

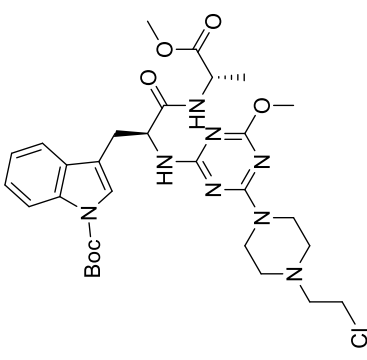
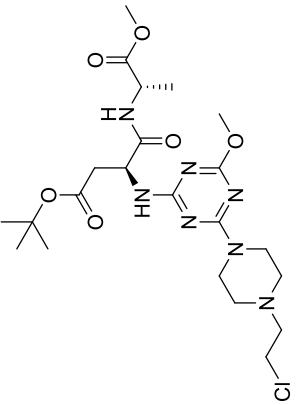
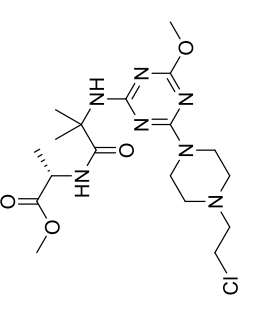
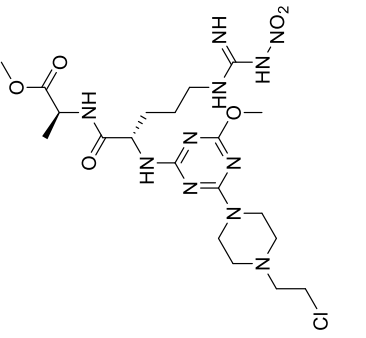
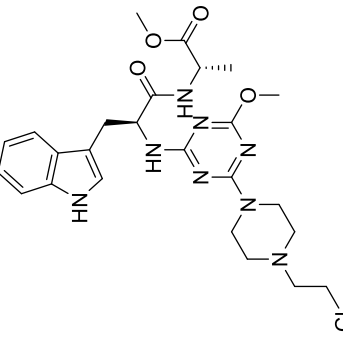
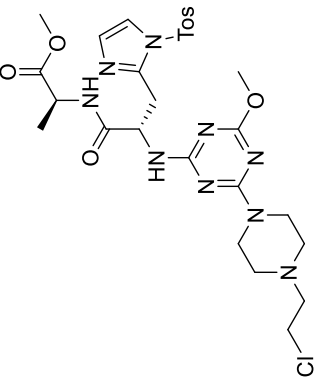
<p><b>4c</b> 2-[4-(2-chloroethyl)piperazin-1-yl]-4-methoxy-6-(NH-Trp(Boc)-Ala-OMe)-1,3,5-triazine</p>		<p>yield = 98.9 %, colorless oil.  <sup>1</sup>H NMR (700 MHz, CDCl<sub>3</sub>): δ 1.41 (d, 3H, J = 5.18 Hz, CH<sub>3</sub>-CH-); 1.42 (s, 9H, (CH<sub>3</sub>)<sub>3</sub>C); 2.66 (t, 2 x 2H, J = 6.32 Hz, N-CH<sub>2</sub>-CH<sub>2</sub>-N); 2.85 (t, 2H, J = 6.24 Hz, N-CH<sub>2</sub>-CH<sub>2</sub>); 3.58 (t, 2 x 2H, J = 6.31 Hz, N-CH<sub>2</sub>-CH<sub>2</sub>-N); 3.05 (d, 2H, J = 6.82 Hz, CH-CH<sub>2</sub>); 3.72 (s, 3H, CH<sub>3</sub>OCO); 3.88 (t, 2H, J = 6.24 Hz, Cl-CH<sub>2</sub>); 4.02 (s, 3H, CH<sub>3</sub>O-); 4.36 (q, 1H, J = 5.18 Hz, CH<sub>3</sub>-CH-); 4.80 (t, 1H, J = 6.82 Hz, CH-CH<sub>2</sub>); 6.98-7.62 (m, 5H, Ar) [ppm].  <sup>13</sup>C NMR (176 MHz, CDCl<sub>3</sub>): δ 17.8, 27.6, 28.2, 41.2, 44.1, 47.8, 51.8, 52.3, 53.0, 53.6, 54.6, 81.4, 115.2, 117.1, 118.8, 120.2, 122.9, 123.7, 129.8, 135.3, 149.2, 162.2, 163.4, 171.7, 172.5, 172.9 [ppm].            HRMS: 646.2837, ([M+H]<sup>+</sup>, C<sub>30</sub>H<sub>42</sub>ClN<sub>8</sub>O<sub>6</sub><sup>+</sup>; calc. 646.1495).</p>
<p><b>4d</b> 2-[4-(2-chloroethyl)piperazin-1-yl]-4-methoxy-6-(NH-Asp(OtBu)-Ala-OMe)-1,3,5-triazine</p>		<p>yield = 99.1 %, colorless oil.  <sup>1</sup>H NMR (700 MHz, CDCl<sub>3</sub>): δ 1.37 (s, 9H, (CH<sub>3</sub>)<sub>3</sub>C); 1.41 (d, 3H, J = 5.18 Hz, CH<sub>3</sub>-CH-); 2.66 (t, 2 x 2H, J = 6.32 Hz, N-CH<sub>2</sub>-CH<sub>2</sub>-N); 2.85 (t, 2H, J = 6.24 Hz, N-CH<sub>2</sub>-CH<sub>2</sub>); 3.01 (d, 3H, J = 6.23 Hz, CH-CH<sub>2</sub>); 3.58 (t, 2 x 2H, J = 6.31 Hz, N-CH<sub>2</sub>-CH<sub>2</sub>-N); 3.72 (s, 3H, CH<sub>3</sub>OCO); 3.88 (t, 2H, J = 6.24 Hz, Cl-CH<sub>2</sub>); 4.01 (s, 3H, CH<sub>3</sub>O-); 4.36 (q, 1H, J = 5.18 Hz, CH<sub>3</sub>-CH-); 5.03 (t, 1H, J = 6.23 Hz, CH-CH<sub>2</sub>) [ppm].  <sup>13</sup>C NMR (176 MHz, CDCl<sub>3</sub>): δ 17.7, 28.1, 37.9, 41.2, 44.0, 47.8, 51.8, 52.3, 53.1, 53.6, 54.6, 81.4, 162.2, 163.4, 171.7, 172.3, 172.5, 172.9 [ppm].            HRMS: 531.2773, ([M+H]<sup>+</sup>, C<sub>22</sub>H<sub>37</sub>ClN<sub>7</sub>O<sub>6</sub><sup>+</sup>; calc. 531.0175).</p>
<p><b>4e</b> 2-[4-(2-chloroethyl)piperazin-1-yl]-4-methoxy-6-(NH-Alb-Ala-OMe)-1,3,5-triazine</p>		<p>yield = 98.3 %, colorless oil.  <sup>1</sup>H NMR (700 MHz, CDCl<sub>3</sub>): δ 1.36 s, 6H, (CH<sub>3</sub>)<sub>2</sub>; 1.41 (d, 3H, J = 5.18 Hz, CH<sub>3</sub>-CH-); 2.66 (t, 2 x 2H, J = 6.32 Hz, N-CH<sub>2</sub>-CH<sub>2</sub>-N); 2.85 (t, 2H, J = 6.24 Hz, N-CH<sub>2</sub>-CH<sub>2</sub>); 3.58 (t, 2 x 2H, J = 6.31 Hz, N-CH<sub>2</sub>-CH<sub>2</sub>-N); 3.72 (s, 3H, CH<sub>3</sub>OCO); 3.86 (t, 2H, J = 6.24 Hz, Cl-CH<sub>2</sub>); 4.01 (s, 3H, CH<sub>3</sub>O-); 4.36 (q, 1H, J = 5.18 Hz, CH<sub>3</sub>-CH-) [ppm].  <sup>13</sup>C NMR (176 MHz, CDCl<sub>3</sub>): δ 17.8, 27.1, 41.2, 44.0, 48.1, 54.6, 51.8, 52.3, 53.0, 58.1, 163.4, 167.9, 171.7, 172.9, 175.6 [ppm].            HRMS: 445.0345, ([M+H]<sup>+</sup>, C<sub>18</sub>H<sub>31</sub>ClN<sub>7</sub>O<sub>4</sub><sup>+</sup>; calc. 444.9283).</p>

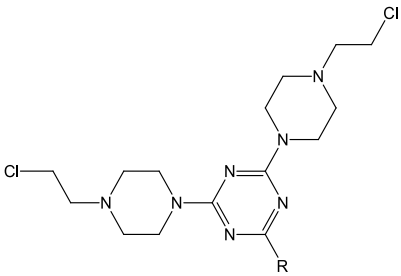
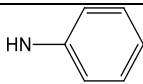
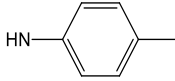
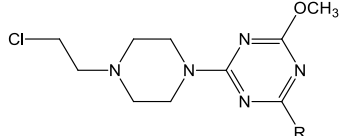
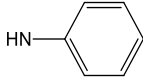
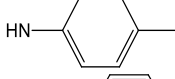
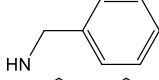
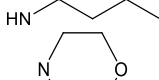
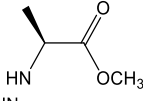
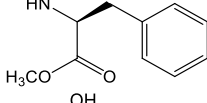
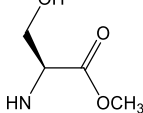
Table 1. Characterization of s-triazine derivatives

<p><b>4f</b> 2-[4-(2-chloroethyl)piperazin-1-yl]-4-methoxy-6-(NH-Arg(NO<sub>2</sub>)-Ala-OMe)-1,3,5-triazine</p>		<p>yield = 98.4 %, colorless oil.  <sup>1</sup>H NMR (700 MHz, CDCl<sub>3</sub>): δ 1.41 (d, 3H, J = 5.18 Hz, CH<sub>3</sub>-CH-); 1.594 (quint, 2H, J = 4.72 Hz, CH<sub>2</sub>-CH<sub>2</sub>); 1.94 (q, 2H, J = 6.47 Hz, -CH-CH<sub>2</sub>); 2.66 (t, 2 x 2H, J = 6.32 Hz, N-CH<sub>2</sub>-CH<sub>2</sub>-N); 2.85 (t, 2H, J = 6.24 Hz, N-CH<sub>2</sub>-CH<sub>2</sub>); 3.12 (t, 2H, J = 6.25 Hz, CH<sub>2</sub>-CH<sub>2</sub>); 3.58 (t, 2 x 2H, J = 6.31 Hz, N-CH<sub>2</sub>-CH<sub>2</sub>-N); 3.72 (s, 3H, CH<sub>3</sub>OCO); 3.86 (t, 2H, J = 6.24 Hz, Cl-CH<sub>2</sub>); 4.01 (s, 3H, CH<sub>3</sub>O-); 4.33 (t, 1H, J = 6.55 Hz, CH-CH<sub>2</sub>); 4.36 (q, 1H, J = 5.18 Hz, CH<sub>3</sub>-CH-) [ppm]  <sup>13</sup>C NMR (176 MHz, CDCl<sub>3</sub>): δ 17.7, 25.7, 30.7, 41.0, 41.2, 44.0, 47.8, 51.8, 52.3, 53.0, 53.6, 54.6, 154.7, 162.2, 163.4, 171.7, 172.5, 172.9 [ppm]            HRMS: 561.0123, ([M+H]<sup>+</sup>, C<sub>20</sub>H<sub>35</sub>CIN<sub>11</sub>O<sub>6</sub><sup>+</sup>; calc. 561.0071).</p>
<p><b>4g</b> 2-[4-(2-chloroethyl)piperazin-1-yl]-4-methoxy-6-(NH-Trp-Ala-OMe)-1,3,5-triazine</p>		<p>yield = 99.2 %, colorless oil.  <sup>1</sup>H NMR (700 MHz, CDCl<sub>3</sub>): δ 1.41 (d, 3H, J = 5.18 Hz, CH<sub>3</sub>-CH-); 2.66 (t, 2 x 2H, J = 6.32 Hz, N-CH<sub>2</sub>-CH<sub>2</sub>-N); 3.05 (d, 2H, J = 6.82 Hz, CH-CH<sub>2</sub>); 3.72 (s, 3H, CH<sub>3</sub>OCO); 2.85 (t, 2H, J = 6.24 Hz, N-CH<sub>2</sub>-CH<sub>2</sub>); 3.58 (t, 2 x 2H, J = 6.31 Hz, N-CH<sub>2</sub>-CH<sub>2</sub>-N); 3.86 (t, 2H, J = 6.24 Hz, Cl-CH<sub>2</sub>); 4.02 (s, 3H, CH<sub>3</sub>O-); 4.36 (q, 1H, J = 5.18 Hz, CH<sub>3</sub>-CH-); 4.80 (t, 1H, J = 6.82 Hz, CH-CH<sub>2</sub>); 6.98-7.62 (m, 5H, Ar) [ppm].  <sup>13</sup>C NMR (176 MHz, CDCl<sub>3</sub>): δ 17.8, 27.7, 41.2, 44.1, 47.8, 51.8, 52.3, 53.1, 53.6, 54.6, 109.9, 111.6, 118.7, 120.2, 122.3, 124.4, 127.7, 136.4, 162.2, 163.4, 171.7, 172.5, 172.9 [ppm].            HRMS: 546.2377, ([M+H]<sup>+</sup>, C<sub>25</sub>H<sub>34</sub>CIN<sub>8</sub>O<sub>4</sub><sup>+</sup>; calc. 546.0337).</p>
<p><b>4h</b> 2-[4-(2-chloroethyl)piperazin-1-yl]-4-methoxy-6-(NH-His(Tos)-Ala-OMe)-1,3,5-triazine</p>		<p>yield = 98.7 %, colorless oil.  <sup>1</sup>H NMR (700 MHz, CDCl<sub>3</sub>): δ 1.41 (d, 3H, J = 5.18 Hz, CH<sub>3</sub>-CH-); 2.47 (s, 3H, CH<sub>3</sub>); 2.67 (t, 2 x 2H, J = 6.32 Hz, N-CH<sub>2</sub>-CH<sub>2</sub>-N); 2.85 (t, 2H, J = 6.24 Hz, N-CH<sub>2</sub>-CH<sub>2</sub>); 3.45 (d, 2H, J = 6.38 Hz, CH-CH<sub>2</sub>); 3.58 (t, 2 x 2H, J = 6.31 Hz, N-CH<sub>2</sub>-CH<sub>2</sub>-N); 3.71 (s, 3H, CH<sub>3</sub>OCO); 3.86 (t, 2H, J = 6.24 Hz, Cl-CH<sub>2</sub>); 4.02 (s, 3H, CH<sub>3</sub>O-); 4.36 (q, 1H, J = 5.18 Hz, CH<sub>3</sub>-CH-); 5.03 (t, 1H, J = 6.38 Hz, CH-CH<sub>2</sub>); 7.28-7.79 (m, 6H, Ar) [ppm].  <sup>13</sup>C NMR (176 MHz, CDCl<sub>3</sub>): δ 17.8, 21.3, 30.5, 41.2, 44.0, 47.8, 51.8, 52.3, 53.0, 127.5, 129.7, 128.8, 135.1, 162.2, 163.4, 171.7, 172.5, 172.9 [ppm].            HRMS: 651.5463, ([M+H]<sup>+</sup>, C<sub>27</sub>H<sub>37</sub>CIN<sub>9</sub>O<sub>6</sub>S<sup>+</sup>; calc. 651.1494).</p>

## 4.2. Antimicrobial activity

The antimicrobial activity of all the compounds was tested *in vitro* on pathogenic bacteria, yeast, and filamentous fungi by using the microbroth dilution method and compared with 11 s-triazine derivatives (Table 2) described by Frączyk et al. [80], and also antibacterial (Streptomycin) and antifungal (Ketoconazole and Nystatin) drugs. Generally, the compounds were more effective against *Candida albicans* than other filamentous fungi and bacteria. The anticandidal activity of the compounds were found more successful with a lower dose than the tested standard antifungal antibiotics (250 µg/ml). Many of these antifungals have an important limitation to their spectrum of activity, pharmacokinetics, drug-drug interactions and unusual toxicities associated with long-term use [90, 91]. For these reasons, the compounds that we have synthesized and examined as new antibiotic candidates are very promising.

Table 2. Structures of s-triazine derivatives presented by Frączyk et al.

Structure	Compound	R	Structure
	<b>5a</b>	C <sub>6</sub> H <sub>5</sub>	
	<b>5b</b>	4-CH <sub>3</sub> (C <sub>6</sub> H <sub>4</sub> )	
	<b>6a</b>	C <sub>6</sub> H <sub>5</sub>	
	<b>6b</b>	4-CH <sub>3</sub> (C <sub>6</sub> H <sub>4</sub> )	
	<b>6c</b>	CH <sub>2</sub> C <sub>6</sub> H <sub>5</sub>	
	<b>6d</b>	n-C <sub>4</sub> H <sub>9</sub>	
	<b>6e</b>	morpholine	
	<b>6f</b>	piperidine	
	<b>7a</b>	AlaOMe	
	<b>7b</b>	PheOMe	
	<b>7c</b>	SerOMe	

In addition to the high anticandidal effects at a low dose, another important finding of our study is that the studied compounds show a broad-spectrum antimicrobial effect. Although some compounds required higher doses than standard antibiotics, compounds **4c**, **4d** and **7b** exhibited the highest inhibitory activity on both bacteria and yeasts such as *S. aureus*, *B. subtilis*, *M. luteus* and *C. albicans* with MIC values between 7.81 – 62.5 µg/ml. Especially **7b** and **4d** showed antibacterial activity while using a lower dose in *M. luteus* than standard antibiotics (31.25 µg/ml) (Tables 3).

Table 3. Antibacterial and antifungal activities of compounds (µg/ml)

Compound	Antibacterial activities				Antifungal activities				
	A	B	C	D	E	F	G	H	I
<b>4a</b>	250	<b>500</b>	250	250	250	250	500	250	250
<b>4b</b>	250	250	250	250	250	250	500	250	125
<b>4c</b>	125	125	<b>62.5</b>	<b>62.5</b>	250	250	500	250	<b>62.5</b>
<b>4d</b>	125	<b>62.5</b>	<b>31.25</b>	<b>15.62</b>	250	250	500	250	<b>15.62</b>
<b>4e</b>	250	250	250	250	250	250	500	250	250
<b>4f</b>	250	500	500	250	250	500	250	250	125
<b>4g</b>	250	500	250	250	250	250	500	250	250
<b>4h</b>	250	500	500	250	500	250	250	250	250
<b>5a</b>	250	250	250	125	250	250	500	250	250
<b>5b</b>	250	250	125	<b>62.5</b>	250	250	500	250	<b>125</b>
<b>6a</b>	250	250	250	250	250	250	500	250	250
<b>6b</b>	250	250	250	125	250	250	250	250	<b>125</b>
<b>6c</b>	250	250	250	250	250	250	250	250	250
<b>6d</b>	250	125	125	125	250	250	500	250	<b>125</b>
<b>6e</b>	500	500	500	500	250	250	250	250	500
<b>6f</b>	250	250	250	125	250	250	500	250	<b>125</b>
<b>7a</b>	500	500	250	250	250	250	500	250	250
<b>7b</b>	500	<b>62.5</b>	<b>31.25</b>	<b>7.81</b>	250	250	500	250	<b>7.81</b>
<b>7c</b>	250	250	250	250	250	250	500	250	250
<b>Streptomycin</b>	15.625	31.25	7.81	31.25	-	-	-	-	-
<b>Ketoconazole</b>	-	-	-	-	62.5	15.62	62.52	31.25	250
<b>Nystatin</b>	-	-	-	-	3.90	3.90	3.90	1.95	250

A: *E. coli* (ATCC-25922), B: *S. aureus* (NRRL B-767), C: *B. subtilis* (NRS-744), D: *M. luteus* (NRRL B-4375), E: *A. fumigatus* (NRRL 163), F: *A. flavus* (NRRL 980), G: *F. solani* (NRRL 13414), H: *P. citrinum* (NRRL 1841), I: *C. albicans* (ATCC 90028)

Although compounds **5a** and **5b** showed poor antimicrobial activity, the main MIC values of these compounds were found to be 62.5 - 250 µg/ml for bacteria and 250 – 500 µg/ml for filamentous fungi. **5b** exhibited anticandidal activity at a lower dose than standard antibiotics for *C. albicans* with a MIC value of 125 µg/ml (Tables 3).

Similarly, we found compound group **6** to be antimicrobial at concentrations between 125-500 µg/ml, but **6b**, **6d**, and **6f** showed anticandidal activity at a lower dose than ketoconazole and Nystatin at 125 µg/ml MIC (Tables 3).

Synthetic derivatives from **4c-4d** and **7a-7c** proved themselves to be more active against Gram-positive bacteria than Gram-negative. Compound **7b** was the most active (highly effective) against Gram-positive bacilli, especially against *M. luteus* with an MIC value of 7.81, when the MIC of Streptomycin is 31.25 µg/ml. Derivatives **4c** and **4d** had similar activity to **7b** against *S. aureus* and *B. subtilis*, but it was not more active than Streptomycin. Compounds **4a**, **4b**, **4e**, **4f**, **4g** and **4h** antibacterial and antifungal activity were reached in concentration 125 – 500 µg/ml range.

Compounds **5a-5g** showed an antifungal activity of average value 250 µg/ml. *C. albicans* turned out to be the most susceptible to compounds **5b** (7.81 µg/ml), **5e** (15.62 µg/ml) and **5g** (62.5 µg/ml).

DNA gyrases were an extremely useful research strategy for the potential antimicrobial drugs [34]. Ciprofloxacin blocked activity of *S. aureus* DNA and *E. coli* gyrases [92]. Figure 1 and Figure 2 shows the results of electrophoresis analysis of the examined substances after staining with ethidium bromide. (Figure 1) demonstrates that at concentration of 100 and 300 nM all of the s-triazine analogs (**4c**, **4a**, **4d**, **4e**, **7b**, **6f**, **7b** and **6c**) have visible effect on the ability of *S. aureus* DNA gyrase to transform supercoiled kDNA into several topological forms of relaxed kDNA. In turn, substances **4c**, **4d** and **7b** (100 nM) and **4a**, **4d**, **4e**, **6f** and **6c** (300 nM) inhibited *E. coli* gyrase action on supercoiled kDNA (Figure 2). Interesting is the fact, that demonstrated 1,3,5-triazine mono [4-(2-chloroethyl)piperazin-1-yl] are strong alkylating agents with the most of nucleophilic functional groups, that are typical for nucleic acids and proteins. Moreover, intensive structural modifications of compounds bearing triazine core diversified derivatives associated with anti-bacterial, anti-cancer or anti-inflammatory properties [93–95]. We observed a high potential of s-triazine derivatives containing in nitrogen mustard **6f** (piperidine), dipeptide groups: **4c** (Trp(Boc)-Ala-OMe), **4d** (Asp(OtBu)-Ala-OMe), and **7b** (Phe-OMe). Triazine analogues: **4a**, **4e** and **6c** not inhibited *E. coli* gyrase at neither concentration. The mechanism of action of tested 1,3,5-triazine derivatives needs further studies.

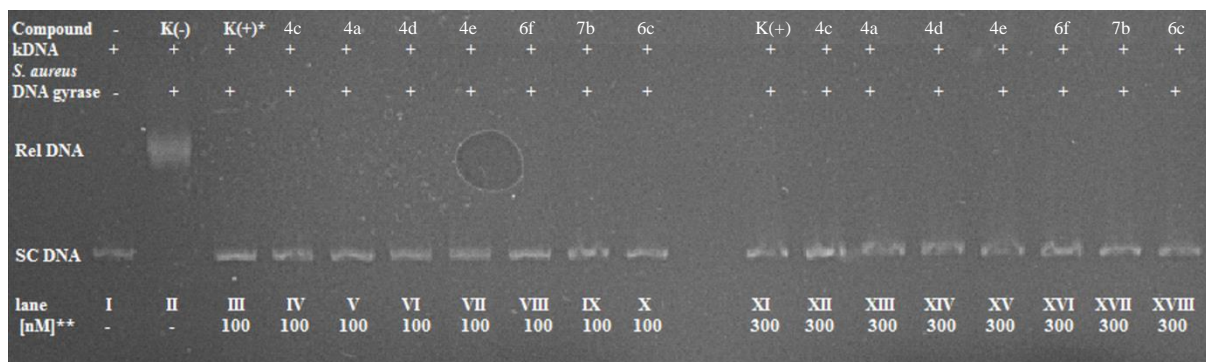


Figure 1. Effect of *S. aureus* DNA gyrase on relaxation of kDNA in the presence of compounds **4c**, **4a**, **4d**, **4e**, **7b**, **6f**, **7b** and **6c** \*(lane IV-X 100 nM; lane XII-XVIII 300 nM). Lane I: Kinetoplast DNA (kDNA). \* Lane II: K(-) Purified *S. aureus* DNA gyrase and kDNA. \*Lane III and XI: K(+) Purified *S. aureus* DNA gyrase, kDNA and ciprofloxacin (100 nM and 300nM respectively). Rel DNA (relaxed DNA); SC (supercoiled DNA).

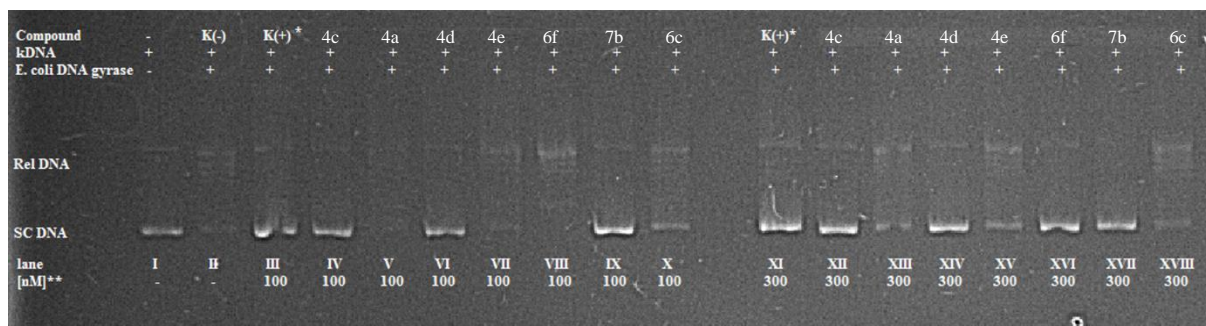


Figure 2. Effect of *E. coli* DNA gyrase on relaxation of kDNA in the presence of compounds **4c**, **4a**, **4d**, **4e**, **7b**, **6f**, **7b** and **6c** \*(lane IV-X 100 nM; lane XII-XVIII 300 nM). Lane I: Kinetoplast DNA (kDNA). \*Lane II: K(-) Purified *E. coli* DNA gyrase and kDNA. \*Lane III and XI: K(+) Purified *E. coli* gyrase, kDNA and ciprofloxacin (100 nM and 300nM respectively). Rel DNA (relaxed DNA); SC (supercoiled DNA).

We began our molecular docking studies by investigating the potential binding sites for our inhibitors. As mentioned in the methods section, we performed a scan of the whole DNA-binding/cleavage domain to look for the potential binding sites. The theoretical experiment showed, that our inhibitors do not fit into typical binding sites reported in the literature [45,48–50,58,84,96]. Instead, the binding modes from all investigated sites during the scan indicated, that the tested molecules have a strong preference for binding with DNA. It was found out, that all inhibitors show the highest affinity to the same site located at the minor groove of DNA, next to the simocyclinone binding site (Figure 3). This was the case for both *E. coli* and *S. aureus* DNA gyrase. We have also observed, that as it is with other inhibitors (Figure 3), our derivatives bind symmetrically into the suggested binding site in each GyrA subunits, showing the same binding energy and binding modes. Therefore, we only present results for one of the two identical binding sites.

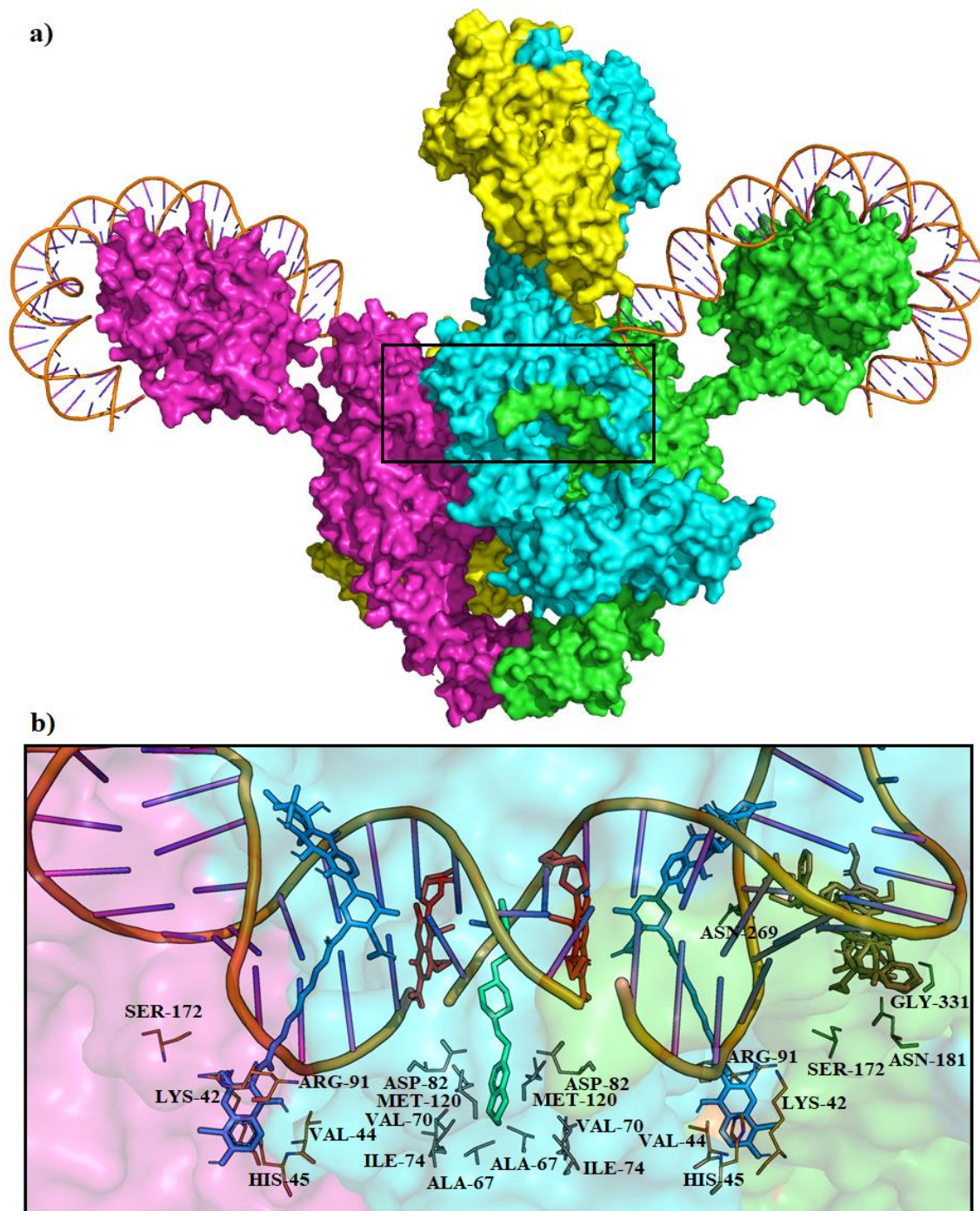


Figure 3. Structure of *E. coli* DNA gyrase bound to a DNA duplex (PDB: 6RKW). a) Surface of the protein is colored according to the subunit of the enzyme, where magenta and green are GyrA subunits, whereas blue and yellow are GyrB subunits. Potential inhibitor binding area is marked with a black rectangle. b) Close-up of the potential inhibitor binding area with DNA duplex and residues involved in binding inhibitors of DNA gyrase. Other inhibitors are presented for comparison: red – moxifloxacin (PDB: 4Z2C); blue – simocyclinone D8 (PDB: 2Y3P); and aquamarine – gepotidacin (PDB: 6RKW). Inhibitors **4c**, **4d** and **7b** are superimposed and colored brown. Residues that belong to the simocyclinone binding site are orange, residues in NBTI binding site are grey and residues involved in binding our inhibitors are green.

To fully explore the activity of our inhibitors we conducted the molecular docking study at the ATP/aminocoumarin binding site within the GyrB subunit of DNA gyrase. In case of *E. coli*, the complete enzyme structure was available (PDB: 6RKW), but for the *S. aureus* the N-terminal domain of DNA gyrase GyrB (24 kDa) was obtained from Protein Data Bank (PDB: 4URO) [90]. The grid-box with dimensions 20x20x20 Å was set at the ATP binding pocket. The resulting ATP side binding energies are: -7.8 kcal/mol for **7b**, -7.7 kcal/mol for **4d** and -7.4 kcal/mol for **4c** in case of *E. coli* and -7.3 kcal/mol for **7b**, -6.0 kcal/mol for **4d** and -7.1 kcal/mol for **4c** in case of *S. aureus*. However, they are significantly lower when compared to the binding energies at the DNA-binding/cleavage domain (Table 4). For that reason, we do not report details about the binding modes at the ATP binding site.

Table 4. Binding energies, Inhibition Constants and Ligand Efficiencies of tested ligand-enzyme complexes. Inhibition Constants and Ligand Efficiencies were calculated based on the binding energies from AutoDock Vina scoring function.

<i>E. coli</i>				
Molecule	Binding Energy [kcal/mol]	Inhibition Constant (μM)	Ligand Efficiency	
<b>7b</b>	-8.8	0.354	-0.29	
<b>4d</b>	-8.8	0.354	-0.24	
<b>4c</b>	-10.0	0.047	-0.22	
<i>S. aureus</i>				
Molecule	Binding Energy [kcal/mol]	Inhibition Constant (μM)	Ligand Efficiency	
<b>7b</b>	-9.2	0.180	-0.31	
<b>4d</b>	-8.6	0.496	-0.24	
<b>4c</b>	-10.2	0.033	-0.23	

Calculations were carried out with Blind Docking Server [86], available at: <http://bio-hpc.eu/software/blind-docking-server/> to find the binding site of our inhibitors for both bacterial DNA gyrases. This tool performs an exhaustive series of docking calculations across the whole protein surface in order to find the spots with the best binding affinities. However, only the **7b** could be used molecule for the Blind Docking calculation, since it only allows small ligands with up to 12 degrees of freedom. The results showed, that this inhibitor had the highest affinity at the same location in both enzymes as in our study (Figure 4), which further validates our assumption about this binding site. Binding energies from Blind Docking Server are: -9.3 kcal/mol for *E. coli* and -9.4 kcal/mol for *S. aureus*. These values are comparable to those in our study estimated by AutoDock Vina: - 8.8 kcal/mol for *E. coli* and -9.2 kcal/mol for *S. aureus*.

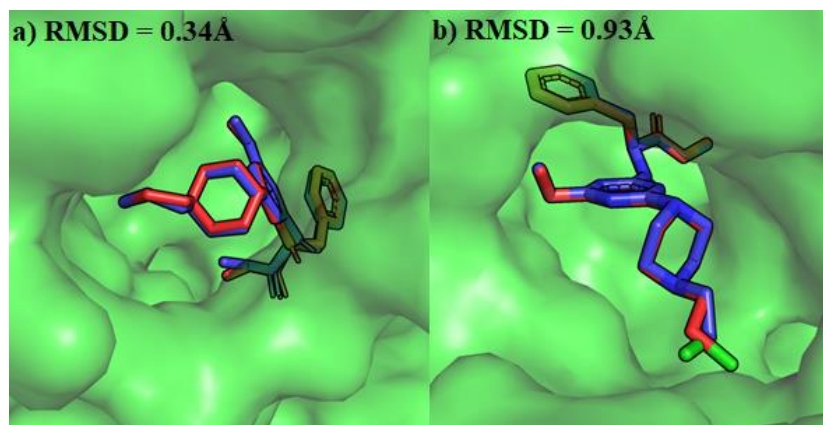


Figure 4. Superimposed binding modes of **7b** estimated by AutoDock Vina (red) and the binding modes of **7b** from Blind Docking Server (blue) within the putative binding site of a) *E. coli* (PDB: 6RKW) and b) *S. aureus* (PDB: 7MVS).

Binding energies, inhibition constants and ligand efficiencies are presented in the Table 4. It can be seen that the best binding energy in case of both *E. coli* and *S. aureus* is inhibitor **4c**. However, the value of ligand efficiency shows that the most promising derivative is **7b**, followed by **4c** and **4d**. Ligand efficiency is a value that expresses the binding energy of a compound normalized by the compound's size, and is an important property to consider when assessing the quality of binding modes. Larger compounds tend to show greater binding energy due to the larger number of interactions they form in molecular docking experiment but may not necessarily be the most efficient inhibitors [45]. As with the binding energy, the smaller the value of ligand efficiency the more affinity it shows towards the receptor. Using the BIOVIA Discovery Studio software we managed to find interactions involved in forming DNA gyrase-ligand complex. As can be seen in Figure 5, mainly hydrogen-bonds (H-bonds) were formed, although a few hydrophobic interactions as well as  $\pi$ - $\pi$  interactions were observed. In most cases our inhibitors had a tendency to bind with nucleotides in the minor-groove of DNA but interactions with residues in GyrA subunit are also present. This is to be expected since our inhibitors are analogous to the minor-groove binding agents such as netropsin or distamycin. The details of H-bonds formed between our derivatives and receptors are presented in Table 5.

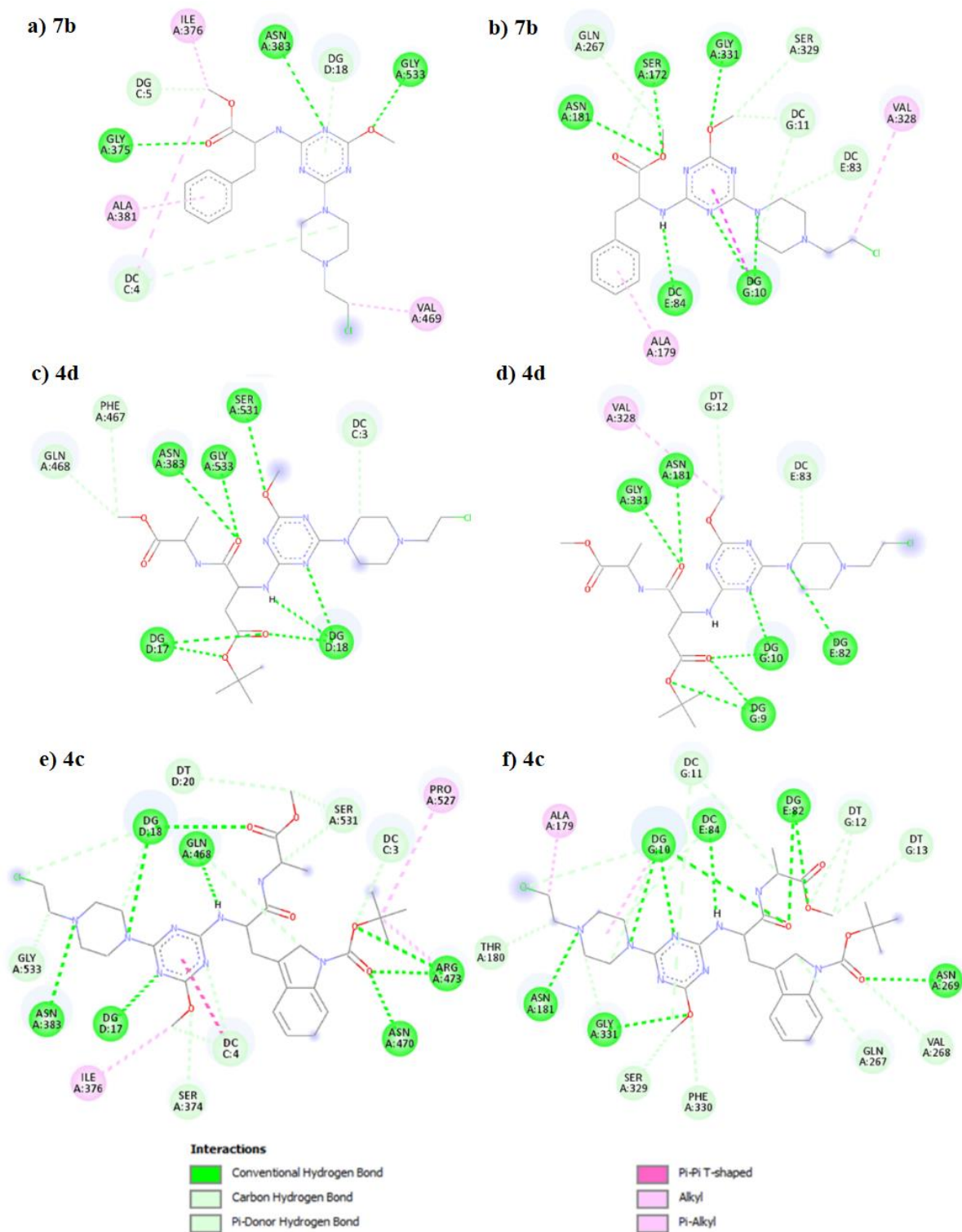


Figure 5. Interactions between inhibitors from this study and residues or nucleotides from molecular docking studies. Subfigures on the left-hand side (a), (c) and (e)) refer to ligands **7b**, **4d** and **4c** bound to the *S. aureus* DNA gyrase (PDB: 7MVS). Subfigures on the right-hand side (b), (d) and (f)) refer to ligands **7b**, **4d** and **4c** bound to the *E. coli* DNA gyrase (PDB: 6RKW).

Table 5. Residues and nucleotides involved in binding of **7b**, **4d** and **4c** with the length of H-bonds.

<i>E. coli</i>			<i>S. aureus</i>		
No.	Residue	H-Bond Length [Å]	No.	Residue	H-Bond Length [Å]
<b>7b</b>	DG10	2.33	<b>7b</b>	Gly-375	2.88
	DG10	2.73		Asn-383	2.73
	DC84	2.25		Gly-533	2.21
	Ser-172	2.68	DG17	2.33	
	Asn-181	2.77	DG17	3.07	
	Gly-331	2.41	DG18	2.52	
<b>4d</b>	DG9	2.38	<b>4d</b>	DG18	2.70
	DG9	2.34		DG18	2.72
	DG10	3.00		Asn-383	2.75
	DG10	2.42		Gly-533	2.12
	DG82	2.54		Ser-531	2.51
	Asn-181	2.46		DG17	3.01
Gly-331	2.04	DG18	2.23		
<b>4c</b>	DG10	2.63	<b>4c</b>	DG18	2.89
	DG10	2.76		Asn-383	2.78
	DG10	2.84		Gln-468	1.91
	DG82	2.62		Asn-470	2.32
	DG82	2.97		Arg-473	2.80
	DC84	2.28		Arg-473	2.90
	Asn-181	2.47			
	Asn-269	2.88			
	Gly-331	2.57			

#### 4.3. Anticancer activity.

The results of *in vitro* studies on the MCF-7 and MDA-MB-231 breast cancer cell lines showed that all s-triazine derivatives **4a-4h** exhibits antiproliferative activity. The activity was described by IC<sub>50</sub> values ranging from 118.67 to 18.99 μM and from 169.46 to 79.30 μM, respectively. These results indicate that all compounds exerted stronger inhibitory effects on MCF-7 breast cancer cell proliferation. Table 6 clearly present **4a** as the strongest anti-tumor derivative with inhibition activity equals IC<sub>50</sub> = 18.99 μM, which compared to the reference compound Chlorambucil (IC<sub>50</sub> = 29.14 μM), obtained a lower value. Table 6 and 7 presents the results of the determination of the type of MCF-7 cells treated by new compounds (reading after 24h). Compounds **4b-4h** showed similar properties. **4f** was the most effective. On the other hand, the compound **4h** required the highest molar concentration to half-decrease the population of breast cancer cells.

Table 6. The IC<sub>50</sub> of the compounds **4a-h** against MCF-7 breast cancer cells

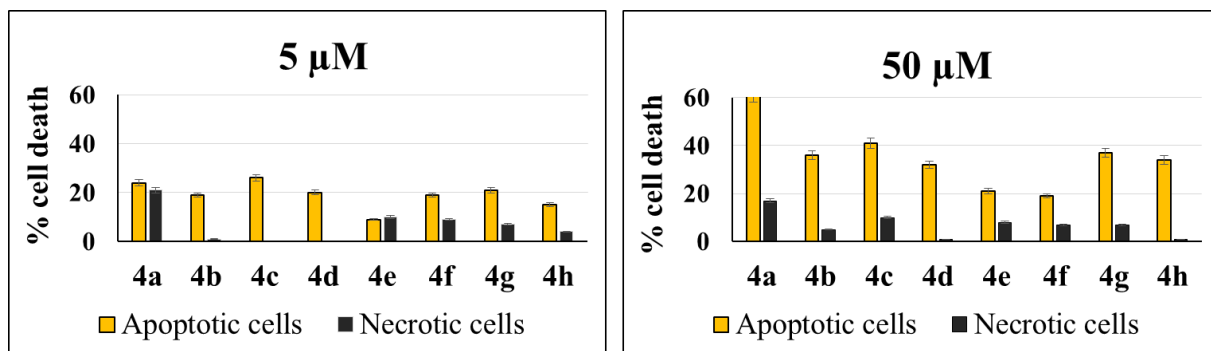
Compound	IC <sub>50</sub> [μM]	
	MCF-7	MDA-MB-231
<b>4a</b>	<b>18.99</b>	110.89
<b>4b</b>	76.29	86.20
<b>4c</b>	77.07	110.15
<b>4d</b>	79.42	79.30
<b>4e</b>	80.76	169.46
<b>4f</b>	65.62	121.86
<b>4g</b>	97.96	120.21
<b>4h</b>	118.67	149.52
<b>Chlorambucil</b>	<b>29.14<sup>a</sup></b>	<b>84.50<sup>b</sup></b>

<sup>a</sup> according to [80]. <sup>b</sup> according to [97]

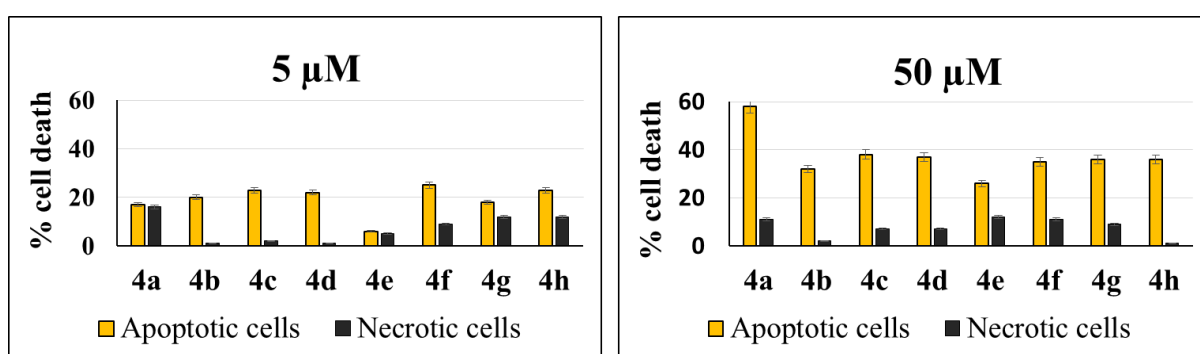
Flow cytometry analysis, based on detection of morphological changes, DNA fragmentation, DNA loss and membrane alterations, allowed us to study the effect of compounds on inducing apoptosis. It was measured by evaluating phosphatidylserine exposure to annexin V-FITC. Phosphatidylserine is translocated during the early stages of apoptosis from the inside to the outside of the plasma membrane. Therefore, it becomes visible on the cell surface, and can be recognized by macrophages [98]. After 24 h incubation of MCF-7 breast cancer cells with the compounds, phosphatidylserine exposure was very pronounced. I observed that all analyzed compounds induced concentration-dependent apoptosis (Table 7 and Scheme 16 and 17). Compounds **4a-h** induced apoptosis much more strongly than necrosis at both 5 μM and 50 μM concentrations (Scheme 18). Some of the compounds did not increase necrotic cell death.

Table 7. MCF-7 breast cancer cells treated by the compounds 4a-h (fluorescent microscopy assay/flow cytometry analysis).

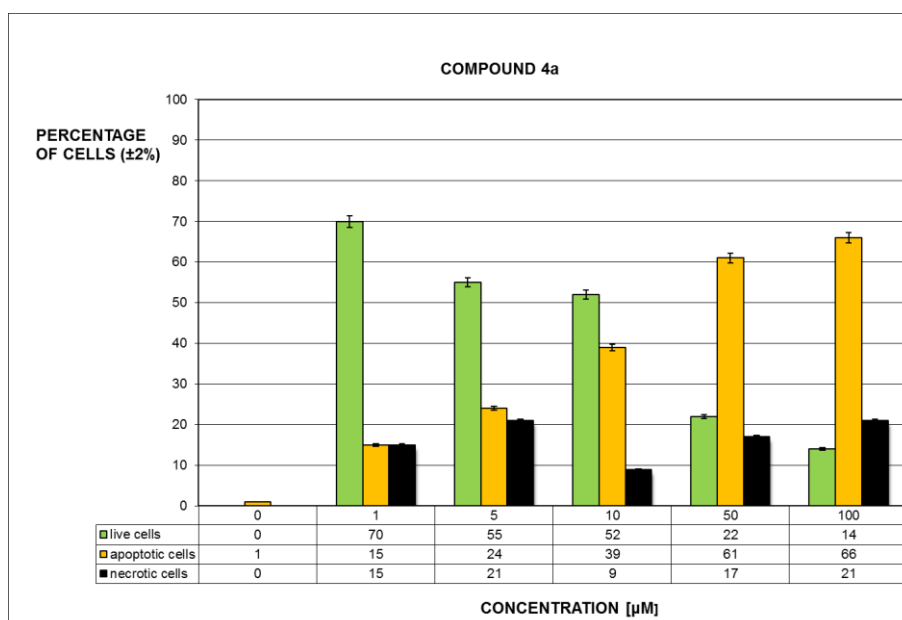
Compound		Concentration				
		1 $\mu$ M	5 $\mu$ M	10 $\mu$ M	50 $\mu$ M	100 $\mu$ M
4a	<i>Live</i>	70/76	55/67	52/48	22/31	14/21
	<i>Apoptotic</i>	15/14	24/17	39/41	61/58	66/62
	<i>Necrotic</i>	15/10	21/16	9/11	17/11	21/17
4b	<i>Live</i>	85/92	80/80	68/73	59/66	42/42
	<i>Apoptotic</i>	12/8	19/20	26/27	36/32	52/55
	<i>Necrotic</i>	3/0	1/0	6/0	5/2	6/3
4c	<i>Live</i>	82/86	74/71	65/62	49/55	48/57
	<i>Apoptotic</i>	15/14	26/24	31/36	41/39	37/41
	<i>Necrotic</i>	3/0	0/5	4/2	10/6	5/2
4d	<i>Live</i>	85/81	80/70	72/65	50/56	48/52
	<i>Apoptotic</i>	6/3	20/22	27/33	32/37	41/39
	<i>Necrotic</i>	9/16	0/8	1/2	1/7	11/9
4e	<i>Live</i>	83/84	81/79	80/78	71/62	38/38
	<i>Apoptotic</i>	10/5	9/6	12/15	21/26	51/50
	<i>Necrotic</i>	7/11	10/15	8/7	8/12	11/12
4f	<i>Live</i>	79/73	72/66	63/60	58/54	37/30
	<i>Apoptotic</i>	11/16	19/25	27/24	33/34	59/63
	<i>Necrotic</i>	10/11	9/9	10/16	9/12	4/7
4g	<i>Live</i>	83/80	72/70	70/67	56/55	53/49
	<i>Apoptotic</i>	9/11	21/18	27/28	37/37	46/50
	<i>Necrotic</i>	8/9	7/12	3/5	7/10	1/1
4h	<i>Live</i>	85/88	81/65	70/73	65/63	56/51
	<i>Apoptotic</i>	10/8	15/23	23/25	34/36	41/44
	<i>Necrotic</i>	5/4	4/12	7/2	1/1	3/5



Scheme 16. Morphological evaluation of apoptosis in MCF-7 cells treated for 24 h with compounds **4a-h** at 5 μM or 50 μM in an annexin V-FITC assay. Yellow columns represent annexin+/propidium iodide-cells in the apoptotic stage and the black columns annexin+/propidium iodide- cells in the necrotic stage. Mean percentages ± S.D. from three independent experiments.



Scheme 17. Evaluation of apoptosis induction in MCF-7 cells treated for 24 h with compounds **4a-h** at 5 and 50 μM in a fluorescent microscopy assay after staining with acridine orange and ethidium bromide. Mean percentage ± S.D. from three independent experiments.



Scheme 18. Dose-response graph for apoptotic and necrotic MCF-7 cells for the most active compound **4a**.

#### 4.4. Evaluation of AChE and BACE1 inhibition potency of s-triazine derivatives

s-Triazine derivatives were attempted to bind to AChE and BACE1. The activities of the investigated compounds **4a-4h** against both enzymes are presented in Table 8. The obtained IC<sub>50</sub> results were in the range of 0.051-1.44 μM (AChE), while the reference compound - donepezil obtained an IC<sub>50</sub> = 0.046 μM. On the other hand, in relation to BACE1, the chemical compounds obtained an IC<sub>50</sub> in the range of 9.00-58.09 μM, and the IC<sub>50</sub> of the reference compound - Quercetin was equal 4.89 μM. The AChE inhibitory effect of the compounds **4a**, **4d** and **4h** is evident. These derivatives contained the dipeptide groups Lys-Ala-OMe, Asp-Ala-OMe and His-Ala-OMe, exhibited IC<sub>50</sub> were 0.055; 0.065; 0.067 μM, respectively. The most active BACE1 binding structures were **4a**, **4c** (contains the Trp(Boc)-Ala-OMe group) and **4h**. IC<sub>50</sub> of the mentioned analogues, were respectively 11.09, 18.09 and 14.25 μM. The remaining derivatives showed a slightly weaker inhibitory effect. The compound **5a** containing an aniline and two 2-chloroethylpiperazine groups was synthesized in earlier investigation [80]. It showed the highest inhibitory activity against AChE (IC<sub>50</sub> = 0.051 μM) and BACE1 (IC<sub>50</sub> = 9.00 μM).

Table 8. *In vitro* inhibition of AChE and BACE1 of the target compounds.

Compounds	AChE IC <sub>50</sub> (μM) <sup>a</sup>	BACE1 IC <sub>50</sub> (μM) <sup>b</sup>
<b>4a</b>	0.055 ± 0.001	11.09 ± 2.29
<b>4b</b>	0.387 ± 0.054	58.09 ± 9.69
<b>4c</b>	0.114 ± 0.012	18.09 ± 2.69
<b>4d</b>	0.065 ± 0.002	33.82 ± 3.91
<b>4e</b>	0.789 ± 0.031	51.03 ± 7.99
<b>4f</b>	1.44 ± 0.029	52.04 ± 8.55
<b>4g</b>	0.122 ± 0.014	28.09 ± 3.69
<b>4h</b>	0.067 ± 0.003	14.25 ± 3.45
<b>5a</b>	0.051 ± 0.001	9.00 ± 0.22
<i>Donepezil</i>	0.046 ± 0.013	- <sup>c</sup>
<i>Tacrine</i>	0.274 ± 0.08	- <sup>c</sup>
<i>Quercetin</i> <sup>d</sup>	- <sup>c</sup>	4.89 ± 2.31

<sup>a</sup> AChE from electric eel; IC<sub>50</sub>, inhibitor concentration (mean ± SD of three independent experiments) resulting in 50% inhibition of AChE. <sup>b</sup> BACE1 from *equine serum*; IC<sub>50</sub>, inhibitor concentration (mean ± SD of three independent experiments) resulting in 50% inhibition of BuChE. <sup>c</sup> n.d., not determined. <sup>d</sup> Quercetin was used as a standard positive control agent.

## V. Discussion

The work carried out as part of doctoral studies included the creation of a group of chemical compounds. The research continues the subject matter conducted at the Department of Organic Chemistry of the Medical University of Bialystok, as well as at the Institute of Organic Chemistry of the Lodz University of Technology. Both research units have been cooperating for years [78–80,93,99,100]. The collected experience allowed to generate a trend that led to the formation of dipeptide derivatives based on *s*-triazine conjugated with DABCO. The synthesis of the planned compounds was to be carried out in the way of simple and high-efficiency reactions (Scheme 14). A 4-step solution synthesis was planned. In the first step, 4-(4,6-Dimethoxy-1,3,5-triazin-2-yl)-4-methylmorpholinium toluene-4-sulfonate (DMT/NMM/TsO<sup>-</sup>), a connecting compound developed by scientists from the Institute of Organic Chemistry of the Lodz University of Technology [101], was used for the coupling of two amino acids. Alanine (with a methylated carboxyl group and a free N-terminus) and a second amino acid (with an amino-blocked group using Fmoc or Boc, depending on the presence of other functional groups) were used for the condensation. This allowed to get the first main product. The following procedure involves the removal of the protecting group (Pg) and preparation of the free amino group for further reaction with DCMT. The problem of the next step arises from the presence of two reactive chlorine atoms. It does not matter which chlorine reacts with the dipeptide because DCMT is symmetrical. It is important that only one reacts. As a consequence of the substitution of two chlorines with a dipeptide in the post-reaction mixture, where the dipeptide is consumed, an unused amount of DCMT, as well as two and three substituted *s*-triazine remains. This generates theoretical complications in the purification and preparation for the third step of synthesis disubstituted *s*-triazine. However, thermodynamic control of the reaction allowed this process to be carried out with over 90% yield. Only one chlorine is susceptible to reaction at the lowered temperature. The reaction is carried out until one substrate is consumed in the equivalent mixture. The reaction state is monitored by TLC. Chlorine containing substances on the *s*-triazine ring turn red after spraying with the NBP solution and heating the plate. The last step, the reaction with DABCO, started in the ice bath. The temperature was successively increased with the consumption of substrates, until at the end of consumption of substrates, the reaction mixture was heated to 40°C. The reaction with DABCO initially led to the formation of a quaternary ammonium salt, inducing the TLC plate with DCM R<sub>f</sub> was 0. Over time, said salt started to convert to the designed end product. On the TLC, the spot disappearance (R<sub>f</sub> = 0) and the appearance of the signal were

visible in the higher ceilings depending on the dipeptides used. The yields of the last stage oscillated between 98.3-99.2%.

Compounds **4a-4h** were initially tested in three areas. At this point, it is important to note that the tests performed screen out the most active ones that can be used in further evaluation. The results from the three studies are not sufficient to define a mechanism of action. The conclusions drawn in the following paragraphs will be speculation.

Tests carried out on fungi and bacteria showed antimicrobial properties of the mentioned compounds, in particular compounds **4c** and **4d**. Studies on *E. coli* gyrase and *S. aureus* revealed the inhibitory potential for topoisomerases II. The theoretical experiment showed, that inhibitors do not fit into typical binding sites reported in the literature [45,48–50,87,102]. Instead, the binding modes from all investigated sites during the scan indicated, that the tested molecules have a strong preference for binding with DNA. It was found out, that all inhibitors show the highest affinity to the same site located at the minor groove of DNA, next to the simocyclinone binding site (Figure 3). This was the case for both *E. coli* and *S. aureus* DNA gyrase. Theoretical calculations allowed to find the active site on the enzyme topography and confirmed the inhibitory nature of the compounds. Molecular docking studies show that our inhibitors have a high affinity towards the DNA-gyrase enzyme in both *E. coli* and *S. aureus*. Therefore, we suggest a new binding site for our molecules involving residues Ser-172, Asn-181, Asn-269 and Gly-331 in case of *E. coli*, and Gly-375, Asn-383, Gln-468, Asn-470, Arg-473, Ser-531 and Gly-533 in case of *S. aureus* (Figure 5 and Table 5). However, further experimental study is required to unambiguously confirm our assumption about this binding site. Binding energies, inhibition constants and ligand efficiencies are presented in the Table 4. It can be seen that the best binding energy in case of both *E. coli* and *S. aureus* is inhibitor **4c**. However, the value of ligand efficiency shows that the most promising derivative is **7b**, followed by **4c** and **4d**. Ligand efficiency is a value that expresses the binding energy of a compound normalized by the compound's size, and is an important property to consider when assessing the quality of binding modes. Larger compounds tend to show greater binding energy due to the larger number of interactions they form in molecular docking experiment but may not necessarily be the most efficient inhibitors [45]. As with the binding energy, the lower the ligand's efficiency value, the greater its affinity towards the receptor. We can see from Table 3 and Table 4 that there is a correlation between experimental values of MIC and the ligand efficiency from theoretical calculations. This affinity is better reflected when comparing the values of ligand efficiency to take into consideration the molecule size. Theoretical and

experimental results are in great agreement and show that the most potent inhibitor in our study is **4c** and **4d**. Due to the increasing drug resistance in microorganisms, it is necessary to develop therapeutic methods based on chemotherapy and topoisomerase II is an important target. The triazine scaffold is very well suited for development and modification to obtain more active compounds overcoming the drug resistance of microbes. The obtained results suggest future studies should expand the group of tested microorganisms as prospective targets. However, it is important to improve the structure to increase antimicrobial potency.

The antitumor activity of s-triazine derivatives is an important aspect of the research of many teams, as the literature review has already proved. Breast cancer, as one of the leading causes of death among women worldwide, is an appropriate target to begin testing the anticancer activity of new derivatives.

Presented study provides new information on the cellular effects of 1,3,5-triazine nitrogen mustards with different peptide groups in MCF-7 and MDA-MB-231 human breast cancer cell lines. The current study continues to investigate the effect of the type of substituents in the triazine ring on activity against breast cancer cells. The s-triazine derivatives **4a-h** obtained by functionalization of the melamine scaffold with 2-chloroethylamino fragment attached via the piperazine ring were found to induce apoptosis at a much higher rate than necrosis. This confirms the results obtained by Frączyk et al. for compounds of groups 5, 6 and 7 (Table 2.), where the most active compounds against MCF-7 cells were derivatives bearing an arylamino group i.e. triazines substituted with phenylamine **6a** ( $IC_{50} = 12.30 \mu M$ ) and p-tolylamine **6b** ( $IC_{50} = 7.40 \mu M$ ) fragments [80].

The inhibitory effect on MCF-7 cancer cells was found to be strongly dependent on the structure of the substituents in the triazine ring. The most active compound in our study **4a**, derivative with an Lys(Boc)-Ala-OMe substituent on the ring with an  $IC_{50}$  equal to  $18.99 \mu M$ , is more active against MCF-7 cells than used as the reference Chlorambucil, with a cytotoxic activity value of  $IC_{50} = 29.14 \mu M$ . A difference was observed in activity of **4a** towards estrogen responsive and nonresponsive breast cancer cell line. However, this compound, like the others, inhibits proliferation in both cell types, that may suggest that such compounds could be potential pharmacological agents for the treatment of both hormone responsive and nonresponsive breast cancer cells.

It was confirmed that the high apoptotic index of the investigated compounds that the alkylating 2-chloroethylamine fragment would not dominate the activity profile of hybrid

triazine derivatives **4a-h**. In order to verify this hypothesis, additional experiments were performed using triazines substituted with two alkylating 2-chloroethylamine fragments. The compounds **5a** and **5b** with two alkylating moieties did not work for brain cancer cells. In the case of glioblastoma LBC3, LN-18 and LN-22 cell lines the most active was the compound with three 2-chloroethylamino fragments attached via the piperazine rings. After 24 h of incubation IC<sub>50</sub> of this compound was: 49 ± 3 μM, 60 ± 2 μM, 52 ± 3 μM for LN-18, LN-229 or LBC3 cell lines, respectively and its toxicity was due to the induction of apoptosis. Glioma LBC3, LN-18 and LN-229 cell lines were resistant to other studied compounds with one or two alkylating chains. All of these compounds of this group induced dose-dependent apoptosis and necrosis of MCF-7 cell line [78].

In an earlier study, it was found that the derivative was also the most active towards DLD-1 and HT-29 colon cancer cells, with IC<sub>50</sub> values of 13.71 μM. The IC<sub>50</sub> value was at least 2-fold lower than the values for 5-FU, for which the IC<sub>50</sub> was equal to 27.22 μM. The investigated in detail mechanism of **4a** action was determined that this triazine derivative induces apoptosis through intracellular signalling pathway attenuation [79].

My research confirms the value of triazine derivatives as potential anticancer agents. Further investigations are needed to ascertain whether the studied compounds should be considered for possible therapeutic applications.

As can be seen, the introduction of peptide fragments does not significantly improve antiproliferative activity. However, only a few amino acid combinations have been studied, and it is conceivable that further derivatives may be more active.

The mechanism of action of currently available and experimental therapeutic methods is closely related to the pathogenetic basis of Alzheimer's disease, which is amyloidosis, i.e. a neurodegenerative process in which there is an abnormal accumulation of amyloid protein in the brain as a result of the so-called amyloid cascade is based on abnormalities associated with defective fragmentation of the amyloid precursor protein (APP), an endothelial peptide made of 700 amino acids, which is one of the components of the neuron cell membrane, plays a role in axonal transport and probably shows neuroprotective and neuroprotective activity. neurotrophic. In a healthy brain, APP is split into soluble fragments by the enzyme  $\alpha$ -secretase [103]. In Alzheimer's disease, with the participation of malfunctioning enzymes,  $\beta$ - and  $\gamma$ -secretases, APP fragmentation into insoluble forms of  $\beta$ -amyloid, deposited in the form of

senile plaques. One of the currently investigated therapeutic methods is the use of monoclonal antibodies directed against  $\beta$ -amyloid, which are supposed to bind to it and facilitate the removal of plaque. Another potential point of action is the inhibition of the activity of  $\beta$ - and  $\gamma$ -secretases by the use of their inhibitors. The insoluble fragments of  $\beta$ -amyloid cause abnormal changes in tau in the form of hyperphosphorylation. The tau protein stabilizes intra-neuronal microtubules and disrupts its structure and function significantly disturbs axonal transport. Currently available pharmacotherapy for Alzheimer's disease includes acetylcholinesterase inhibitors and N-methyl-D-aspartate (NMDA) receptor antagonists. These drugs were registered over 20 years ago and the search for new therapeutic strategies is still ongoing [104,105].

The two proteins acetylcholinesterase (AChE) and beta-secretase 1 (BACE) were used to verify the potential inhibitory effect on the development of neurodegenerative diseases. All compounds showed inhibitory activity. However, they showed a higher affinity for AChE than for BACE (Table 8). As each of the molecules has an affinity for proteins, it can be said that the 2-chloroethylpiperazyl group plays the main role here. Derivative **5a** was selected for the group of tested compounds, with one group 2-chloroethylpiperazyl more. The results obtained by **5a** turned out to be better. The presence of the 2-chloroethylpiperazyl moiety reduces the polarity of the molecule (Table 9).

Table 9. Selected parameters describing the properties of potentially active molecules.

Derivatives	Polar Surface Area	ALogP	Hydrogen Acceptor Count	Hydrogen Donor Count
<b>4a</b>	160.14	3.3377	12	3
<b>4b</b>	148.11	2.3588	12	2
<b>4c</b>	153.04	5.2349	12	2
<b>4d</b>	131.04	2.9248	11	2
<b>4e</b>	121.81	2.1327	10	2
<b>4f</b>	215.54	3.3592	13	5
<b>4g</b>	137.6	3.6704	10	3
<b>4h</b>	182.14	3.2279	13	2
<b>5a</b>	63.66	4.6282	8	1

Among the compounds **4a-4h**, **4a** turned out to be the most active, and **4f** - the least active. As a result of the simulation of selected parameters (BIOVIA program) characterizing potentially active molecules, it is easy to notice that the only parameter significantly differentiating **4a-4h** and **5a** derivatives (Table 9) is the polar surface area. For derivative **5a**,

the value is less than 100, while for the other compounds **4a-4h**, the value is greater than 100. Compound **5a** also meets the assumptions of Lipinski's rule [106] that the number of hydrogen bond acceptors should not exceed ten. For compounds **4a-4h**, the determined values are ten or slightly higher. Another Lipinski's rule of not exceeding five hydrogen bond donors was met for all tested compounds. Regarding the postulate that the molecular mass should be less than 500 daltons, for most of the investigated derivatives, the molar mass was slightly higher than the assumed value. On the other hand, an octanol-water partition coefficient (AlogP) parameter, only for compound **4c**, exceeded the value of five. The derivative **4a** is definitely suitable for further research, *in silico* analysis and *in vitro* research.

## VI. Conclusion

1. The **4a-4h** derivatives were obtained with high yield and purity. The synthesis method can be used to obtain other derivatives with sufficient efficiency.
2. Nineteen 1,3,5-triazine derivatives were subjected to microbiological tests. The compounds **4c**, **4d** and **7b** showed the strongest bactericidal activity. In its structure are containing methoxyl, 2-chloroethylpiperazine and, respectively, -NH-Trp(Boc)-AlaOMe, -NH-Asp(tBu)-AlaOMe and -NH-PheOMe moieties.
3. Compounds **4c**, **4d** and **7b** showed more potent activity against fungi, but the results were weaker than bacterial ones. Aromatic substituents and aliphatic carbon chains reduced the microbial activity of the s-triazine derivative.
4. The tested compounds inhibited the bacterial gyrases of *E. coli* and *S. Aureus*. They blocked the relaxation process of DNA and stopped cell growth.
5. Molecular docking results showed a strong effect on the GyrA subunit at the site of the DNA minor groove. Incorporation of the ligand blocked the proper complexation of gyrase and DNA helix, which may result in incorrect operation of the enzyme.
6. The evaluation of anticancer properties was conducted on two cancer cell lines MCF-7 and MDA-MB-231. All the s-triazine derivative compounds **4a-4h** induced apoptosis and compounds **4a** and **4d** showed significant antiproliferative activity.
7. The potential inhibitory effect on the development of Alzheimer's disease was carried out on eight 1,3,5-triazine derivatives. All of the compounds were active against AChE and BACE1, especially compounds **4a**, **4d**, **4h**
8. Compounds **4a** (with -NH-Lys(Boc)-AlaOMe moiety) and **4d** (with -NH-Ser (Bn)-Ala-OMe moiety), as new 1,3,5-triazine derivatives of multi-target nature, are suitable for further studies, such as on healthy tissues or on animals.
9. Further development of research into the effect of the presence of a 2-chloroethylpiperazine substituent, as well as dipeptide fragments built from other amino acids, offers the prospect of obtaining derivatives with high biological activity.

## VII. Abstract

The theoretical part of the dissertation proves that among the vast number of chemical compounds, those based on the s-triazine (1,3,5-triazine) structure play an important role. In organic chemistry, the heterocyclic s-triazine ring, which is usually the core of the molecule, has found extensive use in crosslinking polymeric materials and combining the properties of various substituents. The spectrum of biological properties of s-triazine derivatives is broad and includes anti-microbial, anti-cancer, or anti-neurodegenerative activities, among others. Accepted and marketed drugs include Altretamine, Decitabine or Almitrine. However, there are many more s-triazine derivatives in the basic research phase, as well as clinical trials with promising results. Multi-target compounds are being sought as more effective therapeutic formulations. The s-triazine molecule, due to the possibility of substitution of three substituents, offers many opportunities to obtain hybrid compounds with a wide variety of activity.

The experimental part presents the synthesis and study of the biological activity of a group of 1,3,5 triazine derivatives containing a dipeptide, 2-ethylpiperazine and a methoxy group as substituents. The developed compounds were obtained in high yields, and their structures were analysed by  $^1\text{H}$  and  $^{13}\text{C}$  NMR and MS methods. The compounds were subjected to biological tests in three fields: on bacteria and fungi, on cancer cells and on proteins involved in neurodegeneration.

An *in vitro* study was conducted on pathogenic bacteria (*E. coli*, *S. Aureus*, *B. subtilis* and *M. luteus*), yeasts (*C. albicans*) and filamentous fungi (*A. fumigatus*, *A. flavus*, *F. solani*, *P. citrinum*) by microdilution in broth and compared with antibacterial (Streptomycin) and antifungal (Ketoconazole and Nystatin) antibiotics. Several s-triazine analogues have minimal inhibitory concentrations lower than the standard used. To investigate the molecular targets of the most active compounds, a bacterial gyrase inhibition assay was performed. To gain a better insight into the interactions of the most active DNA gyrase inhibitors, a molecular docking study was performed with the two gyrases *E. coli* and *S. aureus*, which confirmed the inhibitory potential of all selected compounds against *S. aureus* gyrase. On the other hand, with regard to *E. coli* gyrase, the most active were s-triazine derivatives with the -NH-Trp(Boc)-AlaOMe and -NH-Asp(OtBu)-AlaOMe groups.

The evaluation of the tumor capacity was performed on two cell lines MCF-7 and MDA-MB-231. Cells were derivatized at various concentrations (1, 5, 10, 50 and 100  $\mu\text{M}$ ) and this was related to the reference compound - Chlormabucil. The number of healthy, apoptotic

and necrotic cells was observed. Based on these data, the  $IC_{50}$  was determined. All tested compounds showed antiproliferative activity against both lines of tumor cells. The most active against MCF-7 breast cancer cells was derivative containing the Lys(Boc)AlaOMe dipeptide fragment. The derivative with the Asp(OtBu)AlaOMe group showed a lower  $IC_{50}$  value than Chlorambucil against to the MDA-MB-231 line.

The group of s-triazine derivatives was also tested for the ability to inhibit the enzymes AChE and BACE1. The study of the inhibitory potential against AChE was carried out using the Ellman colorimetric method, the BACE1 study was carried out using FRET. All derivatives showed an inhibitory effect. The derivative with the Lys(Boc)AlaOMe group showed the greatest inhibitory capacity.

The performed and presented studies confirmed that 1,3,5-triazine derivatives have great potential in the field of synthesis and biological research as new potential multifunctional agents.

## VIII. Streszczenie w języku polskim

Część teoretyczna pracy udowadnia, że wśród ogromnej ilości związków chemicznych ważną rolę odgrywają te oparte na strukturze s-triazyny (1,3,5-triazyny). W chemii organicznej heterocykliczny pierścień s-triazynowy, stanowiący zazwyczaj rdzeń cząsteczki, znalazł szerokie zastosowanie w sieciowaniu materiałów polimerowych oraz łączeniu właściwości różnych podstawników. Spektrum właściwości biologicznych pochodnych s-triazyny jest szerokie i obejmuje m.in. działanie przeciwmikrobiologiczne, przeciwnowotworowe, a także przeciweurodegeneracyjne. Do zaakceptowanych i wprowadzonych na rynek leków należą Altretamina, Decytabina czy Almitryna. Jednak pochodnych s-triazyny w fazie badań podstawowych, jak też klinicznych dających obiecujące rezultaty, jest znacznie więcej. Poszukiwane są związki wielocelowe jako skuteczniejsze preparaty lecznicze. Cząsteczka s-triazyny ze względu na możliwość podstawienia trzech podstawników daje możliwość do uzyskania hybrydowych związków o różnorodnej aktywności.

W części eksperymentalnej przedstawiono syntezę i badania aktywności biologicznej pochodnych 1,3,5-triazyny zawierających dipeptyd, 2-etylopiperazynę i grupę metoksyłową jako podstawniki. Opracowane związki chemiczne uzyskano z wysoką wydajnością, a ich struktury potwierdzono metodami  $^1\text{H}$  i  $^{13}\text{C}$  NMR oraz MS. Związki poddano badaniom biologicznym w trzech kierunkach: na bakteriach i grzybach, na komórkach nowotworowych oraz białkach biorących udział w neurodegeneracji.

Przeprowadzono badanie *in vitro* na bakteriach chorobotwórczych (*E. coli*, *S. Aureus*, *B. subtilis* i *M. luteus*), drożdżach (*C. albicans*) i grzybach strzępkowych (*A. fumigatus*, *A. flavus*, *F. solani*, *P. citrinum*) metodą mikrorozcieńczeń i porównano z antybiotykami przeciwbakteryjnymi (Streptomycyna) i przeciwgrzybiczymi (Ketokonazol i Nystatyna). Kilka analogów 1,3,5-triazyny ma minimalne stężenia hamujące niższe niż stosowany standard. W celu określenia celu molekularnego najbardziej aktywnych związków, przeprowadzono test hamowania gyrazy bakteryjnej. Aby uzyskać lepszy wgląd w interakcje najbardziej aktywnych inhibitorów, wykonano dokowanie molekularne z dwoma gyrazami *E. coli* i *S. aureus*, które potwierdziło potencjał hamujący wszystkich wybranych związków względem gyrazy *S. aureus*. Natomiast względem gyrazy *E. coli* najaktywniejsze okazały się pochodne s-triazyny z ugrupowaniem -NH-Trp(Boc)AlaOMe oraz -NH-Asp(OtBu)AlaOMe.

Ewaluacja zdolności przeciwnowotworowej przeprowadzona została na dwóch liniach komórkowych MCF-7 and MDA-MB-231. Komórki poddano działaniu pochodnych w różnych

stężeniach (1, 5, 10, 50 i 100  $\mu\text{M}$ ) i odniesiono do związku referencyjnego - Chlormabucylu. Obserwowano ilość komórek zdrowych, apoptycznych i nekrotycznych. Na podstawie tych danych wyznaczone  $\text{IC}_{50}$ . Wszystkie badane związki wykazały działanie antyproliferacyjne względem obu linii komórek nowotworowych. Szczególnie dobre wyniki względem komórek MCF-7 wykazała pochodna zawierająca dipeptyd Lys(Boc)AlaOMe. Wartość  $\text{IC}_{50}$  względem linii MDA-MB-231 niższą od Chlorambucylu wykazała pochodna z grupą Asp(OtBu)AlaOMe.

Zbadano także zdolność pochodnych 1,3,5-triazyny do hamowania enzymów AChE i BACE1. Badanie potencjału hamującego wobec acetylocholinesterazy AChE przeprowadzone zostało przy pomocy kolorymetrycznej metody Ellman'a, zaś badanie stopnia hamowania aktywności  $\beta$ -sekreazy BACE1 przeprowadzono przy użyciu metody FRET. Wszystkie pochodne wykazały działanie hamujące wobec enzymów. Największą zdolność hamującą wykazała pochodna z grupą Lys(Boc)AlaOMe.

Wykonane i przedstawione badania potwierdzają, że pochodne s-triazyny mają duży potencjał w dziedzinie syntezy i badań biologicznych nowych potencjalnych leków wielofunkcyjnych.

## IX. References

1. Drug Bank Stat [Internet]. [cited 2022 Aug 30]. Available from: <https://go.drugbank.com/stats>
2. Sharma A, Sheyi R, de la Torre BG, El-Faham A, Albericio F. s-Triazine: A Privileged Structure for Drug Discovery and Bioconjugation. *Molecules*. 2021 Feb 6;26(4):864.
3. Chen X, Du C, Guo JP, Wei XH, Liu DS. Addition reactions of bis(trimethylsilyl)methyl- and 1-allyl-lithium with cyanoamines into triazines or  $\beta$ -diketiminatolithium compounds. *J Organomet Chem*. 2002 Aug;655(1–2):89–95.
4. Shibuya I, Oishi A, Yasumoto M. Reaction of Disubstituted Cyanamides with Formamides under High Pressure. *HETEROCYCLES*. 1998;48(8):1659.
5. Arya K, Dandia A. Synthesis and cytotoxic activity of trisubstituted-1,3,5-triazines. *Bioorg Med Chem Lett*. 2007 Jun;17(12):3298–304.
6. Reddy ND, Elias AJ, Vij A. N-Dealkylation of Aliphatic Tertiary Amines and Diamines with Cyanuric Chloride: Crystal Structure of 2,4-Dichloro-6-(N-ethyl-N-isopropylamino)-s-triazine. *J Chem Res*. 1998;(9):504–5.
7. Damia G, D’Incalci M. Clinical Pharmacokinetics of Altretamine: *Clin Pharmacokinet*. 1995 Jun;28(6):439–48.
8. Yan H fa, Zou T, Tuo Q zhang, Xu S, Li H, Belaidi AA, et al. Ferroptosis: mechanisms and links with diseases. *Signal Transduct Target Ther*. 2021 Dec;6(1):49.
9. Chan J. Oral altretamine used as salvage therapy in recurrent ovarian cancer. *Gynecol Oncol*. 2004 Jan;92(1):368–71.
10. Malik IA. Altretamine is an Effective Palliative Therapy of Patients with Recurrent Epithelial Ovarian Cancer. *Jpn J Clin Oncol*. 2001 Feb 1;31(2):69–73.
11. Chen M, Suzuki A, Thakkar S, Yu K, Hu C, Tong W. DILIrank: the largest reference drug list ranked by the risk for developing drug-induced liver injury in humans. *Drug Discov Today*. 2016 Apr;21(4):648–53.
12. Thakkar S, Li T, Liu Z, Wu L, Roberts R, Tong W. Drug-induced liver injury severity and toxicity (DILiSt): binary classification of 1279 drugs by human hepatotoxicity. *Drug Discov Today*. 2020 Jan;25(1):201–8.
13. Woo JH, Shimoni Y, Yang WS, Subramaniam P, Iyer A, Nicoletti P, et al. Elucidating Compound Mechanism of Action by Network Perturbation Analysis. *Cell*. 2015 Jul;162(2):441–51.
14. Germing U, Kobbe G, Haas R, Gattermann N. Myelodysplastic syndromes: diagnosis, prognosis, and treatment. *Dtsch Arzteblatt Int*. 2013 Nov 15;110(46):783–90.
15. Deschler B, Lübbert M. Acute myeloid leukemia: Epidemiology and etiology. *Cancer*. 2006 Nov 1;107(9):2099–107.

16. Wang C. Synthesis method of decitabine for treating primary or secondary leukemia. CN106117290.
17. Daskalakis M, Blagitko-Dorfs N, Hackanson B. Decitabine. In: Martens UM, editor. *Small Molecules in Oncology* [Internet]. Berlin, Heidelberg: Springer Berlin Heidelberg; 2010 [cited 2022 Sep 28]. p. 131–57. (Recent Results in Cancer Research; vol. 184). Available from: [http://link.springer.com/10.1007/978-3-642-01222-8\\_10](http://link.springer.com/10.1007/978-3-642-01222-8_10)
18. Kantarjian HM, O'Brien S, Cortes J, Giles FJ, Faderl S, Issa JP, et al. Results of decitabine (5-aza-2'-deoxycytidine) therapy in 130 patients with chronic myelogenous leukemia. *Cancer*. 2003 Aug 1;98(3):522–8.
19. Coccolini F. Advanced gastric cancer: What we know and what we still have to learn. *World J Gastroenterol*. 2016;22(3):1139.
20. Sanford M. S-1 (Teysuno®): A Review of Its Use in Advanced Gastric Cancer in Non-Asian Populations. *Drugs*. 2013 Jun;73(8):845–55.
21. Matt P, van Zwieten-Boot B, Calvo Rojas G, Ter Hofstede H, Garcia-Carbonero R, Camarero J, et al. The European Medicines Agency review of Tegafur/Gimeracil/Oteracil (Teysuno™) for the treatment of advanced gastric cancer when given in combination with cisplatin: summary of the Scientific Assessment of the Committee for medicinal products for human use (CHMP). *The Oncologist*. 2011;16(10):1451–7.
22. Zhang G, Zhu A, Liu D. Synthesis method of oteracil potassium. CN110655493A.
23. López-López JR, Pérez-García MT, Canet E, Gonzalez C. Effects of Almitrine Bismesylate on the Ionic Currents of Chemoreceptor Cells from the Carotid Body. *Mol Pharmacol*. 1998 Feb 1;53(2):330–9.
24. Markos F, Champion DP, Carey M, O'Connor JJ. An Investigation into the Mechanism of Action of Almitrine on Isolated Rat Diaphragm Muscle Fatigue. *Respiration*. 2002;69(4):339–43.
25. Wilke A, Siegmund W, Schneider T, Wiersbitzky M, Franke G. Pharmacokinetics of almitrine in healthy volunteers and patients with essential hypertension. *Biomed Biochim Acta*. 1991;50(2):183–7.
26. European Medicines Agency. Oral almitrine to be withdrawn by EU Member States [Internet]. 2013 [cited 2022 Sep 28]. Available from: <https://www.ema.europa.eu/en/news/oral-almitrine-be-withdrawn-eu-member-states>
27. Barthélémy R, Blot PL, Tiepolo A, Le Gall A, Mayeur C, Gaugain S, et al. Efficacy of Almitrine in the Treatment of Hypoxemia in Sars-Cov-2 Acute Respiratory Distress Syndrome. *Chest*. 2020 Nov;158(5):2003–6.
28. Bendjelid K, Giraud R, Von Düring S. Treating hypoxemic COVID-19 “ARDS” patients with almitrine: The earlier the better? *Anaesth Crit Care Pain Med*. 2020 Aug;39(4):451–2.

29. Dhainaut A, Regnier G, Atassi G, Pierre A, Leonce S, Kraus-Berthier L, et al. New triazine derivatives as potent modulators of multidrug resistance. *J Med Chem.* 1992 Jun;35(13):2481–96.
30. Kong D, Yamori T. ZSTK474 is an ATP-competitive inhibitor of class I phosphatidylinositol 3 kinase isoforms. *Cancer Sci.* 2007 Oct;98(10):1638–42.
31. Liu F, Wu X, Jiang X, Qian Y, Gao J. Prolonged inhibition of class I PI3K promotes liver cancer stem cell expansion by augmenting SGK3/GSK-3 $\beta$ / $\beta$ -catenin signalling. *J Exp Clin Cancer Res.* 2018 Dec;37(1):122.
32. Namatame N, Tamaki N, Yoshizawa Y, Okamura M, Nishimura Y, Yamazaki K, et al. Antitumor profile of the PI3K inhibitor ZSTK474 in human sarcoma cell lines. *Oncotarget.* 2018 Oct 12;9(80):35141–61.
33. Sugita K, Baba M, T. A. Salim M, Okamoto M, Aoyama H, Hashimoto Y, et al. Synthesis and Anti-Hepatitis C Virus Activity of Morpholino Triazine Derivatives. *HETEROCYCLES.* 2010;81(6):1419.
34. Rewcastle GW, Gamage SA, Flanagan JU, Frederick R, Denny WA, Baguley BC, et al. Synthesis and Biological Evaluation of Novel Analogues of the Pan Class I Phosphatidylinositol 3-Kinase (PI3K) Inhibitor 2-(Difluoromethyl)-1-[4,6-di(4-morpholinyl)-1,3,5-triazin-2-yl]-1 *H* -benzimidazole (ZSTK474). *J Med Chem.* 2011 Oct 27;54(20):7105–26.
35. Cascioferro S, Parrino B, Spanò V, Carbone A, Montalbano A, Barraja P, et al. 1,3,5-Triazines: A promising scaffold for anticancer drugs development. *Eur J Med Chem.* 2017 Dec;142:523–49.
36. Park S, Ahn Y, Kim Y, Roh EJ, Lee Y, Han C, et al. Design, Synthesis and Biological Evaluation of 1,3,5-Triazine Derivatives Targeting hA1 and hA3 Adenosine Receptor. *Molecules.* 2022 Jun 22;27(13):4016.
37. Hashem HE, Amr AEGE, Nossier ES, Anwar MM, Azmy EM. New Benzimidazole-, 1,2,4-Triazole-, and 1,3,5-Triazine-Based Derivatives as Potential EGFR<sup>WT</sup> and EGFR<sup>T790M</sup> Inhibitors: Microwave-Assisted Synthesis, Anticancer Evaluation, and Molecular Docking Study. *ACS Omega.* 2022 Mar 1;7(8):7155–71.
38. Ng HL, Ma X, Chew EH, Chui WK. Design, Synthesis, and Biological Evaluation of Coupled Bioactive Scaffolds as Potential Anticancer Agents for Dual Targeting of Dihydrofolate Reductase and Thioredoxin Reductase. *J Med Chem.* 2017 Mar 9;60(5):1734–45.
39. Maliszewski D, Drozdowska D. Recent Advances in the Biological Activity of s-Triazine Core Compounds. *Pharmaceuticals.* 2022 Feb 12;15(2):221.
40. World Health Organization. 2019 antibacterial agents in clinical development: an analysis of the antibacterial clinical development pipeline [Internet]. Geneva: World Health Organization; 2019 [cited 2022 Sep 25]. Available from: <https://apps.who.int/iris/handle/10665/330420>

41. Srinivasan B, Tonddast-Navaei S, Skolnick J. Ligand binding studies, preliminary structure–activity relationship and detailed mechanistic characterization of 1-phenyl-6,6-dimethyl-1,3,5-triazine-2,4-diamine derivatives as inhibitors of *Escherichia coli* dihydrofolate reductase. *Eur J Med Chem.* 2015 Oct;103:600–14.
42. Collin F, Karkare S, Maxwell A. Exploiting bacterial DNA gyrase as a drug target: current state and perspectives. *Appl Microbiol Biotechnol.* 2011 Nov;92(3):479–97.
43. World Health Organization. Global priority list of antibiotic-resistant bacteria to guide research, discovery, and development of new antibiotics. 2017 [cited 2021 Nov 3]; Available from: [www.who.int/medicines/publications/WHO-PPL-Short\\_Summary\\_25Feb-ET\\_NM\\_WHO.pdf](http://www.who.int/medicines/publications/WHO-PPL-Short_Summary_25Feb-ET_NM_WHO.pdf)
44. World Health Organization. Global antimicrobial resistance and use surveillance system (GLASS) report: 2021 [Internet]. Geneva: World Health Organization; 2021 [cited 2022 Sep 25]. Available from: <https://apps.who.int/iris/handle/10665/341666>
45. Edwards MJ, Flatman RH, Mitchenall LA, Stevenson CEM, Le TBK, Clarke TA, et al. A Crystal Structure of the Bifunctional Antibiotic Simocyclinone D8, Bound to DNA Gyrase. *Science.* 2009 Dec 4;326(5958):1415–8.
46. Lewis RJ, Singh OM, Smith CV, Skarzynski T, Maxwell A, Wonacott AJ, et al. The nature of inhibition of DNA gyrase by the coumarins and the cyclothialidines revealed by X-ray crystallography. *EMBO J.* 1996 Mar 15;15(6):1412–20.
47. Flatman RH, Howells AJ, Heide L, Fiedler HP, Maxwell A. Simocyclinone D8, an Inhibitor of DNA Gyrase with a Novel Mode of Action. *Antimicrob Agents Chemother.* 2005 Mar;49(3):1093–100.
48. Laponogov I, Sohi MK, Veselkov DA, Pan XS, Sawhney R, Thompson AW, et al. Structural insight into the quinolone–DNA cleavage complex of type IIA topoisomerases. *Nat Struct Mol Biol.* 2009 Jun;16(6):667–9.
49. Vanden Broeck A, Lotz C, Ortiz J, Lamour V. Cryo-EM structure of the complete *E. coli* DNA gyrase nucleoprotein complex. *Nat Commun.* 2019 Dec;10(1):4935.
50. Kolarič A, Germe T, Hrast M, Stevenson CEM, Lawson DM, Burton NP, et al. Potent DNA gyrase inhibitors bind asymmetrically to their target using symmetrical bifurcated halogen bonds. *Nat Commun.* 2021 Dec;12(1):150.
51. Masih A, Shrivastava JK, Bhat HR, Singh UP. Potent antibacterial activity of dihydropyrimidine-1,3,5-triazines via inhibition of DNA gyrase and antifungal activity with favourable metabolic profile. *Chem Biol Drug Des.* 2020 Aug;96(2):861–9.
52. Younis MH, Mohammed ER, Mohamed AR, Abdel-Aziz MM, Georgey HH, Abdel Gawad NM. Design, synthesis and anti-*Mycobacterium tuberculosis* evaluation of new thiazolidin-4-one and thiazolo[3,2-a][1,3,5]triazine derivatives. *Bioorganic Chem.* 2022 Jul;124:105807.
53. Patil V, Noonikara-Poyil A, Joshi SD, Patil SA, Patil SA, Lewis AM, et al. Synthesis, molecular docking studies, and in vitro evaluation of 1,3,5-triazine derivatives as promising antimicrobial agents. *J Mol Struct.* 2020 Nov;1220:128687.

54. Mekheimer RA, Abuo-Rahma GEDA, Abd-Elmonem M, Yahia R, Hisham M, Hayallah AM, et al. New s-Triazine/Tetrazole conjugates as potent antifungal and antibacterial agents: Design, molecular docking and mechanistic study. *J Mol Struct.* 2022 Nov;1267:133615.
55. Patel RV, Kumari P, Rajani DP, Chikhaliya KH. Synthesis and studies of novel 2-(4-cyano-3-trifluoromethylphenyl amino)-4-(quinoline-4-yloxy)-6-(piperazinyl/piperidinyl)-s-triazines as potential antimicrobial, antimycobacterial and anticancer agents. *Eur J Med Chem.* 2011 Sep;46(9):4354–65.
56. Gahtori P, Das A, Mishra R. Design, synthesis and antibacterial activity of substituted phenylthiazolyl s-triazines. *Pharm Chem J.* 2011 Aug 5;1.
57. Desai NC, Makwana AH, Senta RD. Synthesis, characterization and antimicrobial activity of some novel 4-(4-(arylamino)-6-(piperidin-1-yl)-1,3,5-triazine-2-ylamino)-N-(pyrimidin-2-yl)benzenesulfonamides. *J Saudi Chem Soc.* 2016 Nov;20(6):686–94.
58. Liu H, Long S, Rakesh KP, Zha GF. Structure-activity relationships (SAR) of triazine derivatives: Promising antimicrobial agents. *Eur J Med Chem.* 2020 Jan;185:111804.
59. Wu WL, Wen ZY, Qian JJ, Zou JP, Liu SM, Yang S, et al. Design, synthesis, characterization and evaluation of 1,3,5-triazine-benzimidazole hybrids as multifunctional acetylcholinesterases inhibitors. *J Mol Struct.* 2022 Jun;1257:132498.
60. Masih A, Singh S, Agnihotri AK, Giri S, Shrivastava JK, Pandey N, et al. Design and development of 1,3,5-triazine-thiadiazole hybrids as potent adenosine A2A receptor (A2AR) antagonist for benefit in Parkinson's disease. *Neurosci Lett.* 2020 Sep;735:135222.
61. Lolak N, Akocak S, Türkeş C, Taslimi P, Işık M, Beydemir Ş, et al. Synthesis, characterization, inhibition effects, and molecular docking studies as acetylcholinesterase,  $\alpha$ -glycosidase, and carbonic anhydrase inhibitors of novel benzenesulfonamides incorporating 1,3,5-triazine structural motifs. *Bioorganic Chem.* 2020 Jul;100:103897.
62. Lolak N, Tuneğ M, Doğan A, Boğa M, Akocak S. Synthesis and biological evaluation of 1,3,5-triazine-substituted ureido benzenesulfonamides as antioxidant, acetylcholinesterase and butyrylcholinesterase inhibitors. *Bioorganic Med Chem Rep.* 2020 Dec 12;3(2):22–31.
63. Lolak N, Boga M, Tuneğ M, Karakoc G, Akocak S, Supuran CT. Sulphonamides incorporating 1,3,5-triazine structural motifs show antioxidant, acetylcholinesterase, butyrylcholinesterase, and tyrosinase inhibitory profile. *J Enzyme Inhib Med Chem.* 2020 Jan 1;35(1):424–31.
64. Gonzalez P, Pota K, Turan LS, da Costa VCP, Akkaraju G, Green KN. Synthesis, Characterization, and Activity of a Triazine Bridged Antioxidant Small Molecule. *ACS Chem Neurosci.* 2017 Nov 15;8(11):2414–23.
65. Maqbool M, Manral A, Jameel E, Kumar J, Saini V, Shandilya A, et al. Development of cyanopyridine–triazine hybrids as lead multitarget anti-Alzheimer agents. *Bioorg Med Chem.* 2016 Jun;24(12):2777–88.

66. Baréa P, Barbosa VA, Yamazaki DA dos S, Gomes CMB, Novello CR, Costa WF da, et al. Anticholinesterase activity of  $\beta$ -carboline-1,3,5-triazine hybrids. *Braz J Pharm Sci.* 2022;58:e19958.
67. Yazdani M, Edraki N, Badri R, Khoshneviszadeh M, Iraj A, Firuzi O. Multi-target inhibitors against Alzheimer disease derived from 3-hydrazinyl 1,2,4-triazine scaffold containing pendant phenoxy methyl-1,2,3-triazole: Design, synthesis and biological evaluation. *Bioorganic Chem.* 2019 Mar;84:363–71.
68. Prati F, De Simone A, Bisignano P, Armirotti A, Summa M, Pizzirani D, et al. Multitarget Drug Discovery for Alzheimer's Disease: Triazinones as BACE-1 and GSK-3 $\beta$  Inhibitors. *Angew Chem Int Ed.* 2015 Jan 26;54(5):1578–82.
69. Ramsay RR, Popovic-Nikolic MR, Nikolic K, Uliassi E, Bolognesi ML. A perspective on multi-target drug discovery and design for complex diseases. *Clin Transl Med [Internet].* 2018 Dec [cited 2022 Sep 29];7(1). Available from: <https://onlinelibrary.wiley.com/doi/abs/10.1186/s40169-017-0181-2>
70. Zhang G, Guo D, Dash PK, Araínga M, Wiederin JL, Haverland NA, et al. The mixed lineage kinase-3 inhibitor URMC-099 improves therapeutic outcomes for long-acting antiretroviral therapy. *Nanomedicine Nanotechnol Biol Med.* 2016 Jan;12(1):109–22.
71. Miller-Rhodes P, Kong C, Baht GS, Saminathan P, Rodriguiz RM, Wetsel WC, et al. The broad spectrum mixed-lineage kinase 3 inhibitor URMC-099 prevents acute microgliosis and cognitive decline in a mouse model of perioperative neurocognitive disorders. *J Neuroinflammation.* 2019 Dec;16(1):193.
72. Miller-Rhodes P, Li H, Velagapudi R, Chiang W, Terrando N, Gelbard HA. URMC-099 prophylaxis prevents hippocampal vascular vulnerability and synaptic damage in an orthopedic model of delirium superimposed on dementia. *FASEB J [Internet].* 2022 Jun [cited 2022 Sep 30];36(6). Available from: <https://onlinelibrary.wiley.com/doi/10.1096/fj.202200184RR>
73. How J, Yee K. ENMD-2076 for hematological malignancies. *Expert Opin Investig Drugs.* 2012 May;21(5):717–32.
74. Matulonis UA, Lee J, Lasonde B, Tew WP, Yehwalashet A, Matei D, et al. ENMD-2076, an oral inhibitor of angiogenic and proliferation kinases, has activity in recurrent, platinum resistant ovarian cancer. *Eur J Cancer.* 2013 Jan;49(1):121–31.
75. Drug Bank Drugs [Internet]. [cited 2022 Aug 30]. Available from: <https://go.drugbank.com/drugs/>
76. Mounnissamy VM, Priya B. Triazine Derivatives and its Pharmacological Potential - A Review. *Int J Pharm Sci Rev Res.* 62(1):143–7.
77. Majeed Ganai A, Khan Pathan T, Hampannavar GA, Pawar C, Obakachi VA, Kushwaha B, et al. Recent Advances on the s-Triazine Scaffold with Emphasis on Synthesis, Structure-Activity and Pharmacological Aspects: A Concise Review. *ChemistrySelect.* 2021 Feb 17;6(7):1616–60.

78. Krętowski R, Drozdowska D, Kolesińska B, Kamiński Z, Frączyk J, Cechowska-Pasko M. The cellular effects of novel triazine nitrogen mustards in glioblastoma LBC3, LN-18 and LN-229 cell lines. *Invest New Drugs*. 2019 Oct;37(5):984–93.
79. Wróbel A, Kolesińska B, Frączyk J, Kamiński ZJ, Tankiewicz-Kwedlo A, Hermanowicz J, et al. Synthesis and cellular effects of novel 1,3,5-triazine derivatives in DLD and Ht-29 human colon cancer cell lines. *Invest New Drugs*. 2020 Aug;38(4):990–1002.
80. Fraczyk J, Kolesinska B, Swiontek M, Lipinski W, Drozdowska D, Jerzy Kaminski Z. Synthesis of Arylamino-1,3,5-triazines Functionalized with Alkylatin 2-chloroethylamine Fragments and Studies of their Cytotoxicity on the Breast Cancer MCF-7 Cell Line. *Anticancer Agents Med Chem*. 2016 Oct 3;16(11):1435–44.
81. Patel JB, et al. M07-A10: Methods for Dilution Antimicrobial Susceptibility Tests for Bacteria That Grow Aerobically; Approved Standard. 10th Ed. CLSI 2015;35.
82. Pfaller MA, National Committee for Clinical Laboratory Standards. Reference method for broth dilution antifungal susceptibility testing of yeasts; Approved Standard - Second Edition. Wayne, Pa.: National Committee for Clinical Laboratory Standards; 2002.
83. Margerrison EE, Hopewell R, Fisher LM. Nucleotide sequence of the *Staphylococcus aureus* gyrB-gyrA locus encoding the DNA gyrase A and B proteins. *J Bacteriol*. 1992 Mar;174(5):1596–603.
84. Lu Y, Vibhute S, Li L, Okumu A, Ratigan SC, Nolan S, et al. Optimization of TopoIV Potency, ADMET Properties, and hERG Inhibition of 5-Amino-1,3-dioxane-Linked Novel Bacterial Topoisomerase Inhibitors: Identification of a Lead with *In Vivo* Efficacy against MRSA. *J Med Chem*. 2021 Oct 28;64(20):15214–49.
85. Trott O, Olson AJ. AutoDock Vina: Improving the speed and accuracy of docking with a new scoring function, efficient optimization, and multithreading. *J Comput Chem*. 2009;NA-NA.
86. Sánchez-Linares I, Pérez-Sánchez H, Cecilia JM, García JM. High-Throughput parallel blind Virtual Screening using BINDSURF. *BMC Bioinformatics*. 2012 Sep;13(S14):S13.
87. Hopkins AL, Groom CR, Alex A. Ligand efficiency: a useful metric for lead selection. *Drug Discov Today*. 2004 May;9(10):430–1.
88. Ellman GL, Courtney KD, Andres V, Featherstone RM. A new and rapid colorimetric determination of acetylcholinesterase activity. *Biochem Pharmacol*. 1961 Jul;7(2):88–95.
89.  $\beta$ -Secretase (BACE1) Activity Detection Kit (Fluorescent) [Internet]. [cited 2021 Mar 24]. Available from: <https://www.sigmaaldrich.com/content/dam/sigmaaldrich/docs/Sigma/Bulletin/cs0010bul.pdf>
90. Chen SCA, Sorrell TC. Antifungal agents. *Med J Aust*. 2007 Oct;187(7):404–9.
91. Lewis RE. Current Concepts in Antifungal Pharmacology. *Mayo Clin Proc*. 2011 Aug;86(8):805–17.

92. Castro W, Navarro M, Biot C. Medicinal potential of ciprofloxacin and its derivatives. *Future Med Chem.* 2013 Jan;5(1):81–96.
93. Kolesińska B, Drozdowska D, Kamiński ZJ. The new analogues of nitrogen mustard with one, two or three 2-chloroethylamino fragments. Reactions with nucleophiles. *Acta Pol Pharm.* 2008 Dec;65(6):709–14.
94. Pomarnacka E, Bednarski P, Grunert R, Reszka P. Synthesis and anticancer activity of novel 2-amino-4-(4-phenylpiperazino)-1,3,5-triazine derivatives. *Acta Pol Pharm.* 2004 Dec;61(6):461–6.
95. Raval JP, Rai AR, Patel HV, Patel PS. Synthesis and in vitro antimicrobial activity of N<sup>2</sup>-(4-(aryloamino)-6-(pirydyln-2-yloamino)-1,3,5,-triazyn-2-yl)benzo-hydrazide. *Int J ChemTech Res.* 2009;1(3):616–20.
96. Gibson EG, Bax B, Chan PF, Osheroff N. Mechanistic and Structural Basis for the Actions of the Antibacterial Gepotidacin against *Staphylococcus aureus* Gyrase. *ACS Infect Dis.* 2019 Apr 12;5(4):570–81.
97. Ma ZY, Wang DB, Song XQ, Wu YG, Chen Q, Zhao CL, et al. Chlorambucil-conjugated platinum(IV) prodrugs to treat triple-negative breast cancer in vitro and in vivo. *Eur J Med Chem.* 2018 Sep;157:1292–9.
98. Martin SJ, Reutelingsperger CP, McGahon AJ, Rader JA, van Schie RC, LaFace DM, et al. Early redistribution of plasma membrane phosphatidylserine is a general feature of apoptosis regardless of the initiating stimulus: inhibition by overexpression of Bcl-2 and Abl. *J Exp Med.* 1995 Nov 1;182(5):1545–56.
99. Maliszewski D, Wróbel A, Kolesińska B, Fraczyk J, Drozdowska D. 1,3,5-Triazine Nitrogen Mustards with Different Peptide Group as Innovative Candidates for AChE and BACE1 Inhibitors. *Molecules.* 2021 Jun 28;26(13):3942.
100. Kolesinska B, Barszcz K, Kaminski ZJ, Drozdowska D, Wietrzyk J, Switalska M. Synthesis and cytotoxicity studies of bifunctional hybrids of nitrogen mustards with potential enzymes inhibitors based on melamine framework. *J Enzyme Inhib Med Chem.* 2012 Oct 1;27(5):619–27.
101. Fraczyk J, Kaminski ZJ, Katarzynska J, Kolesinska B. 4-(4,6-Dimethoxy-1,3,5-triazin-2-yl)-4-methylmorpholinium Toluene-4-sulfonate (DMT/NMM/TsO<sup>-</sup>) Universal Coupling Reagent for Synthesis in Solution. *Helv Chim Acta.* 2018 Jan;101(1):e1700187.
102. Liu H, Long S, Rakesh KP, Zha GF. Structure-activity relationships (SAR) of triazine derivatives: Promising antimicrobial agents. *Eur J Med Chem.* 2020 Jan;185:111804.
103. Yankner BA, Lu T. Amyloid  $\beta$ -Protein Toxicity and the Pathogenesis of Alzheimer Disease. *J Biol Chem.* 2009 Feb;284(8):4755–9.
104. Miller G. Stopping Alzheimer's Before It Starts. *Science.* 2012 Aug 17;337(6096):790–2.
105. Birks JS. Cholinesterase inhibitors for Alzheimer's disease. *Cochrane Dementia and Cognitive Improvement Group, editor. Cochrane Database Syst Rev [Internet].* 2006 Jan

25 [cited 2022 Oct 6];2016(3). Available from:  
<http://doi.wiley.com/10.1002/14651858.CD005593>

106. Lipinski CA, Lombardo F, Dominy BW, Feeney PJ. Experimental and computational approaches to estimate solubility and permeability in drug discovery and development settings 1PII of original article: S0169-409X(96)00423-1. The article was originally published in *Advanced Drug Delivery Reviews* 23 (1997) 3–25. 1. *Adv Drug Deliv Rev.* 2001 Mar;46(1–3):3–26.

## X. List of Figures

Figure 1. Effect of *S. aureus* DNA gyrase on relaxation of kDNA in the presence of compounds **4c**, **4a**, **4d**, **4e**, **7b**, **6f**, **7b** and **6c** \*\* (lane IV-X 100 nM; lane XII-XVIII 300 nM). Lane I: Kinetoplast DNA (kDNA). \* Lane II: K(-) Purified *S. aureus* DNA gyrase and kDNA. \* Lane III and XI: K(+) Purified *S. aureus* DNA gyrase, kDNA and ciprofloxacin (100 nM and 300nM respectively). Rel DNA (relaxed DNA); SC (supercoiled DNA).

Figure 2. Effect of *E. coli* DNA gyrase on relaxation of kDNA in the presence of compounds **4c**, **4a**, **4d**, **4e**, **7b**, **6f**, **7b** and **6c** \*\* (lane IV-X 100 nM; lane XII-XVIII 300 nM). Lane I: Kinetoplast DNA (kDNA). \* Lane II: K(-) Purified *E.coli* DNA gyrase and kDNA. \* Lane III and XI: K(+) Purified *E.coli* gyrase, kDNA and ciprofloxacin (100 nM and 300nM respectively). Rel DNA (relaxed DNA); SC (supercoiled DNA).

Figure 3. Structure of *E. coli* DNA gyrase bound to a DNA duplex (PDB: 6RKW). a) Surface of the protein is colored according to the subunit of the enzyme, where magenta and green are GyrA subunits, whereas blue and yellow are GyrB subunits. Potential inhibitor binding area is marked with a black rectangle. b) Close-up of the potential inhibitor binding area with DNA duplex and residues involved in binding inhibitors of DNA gyrase. Other inhibitors are presented for comparison: red – moxifloxacin (PDB: 4Z2C); blue – simocyclinone D8 (PDB: 2Y3P); and aquamarine – gepotidacin (PDB: 6RKW). Inhibitors **4c**, **4d** and **7b** are superimposed and colored brown. Residues that belong to the simocyclinone binding site are orange, residues in NBTI binding site are grey and residues involved in binding our inhibitors are green.

Figure 4. Superimposed binding modes of **7b** estimated by AutoDock Vina (red) and the binding modes of **7b** from Blind Docking Server (blue) within the putative binding site of a) *E. coli* (PDB: 6RKW) and b) *S. aureus* (PDB: 7MVS).

Figure 5. Interactions between inhibitors from this study and residues or nucleotides from molecular docking studies. Subfigures on the left-hand side (a), c) and e)) refer to ligands **7b**, **4d** and **4c** bound to the *S. aureus* DNA gyrase (PDB: 7MVS). Subfigures on the right-hand side (b), d) and f)) refer to ligands **7b**, **4d** and **4c** bound to the *E. coli* DNA gyrase (PDB: 6RKW).

## XI. List of Schemes

Scheme 1. Three stages of nucleophilic substitution of TCT.

Scheme 2. Structure of Altretamine.

Scheme 3. Structure of Decitabine.

Scheme 4. Structure of Oteracil.

Scheme 5. Structure of Almitrine.

Scheme 6. Structure of ZSTK474.

Scheme 7. Anticancer s-triazine derivatives **1** and **2**.

Scheme 8. Anticancer 4,6-diamino-1,2-dihydro-s-triazine s-triazine derivatives **3** and **4**.

Scheme 9. Antibacterial s-triazine derivatives **5** and **6**.

Scheme 10. Antimicrobial s-triazine derivatives **7-14**.

Scheme 11. Antineurodegenerative s-triazine derivatives **15 -21**.

Scheme 12. Antineurodegenerative s-triazine derivatives **22** and **23**.

Scheme 13. Structure-activity relationship of three substituted s-triazine.

Scheme 14. Total synthesis pathway of 2-dipeptide-[4-(2-chloroethyl)piperin-1-yl]-6methoxy-s-triazine derivatives.

Scheme 15. Structures of s-triazine derivatives **4a-4h**.

Scheme 16. Morphological evaluation of apoptosis in MCF-7 cells treated for 24 h with compounds **4a-h** at 5  $\mu$ M or 50  $\mu$ M in an annexin V-FITC assay. Yellow columns represent annexin+/propidium iodide- cells in the apoptotic stage and the black columns annexin+/propidium iodide- cells in the necrotic stage. Mean percentages  $\pm$  S.D. from three independent experiments.

Scheme 17. Evaluation of apoptosis induction in MCF-7 cells treated for 24 h with compounds **4a-h** at 5 and 50  $\mu$ M in a fluorescent microscopy assay after staining with acridine orange and ethidium bromide. Mean percentage  $\pm$  S.D. from three independent experiments.

Scheme 18. Dose-response graph for apoptotic and necrotic MCF-7 cells for the most active compound **4a**.

## XII. List of Tables

Table 1. Characterization of s-triazine derivatives.

Table 2. Structures of s-triazine derivatives presented by Frączyk et al.

Table 3. Antibacterial and antifungal activities of compounds ( $\mu\text{g/ml}$ ).

Table 4. Binding energies, Inhibition Constants and Ligand Efficiencies of tested ligand-enzyme complexes. Inhibition Constants and Ligand Efficiencies were calculated based on the binding energies from AutoDock Vina scoring function.

Table 5. Residues and nucleotides involved in binding of **7b**, **4d** and **4c** with the length of H-bonds.

Table 6. The  $\text{IC}_{50}$  of the compounds **4a-h** against MCF-7 breast cancer cells.

Table 7. MCF-7 breast cancer cells treated by the compounds **4a-h** (fluorescent microscopy assay/flow cytometry analysis).

Table 8. *In vitro* inhibition of AChE and BACE1 of the target compounds.

Table 9. Selected parameters describing the properties of potentially active molecules.

**XIII. Annex 1**

**Review article**

**Recent Advances in the Biological Activity  
of s-Triazine Core Compounds**

**Dawid Maliszewski and Danuta Drozdowska**



Review

# Recent Advances in the Biological Activity of s-Triazine Core Compounds

Dawid Maliszewski \* and Danuta Drozdowska \*

Department of Organic Chemistry, Medical University of Białystok, 15-222 Białystok, Poland

\* Correspondence: dawid.maliszewski@umb.edu.pl (D.M.); danuta.drozdowska@umb.edu.pl (D.D.)

**Abstract:** An effective strategy for successful chemotherapy relies on creating compounds with high selectivity against cancer cells compared to normal cells and relatively low cytotoxicity. One such approach is the discovery of critical points in cancer cells, i.e., where specific enzymes that are potential therapeutic targets are generated. Triazine is a six-membered heterocyclic ring compound with three nitrogen replacing carbon-hydrogen units in the benzene ring structure. The subject of this review is the symmetrical 1,3,5-triazine, known as s-triazine. 1,3,5-triazine is one of the oldest heterocyclic compounds available. Because of its low cost and high availability, it has attracted researcher attention for novel synthesis. s-Triazine has a weak base, it has much weaker resonance energy than benzene, therefore, nucleophilic substitution is preferred to electrophilic substitution. Heterocyclic bearing a symmetrical s-triazine core represents an interesting class of compounds possessing a wide spectrum of biological properties such as anti-cancer, antiviral, fungicidal, insecticidal, bactericidal, herbicidal and antimicrobial, antimalarial agents. They also have applications as dyes, lubricants, and analytical reagents. Hence, the group of 1,3,5-triazine derivatives has developed over the years. Triazine is not only the core amongst them, but is also a factor increasing the kinetic potential of the entire derivatives. Modifying the structure and introducing new substituents makes it possible to obtain compounds with broad inhibitory activity on processes such as proliferation. In some cases, s-triazine derivatives induce cell apoptosis. In this review we will present currently investigated 1,3,5-triazine derivatives with anti-cancer activities, with particular emphasis on their inhibition of enzymes involved in the process of tumorigenesis.

**Keywords:** 1,3,5-triazine; s-triazine; anticancer; enzyme inhibitory activity

**Citation:** Maliszewski, D.; Drozdowska, D. Recent Advances in the Biological Activity of s-Triazine Core Compounds. *Pharmaceuticals* **2022**, *15*, 221. <https://doi.org/10.3390/ph15020221>

Academic Editor: Paweł Kafarski

Received: 5 January 2022

Accepted: 10 February 2022

Published: 12 February 2022

**Publisher's Note:** MDPI stays neutral with regard to jurisdictional claims in published maps and institutional affiliations.



**Copyright:** © 2022 by the authors. Licensee MDPI, Basel, Switzerland. This article is an open access article distributed under the terms and conditions of the Creative Commons Attribution (CC BY) license (<https://creativecommons.org/licenses/by/4.0/>).

## 1. Introduction

As far as we know, tumors are the most serious cause of death in the world. Cancers with the highest mortality rates in 2018 were lung cancer (2.1 million new cases and 1.8 million deaths), breast cancer (million new cases and 880 thousand deaths), prostate cancer (1.3 million new cases and 360 thousand deaths), and stomach cancer (1 million new cases and 783 thousand deaths) [1].

The fight against cancer has consumed huge amounts of money to find the cure with little effect. Nevertheless, it cannot be defined as a failure. As Napoleon Hill said, “every adversity, every failure, every heartache carries with it the seed of an equal or greater benefit”. Following this thought, we would like to highlight two aspects of the fight against cancer. First, decades of research lead to more and more precise descriptions of the mechanisms taking place in cancer cells, it is possible to determine the most effective aim in targeted therapies. Second and equally important, the development of small molecules. The development of more active, selective and less cytotoxic drugs is due to designing chemical compounds based on a structure-activity relationship (SAR) [2]. In this search, the leading linker is 1,3,5-triazine, a symmetrical heterocyclic aromatic ring enabling the expansion of the structure in a multi-vector manner. Decades of research have revealed a

wide range of properties of s-triazine derivatives. In this review we will present currently investigated 1,3,5-triazine derivatives with anti-cancer activities.

This review presents the current state of knowledge on 1,3,5-triazine derivatives, their structures and anticancer activity, as well as their ability to inhibit different enzymes or their DNA-binding potential. This data could be helpful in the development of new drugs and therapeutic methods. By analysing the presented approach, a series of compounds with high potency and low toxicity can be designed, synthesized, characterized and evaluated for desired pharmacological activity. The collected data are presented in summary Table 1.

**Table 1.** Promising effects of 1,3,5-triazine derivatives on cell lines and/or enzymes. N/A; not available.

No.	Cancer Cells/Effects	Targets/Effects	Reference Substance	Ref.
1	N/A	DNA topoisomerase II $\alpha$ (IC <sub>50</sub> = 57.6 $\mu$ M)	Etoposide: DNA topoisomerase II $\alpha$ (IC <sub>50</sub> = 59.2 $\mu$ M)	[3]
2	A549 (IC <sub>50</sub> = 0.20 $\mu$ M) MCF-7 (IC <sub>50</sub> = 1.25 $\mu$ M) Hela (IC <sub>50</sub> = 1.03 $\mu$ M)	PI3K $\alpha$ (IC <sub>50</sub> = 7.0 nM) mTOR (IC <sub>50</sub> = 48 nM)	GDC-0941: A549 (IC <sub>50</sub> = 1.21 $\mu$ M), MCF-7 (IC <sub>50</sub> = 1.47 $\mu$ M), Hela (IC <sub>50</sub> = 3.72 $\mu$ M), PI3K $\alpha$ (IC <sub>50</sub> = 6.0 nM), mTOR (IC <sub>50</sub> = 525 nM); PI-103: PI3K $\alpha$ (IC <sub>50</sub> = 5.1 nM), mTOR (IC <sub>50</sub> = 21 nM)	[4]
3	MDA-MB321 (IC <sub>50</sub> = 15.83 $\mu$ M) MCF-7 (IC <sub>50</sub> = 16.32 $\mu$ M) Hela (IC <sub>50</sub> = 2.21 $\mu$ M) HepG2 (IC <sub>50</sub> = 12.21 $\mu$ M)	mTOR (IC <sub>50</sub> = 8.45 nM) PI3K $\alpha$ (IC <sub>50</sub> = 3.41 nM)	Gedatolisib: mTOR (IC <sub>50</sub> = 2.5 nM) PI3K $\alpha$ (IC <sub>50</sub> = 6.04 nM)	[5]
7	leukemia (GI <sub>50</sub> = 1.96 $\mu$ M) colon cancer (GI <sub>50</sub> = 2.60 $\mu$ M) CNS (GI <sub>50</sub> = 2.72 $\mu$ M) melanoma (GI <sub>50</sub> = 1.91 $\mu$ M) ovarian (GI <sub>50</sub> = 4.01 $\mu$ M) renal (GI <sub>50</sub> = 3.03 $\mu$ M) prostate (GI <sub>50</sub> = 4.40 $\mu$ M) breast (GI <sub>50</sub> = 2.04 $\mu$ M)	hDHFR (IC <sub>50</sub> = 0.002 $\mu$ M)	Triazine-Benzimidazole: leukemia (GI <sub>50</sub> = 3.71 $\mu$ M) colon cancer (GI <sub>50</sub> = 2.76 $\mu$ M) CNS (GI <sub>50</sub> = 1.86 $\mu$ M) melanoma (GI <sub>50</sub> = 2.70 $\mu$ M) ovarian (GI <sub>50</sub> = 2.41 $\mu$ M) renal (GI <sub>50</sub> = 1.89 $\mu$ M) prostate (GI <sub>50</sub> = 2.75 $\mu$ M) breast (GI <sub>50</sub> = 2.58 $\mu$ M) MTX: hDHFR (IC <sub>50</sub> = 0.02 $\mu$ M)	[6]
8	HCT116 (IC <sub>50</sub> = 0.88 $\mu$ M) A549 (IC <sub>50</sub> = 0.07 $\mu$ M) HL-60 (IC <sub>50</sub> = 0.33 $\mu$ M)	hDHFR (IC <sub>50</sub> = 0.00746 $\mu$ M)		
9	HCT116 (IC <sub>50</sub> = 1.61 $\mu$ M) A549 (IC <sub>50</sub> = 0.5 $\mu$ M) HL-60 (IC <sub>50</sub> = 0.87 $\mu$ M)	hDHFR (IC <sub>50</sub> = 0.00372 $\mu$ M)		
10	HCT116 (IC <sub>50</sub> = 0.02 $\mu$ M) A549 (IC <sub>50</sub> = 0.74 $\mu$ M) HL-60 (IC <sub>50</sub> = 0.35 $\mu$ M) HepG2 (IC <sub>50</sub> = 1.4 $\mu$ M) MDA-MB-234 (IC <sub>50</sub> = 0.44 $\mu$ M)	hDHFR (IC <sub>50</sub> = 0.00646 $\mu$ M)	MTX: HCT116 (IC <sub>50</sub> = 0.75 $\mu$ M) A549 (IC <sub>50</sub> = 0.25 $\mu$ M) HL-60 (IC <sub>50</sub> = 1.09 $\mu$ M) HepG2 (IC <sub>50</sub> = 0.41 $\mu$ M) MDA-MB-234 (IC <sub>50</sub> = 9.49 $\mu$ M) hDHFR (IC <sub>50</sub> = 0.00667 $\mu$ M)	[7]
11	HCT116 (IC <sub>50</sub> = 0.001 $\mu$ M) A549 (IC <sub>50</sub> = 0.21 $\mu$ M) HL-60 (IC <sub>50</sub> = 0.33 $\mu$ M) HepG2 (IC <sub>50</sub> = 1.38 $\mu$ M) MDA-MB-234 (IC <sub>50</sub> = 0.06 $\mu$ M)	hDHFR (IC <sub>50</sub> = 0.00408 $\mu$ M)		
12	HCT116 (GI <sub>50</sub> = 0.026 $\mu$ M) MCF-7 (GI <sub>50</sub> = 0.08 $\mu$ M)	hDHFR (IC <sub>50</sub> = 0.0061 $\mu$ M) rat TrxR (IC <sub>50</sub> = 4.6 $\mu$ M)	MTX: hDHFR (IC <sub>50</sub> = 0.0079 $\mu$ M)	[8]
13	HCT116 (GI <sub>50</sub> = 0.116 $\mu$ M) MCF-8 (GI <sub>50</sub> = 0.127 $\mu$ M)	hDHFR (IC <sub>50</sub> = 0.0026 $\mu$ M) rat TrxR (IC <sub>50</sub> = 5.9 $\mu$ M)	HCT116 (GI <sub>50</sub> = 0.015 $\mu$ M) MCF-8 (GI <sub>50</sub> = 0.024 $\mu$ M)	

Table 1. Cont.

No.	Cancer Cells/Effects	Targets/Effects	Reference Substance	Ref.
14	HeLa (IC <sub>50</sub> = 16 μM) HaCaT (IC <sub>50</sub> = 61 μM)	hCAI (K <sub>i</sub> = 733.3 nM) hCAII (K <sub>i</sub> = 160.8 nM) hCAIX (K <sub>i</sub> = 41.1 nM) hCAXII (K <sub>i</sub> = 77.6 nM)	AAZ: hCAI (K <sub>i</sub> = 250 nM) hCAII (K <sub>i</sub> = 12.1 nM) hCAIX (K <sub>i</sub> = 25.8 nM) hCAXII (K <sub>i</sub> = 5.7 nM)	[9]
15	N/A	hCAI (K <sub>i</sub> = 16.7 nM) hCAII (K <sub>i</sub> = 7.4 nM) hCAIX (K <sub>i</sub> = 0.4 nM)	MZA: hCAI (K <sub>i</sub> = 780 nM) hCAII (K <sub>i</sub> = 14 nM) hCAIX (K <sub>i</sub> = 27 nM)	[10]
16	N/A	hCAI (K <sub>i</sub> = 2679.1 nM) hCAII (K <sub>i</sub> = 380.5 nM) hCAIX (K <sub>i</sub> = 27.0 nM)	hCAXII (K <sub>i</sub> = 3.4 nM) EZA: hCAI (K <sub>i</sub> = 25 nM)	
17	N/A	hCAI (K <sub>i</sub> = 394.9 nM) hCAII (K <sub>i</sub> = 3.1 nM) hCAIX (K <sub>i</sub> = 0.91 nM)	hCAII (K <sub>i</sub> = 8 nM) hCAIX (K <sub>i</sub> = 34 nM) hCAXII (K <sub>i</sub> = 22 nM)	[11]
18	N/A	hCAI (K <sub>i</sub> = 441.7 nM) hCAII (K <sub>i</sub> = 152.9 nM) hCAIX (K <sub>i</sub> = 14.6 nM) hCAXII (K <sub>i</sub> = 44.4 nM)	DCP: hCAI (K <sub>i</sub> = 1200 nM) hCAII (K <sub>i</sub> = 38 nM) hCAIX (K <sub>i</sub> = 50 nM) hCAXII (K <sub>i</sub> = 50 nM)	[12]
19	HeLa (IC <sub>50</sub> = 39.7 μM) MCF-7 (IC <sub>50</sub> = 41.5 μM) HL-60 (IC <sub>50</sub> = 23.1 μM) HepG2 (IC <sub>50</sub> = 31.2 μM)	EGFR-TK (Inhibition rate = 94.3%; C = 10 μM)	Cisplatin: HeLa (IC <sub>50</sub> = 32.5 μM) MCF-7 (IC <sub>50</sub> = 24.4 μM) HL-60 (IC <sub>50</sub> = 12.3 μM) HepG2 (IC <sub>50</sub> = 25.9 μM) Erlotinib: EGFR-TK (Inhibition rate = 100%; C = 10 μM);	[13]
20	N/A	EGFR-TK (IC <sub>50</sub> = 2.54 μM)	Dacomitinib: EGFR-TK (IC <sub>50</sub> = 0.06 μM)	[14]
21	HeLa (IC <sub>50</sub> = 44.5 μM) MCF-7 (IC <sub>50</sub> = 52.2 μM) HL-60 (IC <sub>50</sub> = 40.3 μM) HepG2 (IC <sub>50</sub> = 56.4 μM)	EGFR-TK (Inhibition rate = 96.3%; C = 10 μM)	Cisplatin: HeLa (IC <sub>50</sub> = 31.3 μM) MCF-7 (IC <sub>50</sub> = 22.5 μM) HL-60 (IC <sub>50</sub> = 14.3 μM) HepG2 (IC <sub>50</sub> = 26.4 μM)	[15]
22	HeLa (IC <sub>50</sub> = 32.4 μM) MCF-7 (IC <sub>50</sub> = 32.3 μM) HL-60 (IC <sub>50</sub> = 26.3 μM) HepG2 (IC <sub>50</sub> = 45.3 μM)	EGFR-TK (Inhibition rate = 90.5%; C = 10 μM)	Erlotinib: EGFR-TK (Inhibition rate = 100%; C = 10 μM)	
26	U-87MG (IC <sub>50</sub> = 0.42 μM) HCT-116 (IC <sub>50</sub> = 0.13 μM) MDA-MB-231 (IC <sub>50</sub> = 0.14 μM) PC-3 (IC <sub>50</sub> = 0.63 μM)	FAK (IC <sub>50</sub> = 50 nM)	TAE-226: U-87MG (IC <sub>50</sub> = 0.19 μM) HCT-116 (IC <sub>50</sub> = 0.23 μM) MDA-MB-231 (IC <sub>50</sub> = 1.9 μM) PC-3 (IC <sub>50</sub> = 0.26 μM) FAK (IC <sub>50</sub> = 7 nM)	[16]

Table 1. Cont.

No.	Cancer Cells/Effects	Targets/Effects	Reference Substance	Ref.
27	HT-29 (IC <sub>50</sub> = 9.5 μM) H1299 (IC <sub>50</sub> = 11 μM) A549 (IC <sub>50</sub> = 14.6 μM) MDA-MB-231 (IC <sub>50</sub> = 2.5 μM) OV90 (IC <sub>50</sub> = 8 μM) A2780 (IC <sub>50</sub> = 7.1 μM) MCF-7 (IC <sub>50</sub> = 6 μM)			
28	HT-29 (IC <sub>50</sub> = 5.8 μM) H1299 (IC <sub>50</sub> = 5 μM) A549 (IC <sub>50</sub> = 10.8 μM) MDA-MB-231 (IC <sub>50</sub> = 4.2 μM) OV90 (IC <sub>50</sub> = 12 μM) A2750 (IC <sub>50</sub> = 6.3 μM) MCF-7 (IC <sub>50</sub> = 7.2 μM)	Rad6 ubiquitin conjugating enzyme (nd)	TZ9: HT-29 (IC <sub>50</sub> = 8.3 μM) H1299 (IC <sub>50</sub> = 45 μM) A549 (IC <sub>50</sub> = 7.2 μM) MDA-MB-231 (IC <sub>50</sub> = 4.6 μM) OV90 (IC <sub>50</sub> = 60 μM) A2780 (IC <sub>50</sub> = 7.8 μM) MCF-7 (IC <sub>50</sub> = 5 μM)	[17]
29	HT-29 (IC <sub>50</sub> = 5.2 μM) H1299 (IC <sub>50</sub> = 22 μM) A549 (IC <sub>50</sub> = 11.6 μM) MDA-MB-231 (IC <sub>50</sub> = 3.5 μM) OV90 (IC <sub>50</sub> = 5 μM) A2750 (IC <sub>50</sub> = 3.6 μM) MCF-7 (IC <sub>50</sub> = 4.2 μM)			
30	MCF-7 (IC <sub>50</sub> = 2.95 μg/mL) HepG2 (IC <sub>50</sub> = 3.7 μg/mL)	N/A	Doxorubicin: MCF-7 (IC <sub>50</sub> = 2.98 μg/mL) HepG2 (IC <sub>50</sub> = 3.82 μg/mL)	[18]
31	MCF-7 (IC <sub>50</sub> = 4.8 μM) MDA-MB-231 (IC <sub>50</sub> = 48.3 μM) HT-29 (IC <sub>50</sub> = 9.8 μM) HGC-27 (IC <sub>50</sub> = 15.1 μM)	N/A	ZSTK474: MDA-MB-231 (IC <sub>50</sub> = 10.8 μM) HT-29 (IC <sub>50</sub> = 25.1 μM) HGC-27 (IC <sub>50</sub> = 1.11 μM)	[19]
32	MCF7 (IC <sub>50</sub> = 5 μM) MDA-MB-231 (IC <sub>50</sub> = 15 μM) HepG2 (IC <sub>50</sub> = 21.1 μM) LoVo (IC <sub>50</sub> = 8.4 μM) K-562 (IC <sub>50</sub> = 5.9 μM)	Arrest cell proliferation in S and G2/M phase. None lethal for zebrafish embryos.	N/A	[20]
33	MCF7 (IC <sub>50</sub> = 7.5 μM) MDA-MB-231 (IC <sub>50</sub> = 14 μM) HepG2 (IC <sub>50</sub> = 17.5 μM) LoVo (IC <sub>50</sub> = 6.1 μM) K-562 (IC <sub>50</sub> = 9.8 μM)			
34	MCF-7 (IC <sub>50</sub> = 0.82 μM) MDA-MB-231 (IC <sub>50</sub> = 9.36 μM) HCT-116 (IC <sub>50</sub> = 17.89 μM)	Arrest of MCF-7 cells in the G2/M stage(36.8%). Mortality response of zebrafish embryos—na.	Tamoxifen: MCF-7 (IC <sub>50</sub> = 5.12 μM) MDA-MB-231 (IC <sub>50</sub> = 15.01 μM) HCT-116 (IC <sub>50</sub> = 26.41 μM)	[21]
35	MG-MID (GI <sub>50</sub> = 2.68 μM; TGI = 11 μM; LC <sub>50</sub> = 32.3 μM)	BSA (distance in complex = 7.9 nm)		
36	MG-MID (GI <sub>50</sub> = 1.38 μM; TGI = 3.15 μM; LC <sub>50</sub> = 8.63 μM)	BSA (distance in complex = 6.61 nm)	N/A	[22]
37	MG-MID (GI <sub>50</sub> = 2.37 μM; TGI = 7.16 μM; LC <sub>50</sub> = 7.88 μM)	BSA (distance in complex = 7.62 nm)		
38	MG-MID (GI <sub>50</sub> = 0.72 μM; TGI = 1.8 μM; LC <sub>50</sub> = 4.88 μM)	BSA (distance in complex = 7.98 nm)		

Table 1. Cont.

No.	Cancer Cells/Effects	Targets/Effects	Reference Substance	Ref.
39	A549 (IC <sub>50</sub> = 53 µM)	N/A	Floxuridine: A549 (IC <sub>50</sub> = 5.8 µM)	[23]
40	DAN-G (IC <sub>50</sub> = 2.14 µM) A-427 (IC <sub>50</sub> = 1.51 µM) LCLC-103H (IC <sub>50</sub> = 2.21 µM) SISO (IC <sub>50</sub> = 2.6 µM) RT-4 (IC <sub>50</sub> = 1.66 µM)	Ct-DNA (potential target)	Cisplatin: DAN-G (IC <sub>50</sub> = 0.73 µM) A-427 (IC <sub>50</sub> = 1.96 µM) LCLC-103H (IC <sub>50</sub> = 0.90 µM) SISO (IC <sub>50</sub> = 0.24 µM) RT-4 (IC <sub>50</sub> = 1.61 µM)	[24]
41	UO-31 (GI <sub>50</sub> = 1.54 µM)			
42	RXF 393 (GI <sub>50</sub> = 0.569 µM) HS 578 (GI <sub>50</sub> = 0.644 µM)	N/A	N/A	[25]
43	SF-539 (GI <sub>50</sub> = 1.35 µM)			
44	SF-539 (GI <sub>50</sub> = 1.18 µM)			
45	MDA-MB-231 (IC <sub>50</sub> = 4.3 µg/mL) HeLa (IC <sub>50</sub> = 2.21 µg/mL) KG1a (IC <sub>50</sub> = 6.45 µg/mL) Jurkat (IC <sub>50</sub> = 28.33 µg/mL) SiHa (IC <sub>50</sub> = 1.34 µg/mL) CaSki (IC <sub>50</sub> = 4.56 µg/mL) DoTc2 (IC <sub>50</sub> = 2.15 µg/mL)	Increase concentration of C-caspase-3, C-caspase-9 and Bcl-2. Decrease of Bax. Tumor reduction in nude mouse (C = 10 µM).	Erlotinib: MDA-MB-231 (IC <sub>50</sub> = 0.16 µg/mL) HeLa (IC <sub>50</sub> = 0.21 µg/mL) KG1a (IC <sub>50</sub> = 0.18 µg/mL) Jurkat (IC <sub>50</sub> = 22.43 µg/mL) SiHa (IC <sub>50</sub> = 0.25 µg/mL) CaSki (IC <sub>50</sub> = 0.34 µg/mL) DoTc2 (IC <sub>50</sub> = 0.28 µg/mL)	[26]
46	N/A	TNF-α (IC <sub>50</sub> = 29 µM)		
47	PC-3 (IC <sub>50</sub> = 43.3 µM)	TNF-α (IC <sub>50</sub> = 13 µM), inducing cell-cycle arrest at the G <sub>0</sub> /G <sub>1</sub> phase (J774 cell line).	N/A	[27]
48	DU145 (GI <sub>50</sub> = 3.43 µM)			
49	DU145 (GI <sub>50</sub> = 4.01 µM)			
50	DU145 (GI <sub>50</sub> = 2.38 µM)			
51	DU145 (GI <sub>50</sub> = 0.67 µM)	N/A	Nilotinib: DU145 (GI <sub>50</sub> = 6.35 µM)	[28]
52	MDA-MB231 (GI <sub>50</sub> = 0.007 µM) SKBR-3 (GI <sub>50</sub> = 0.3 µM) MCF-7 (GI <sub>50</sub> = 12.5 µM)	N/A	MTX: MDA-MB231 (GI <sub>50</sub> = 0.01 µM) MCF-7 (GI <sub>50</sub> = 5.79 µM) Nilotinib: MDA-MB231 (GI <sub>50</sub> = 0.04 µM) SKBR-3 (GI <sub>50</sub> = 9.6 µM)	[29,30]
53	MDA-MB231 (GI <sub>50</sub> = 0.001 µM) SKBR-3 (GI <sub>50</sub> = 0.21 µM)			
54	MCF-7 (IC <sub>50</sub> = 14.85 µM) TPC-1 (IC <sub>50</sub> = 9.23 µM)	Phosphorylated TK (Inhibition rate = 94.4%; C = 10 µM)		
55	MCF-7 (IC <sub>50</sub> = 12.5 µM) TPC-1 (IC <sub>50</sub> = 7.16 µM)	Phosphorylated TK (Inhibition rate = 96.4%; C = 10 µM)	Vandatinib: MCF-7 (IC <sub>50</sub> = 10.42 µM) TPC-1 (IC <sub>50</sub> = 7.63 µM) Phosphorylated TK (Inhibition rate = 98.6%; C = 10 µM)	[31]
56	MCF-7 (IC <sub>50</sub> = 14.43 µM) TPC-1 (IC <sub>50</sub> = 8.8 µM)	Phosphorylated TK (Inhibition rate = 94.3%; C = 10 µM)		
57	LN-18 (IC <sub>50</sub> = 46 µM) LN-229 (IC <sub>50</sub> = 50 µM) LBC3 (IC <sub>50</sub> = 40 µM)	N/A	N/A	[32]
58	DLD-1 (IC <sub>50</sub> = 13.71 µM) HT-29 (IC <sub>50</sub> = 17.78 µM)	BAX (increase); Bcl-2 (decrease)	5-FU: DLD-1 (IC <sub>50</sub> = 27.22 µM) HT-29 (IC <sub>50</sub> = 21.72 µM)	[33]

Table 1. Cont.

No.	Cancer Cells/Effects	Targets/Effects	Reference Substance	Ref.
59	HCT-116 (Inhibition = 115.53%) SW-620 (Inhibition = 95.06%) SF-539 (Inhibition = 89.27%) OVCAR-4 (Inhibition = 94.39%) PC786-0 (Inhibition = 93.76%) ACHN (Inhibition = 86.27%) MCF-7 (Inhibition = 94.82%)	CDK2 (Inhibition rate = 82.38%; C = 10 $\mu$ M; IC50 = 1.85 $\mu$ M)	Roscovitine: CDK2 (Inhibition rate = 89.6%; C = 10 $\mu$ M)	[34]
60	ATCC (Inhibition = 90.02%) NCI-H460 (Inhibition = 83.66%) OVCAR-4 (Inhibition = 92.27%)	CDK2 (Inhibition rate = 81.96%; C = 10 $\mu$ M; IC50 = 2.09 $\mu$ M)		
61	SKMEL-103 (IC50 = 25 $\mu$ M)	PI3K (decrease)AMPK (decrease)	N/A	[35]
62	NCI-H460 (Growth Percent = -50%) MDA-MB468 (Growth Percent = -20.7%)			
63	HCC-2998 (Growth Percent = -82.1%) RXF 393 (Growth Percent = -68%) NCI-H460 (Growth Percent = -58.3%) ACHN (Growth Percent = -57%) MDA-MB-468 (Growth Percent = -52.3%)			
64	HCC-2998 (Growth Percent = -69.3%) RXF 393 (Growth Percent = -66%) NCI-H460 (Growth Percent = -64.8%) ACHN (Growth Percent = -45%)	N/A	N/A	[36]
65	HCC-2998 (Growth Percent = -77%) RXF 393 (Growth Percent = -74.4%) NCI-H460 (Growth Percent = -49.4%) MDA-MB-468 (Growth Percent = -47%)			
66	HCC-2998 (Growth Percent = -53.7%) RXF 393 (Growth Percent = -55%) NCI-H460 (Growth Percent = -54.7%) ACHN (Growth Percent = -52.8%) NCI-H322M (Growth Percent = -50.5%)			
67	A549 (IC50 = 144.1 $\mu$ g/mL) Bel7402 (IC50 = 195.6 $\mu$ g/mL)	N/A	N/A	[37]

Table 1. Cont.

No.	Cancer Cells/Effects	Targets/Effects	Reference Substance	Ref.
68	leukemia (Mean GI50 = 0.96 $\mu$ M) colon cancer (Mean GI50 = 1.64 $\mu$ M) CNS (Mean GI50 = 1.80 $\mu$ M) melanoma (Mean GI50 = 1.62 $\mu$ M) ovarian (Mean GI50 = 2.12 $\mu$ M) renal (Mean GI50 = 1.66 $\mu$ M) prostate (Mean GI50 = 1.75 $\mu$ M) breast (Mean GI50 = 1.59 $\mu$ M)			
69	leukemia (Mean GI50 = 2.55 $\mu$ M) colon cancer (Mean GI50 = 1.92 $\mu$ M) CNS (Mean GI50 = 2.09 $\mu$ M) melanoma (Mean GI50 = 3.4 $\mu$ M) ovarian (Mean GI50 = 2.67 $\mu$ M) renal (Mean GI50 = 1.80 $\mu$ M) prostate (Mean GI50 = 1.222 $\mu$ M) breast (Mean GI50 = 2.03 $\mu$ M)	N/A	N/A	[38]
70	leukemia (Mean GI50 = 4.14 $\mu$ M) colon cancer (Mean GI50 = 1.92 $\mu$ M) CNS (Mean GI50 = 3.13 $\mu$ M) melanoma (Mean GI50 = 7.84 $\mu$ M) ovarian (Mean GI50 = 6.05 $\mu$ M) renal (Mean GI50 = 3.28 $\mu$ M) prostate (Mean GI50 = 4.54 $\mu$ M) breast (Mean GI50 = 3.42 $\mu$ M)			

## 2. Results

### 2.1. Topoisomerase Inhibitors

Topoisomerases are a group of enzymes involved in replication, they are responsible for the degree of twist of the double helix. Topoisomerases convert the chemical energy from ATP into the energy of the torsion tension of a molecule with a superhelical structure. In vivo, topoisomerases unravel the DNA double helix, thus providing a template for the replication or transcription of enzymes. Depending on the number of phosphodiester bonds to be broken at one time, there are two types of enzyme. Topoisomerase I hydrolyses one bond, cuts one strand and is responsible for removing superstrands from the DNA molecule (relaxation). Topoisomerase II hydrolyses two bonds, cuts both strands and is responsible for adding supercoils to the DNA molecule [39].

Human topoisomerase II inhibitory properties were shown by 4-(benzylthio)-6-((3-chlorobenzyl)thio)-1,3,5-triazin-2(1H)-one **1** (Figure 1), giving an IC<sub>50</sub> of 57.6  $\mu$ M. Additionally, the binding of compound **1** with the htl $\alpha$  ATPase domain was proved via microscale thermophoresis (MST) and molecular dynamics (MD) [3].

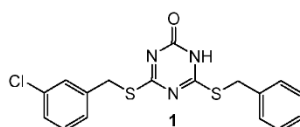


Figure 1. Structure of topoisomerase II inhibitor.

### 2.2. Dual Phosphoinositide 3-Kinase and Mammalian Target of Rapamycin Inhibitors

The phosphoinositide 3-kinase (PI3K) enzymes show a two-way activity including the activity of the lipid kinase and the activity of the protein kinase. They play a crucial role in processes such as proliferation, migration, differentiation, survival, and trafficking. The

PI3K family contains eight isoforms divided into three distinct classes (I, II, and III) which may be different in terms of cellular responsibility [40].

The function of the mammalian target of rapamycin (mTor) is to regulate growth, proliferation and cell traffic, and the processes of translation and transcription. The mTOR catalyzes the phosphorylation ribosomal protein S6 kinase  $\beta$ -1 (S6K1), eukaryotic translation initiation factor 4E binding protein 1 (4E-BP1), Akt, protein kinase C (PKC), and type-I insulin-like growth factor receptor (IGF-IR), thereby regulating protein synthesis, nutrient metabolism, growth factor signaling, cell growth, and migration [41].

The construction of compounds with dual inhibitory effects contributes to obtaining a more selective effect. Potential anti-cancer drugs that inhibit PI3K and mTor at the same time showed greater efficiency and reduced the likelihood of inducing drug resistance [42].

Substituted 2-(thiophen-2-yl)-1,3,5-triazine derivative **2** (Figure 2) exhibited excellent anti-cancer potency for A549, MCF-7 (breast cancer) and HeLa (cervical cancer) cell lines with IC<sub>50</sub> values of 0.20  $\mu$ M, 1.25  $\mu$ M, and 1.03  $\mu$ M, respectively. Western blot analysis proved derivative **2** could suppress the phosphorylation of AKT. The degree of inhibition (%) demonstrated selective inhibition of PI3K $\alpha$ /mTOR, unlike epidermal growth factor receptors (EGFR, c-Met, VEGFR-2, and EGFRL858R/T790M) [4].

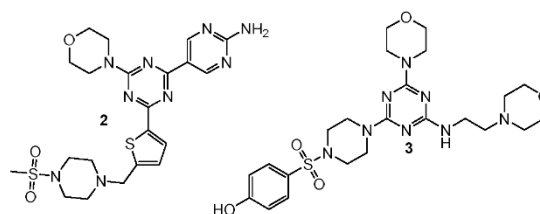


**Figure 2.** Structure of dual PI3K and mTor inhibitors.

From the new series of 1,3,5-triazine derivatives rich in morpholine moiety, 4-((4-(4-morpholino-6-((2-morpholinoethyl)amino)-1,3,5-triazin-2-yl)piperazin-1-yl)sulfonyl)phenol **3** (Figure 2) showed the highest cytotoxic activity against MDA-MB321 (breast cancer), MCF-7, HeLa, and HepG2 (human hepatocellular carcinoma) cells with IC<sub>50</sub> values of 15.83  $\mu$ M, 16.32  $\mu$ M, 2.21  $\mu$ M, and 12.21  $\mu$ M, respectively. Kinase inhibitory activity (IC<sub>50</sub>) of derivative **3** was equal to 3.41 nM for PI3K, and 8.45 nM for mTor [5].

### 2.3. Dihydrofolate Reductase Inhibitors

Dihydrofolate reductase (DHFR) is an enzyme responsible for reducing dihydrofolic acid to tetrahydrofolic acid by catalyzing the transfer of hydride from NADPH, generating the oxidized form of NADP<sup>+</sup> [43]. Inhibiting DHFR induces an amount reduction of tetrahydrofolate (THF), consequently decreasing the synthesis of purines, amino acids, and thymidylate, which are crucial in cell growth and proliferation [44].

Singa et al. demonstrated synthesized triazine-benzimidazole analogs **4–7** (Figure 3) appointed with a hydrogen bond interaction domain, a polar hydrophilic substituent and an intercalating group. The median growth inhibitory (GI<sub>50</sub>) values for these compounds were measured relative to leukemia, non-small cell lung cancer, colon cancer, central nervous system (CNS) tumor, melanoma, ovarian cancer, renal cancer, prostate cancer, and breast cancer cells with values in the range of 1.91–2.72  $\mu$ M. The 50% inhibitory concentration value of DHFR activity was lowest for derivative **7** and was 0.002  $\mu$ M, which was equivalent to methotrexate (MTX) (IC<sub>50</sub> = 0.02  $\mu$ M) [6,45].

Zhou et al. reported hDHFR inhibiting activity in four 1,3,5-triazine analogs bearing a heteroatom (O/S) spiro-ring. Structures **8–11** (Figure 3) presented hDHFR inhibitory activity with IC<sub>50</sub> values of 7.46 nM, 3.72 nM, 6.46 nM, and 4.08 nM, compared with MTX. An in vivo study demonstrated that compound **8** significantly inhibited tumor growth in a nude mouse [7].

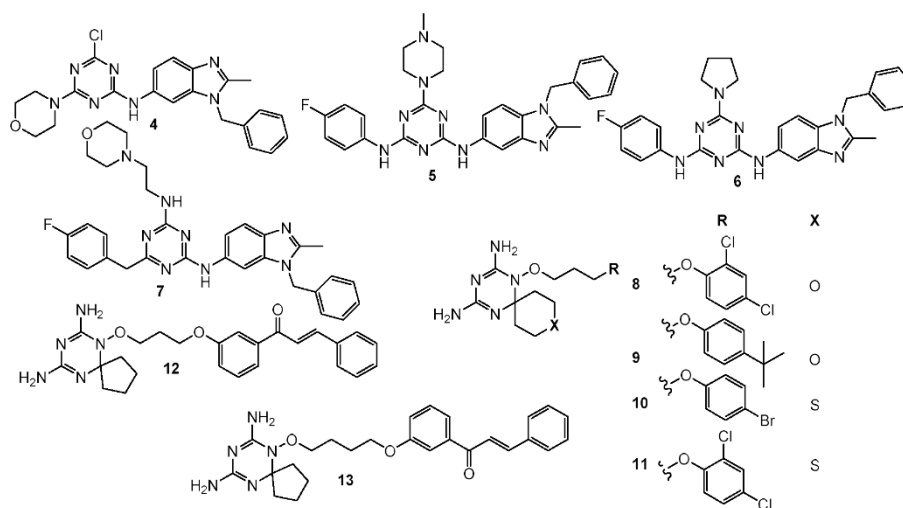


**Figure 3.** Structure of DHFR inhibitors.

A hybrid of 4,6-diamino-1,2-dihydro-1,3,5-triazine and chalcone led to the generation of 15 new compounds as potential DHFR and TrxR (thioredoxin reductase) inhibitors. The greatest results were exhibited by compounds **12** and **13** (Figure 3). Both acted cytotoxic against HCT116 (human colorectal carcinoma) ( $GI_{50} = 0.026 \mu\text{M}$ ;  $GI_{50} = 0.116 \mu\text{M}$ ) and MCF-7 ( $GI_{50} = 0.080 \mu\text{M}$ ;  $GI_{50} = 0.127 \mu\text{M}$ ) cancer cell lines. In addition, studies have shown strong *in vitro* inhibitory activities against recombinant human DHFR ( $IC_{50} = 0.0061 \mu\text{M}$ ;  $IC_{50} = 0.0026 \mu\text{M}$ ) and rat TrxR ( $IC_{50} = 4.6 \mu\text{M}$ ;  $IC_{50} = 5.9 \mu\text{M}$ ) enzymes [8].

#### 2.4. Carbonic Anhydrase Inhibitors

Carbonic anhydrases (CAs), metalloenzymes from the lyase group, are responsible for pH homeostasis and catalyzing the reversible reaction of the formation of the bicarbonate ion  $\text{HCO}_3^-$  from water and carbon dioxide [46].

Among the numerous isoforms we can distinguish the ubiquitous variants CA I and CA II in mammals. In a pathological condition such as hypoxia, increased expression of CA IX and CA XII is observed. These enzyme forms are involved in the regulation of pH homeostasis and intercellular communication and ion transport. 2-[4-Chloro-5-methyl-2-(naphthalen-1-ylmethylthio)-benzenesulfonyl]-1-[4-chloro-6-(4-sulfamoylphenylamino)-1,3,5-triazin-2-ylamino]guanidine **14** (Figure 4) acted with strongest selectivity toward hCA IX versus hCA I (hCA I/hCA IX = 18) and hCA II (hCA II/hCA IX = 4). Compound **14** showed prominent cytotoxicity towards HeLa cancer cells ( $IC_{50} = 17 \mu\text{M}$ ) and did not exhibit toxicity to the non-cancerous HaCaT cells ( $IC_{50} = 61 \mu\text{M}$ ) [9].

Research conducted by Havráňková et al. considered the interaction of CA I, II and IX with 1,3,5-triazine derivatives incorporating piperazine, aminoalcohol and sulfonamide. The results showed that 1,3,5-triazines with a 4-hydroxyaniline substituent achieved the highest ratio of selective inhibition (hCA IX/hCA II): compound **15** (18.50); compound **16** (14.09) (Figure 4) [10].

Based on the structure of SCL-0111, new 1,3,5-triazine derivatives **17** and **18** were synthesized (Figure 4) and their ability to inhibit CA I, II, IX, and XII was investigated. The most promising result was the selective inhibition of CA IX by compound **17** with a KI value = 0.91 nM [11], while compound **18** had a KI value of 14.6 nM [12].

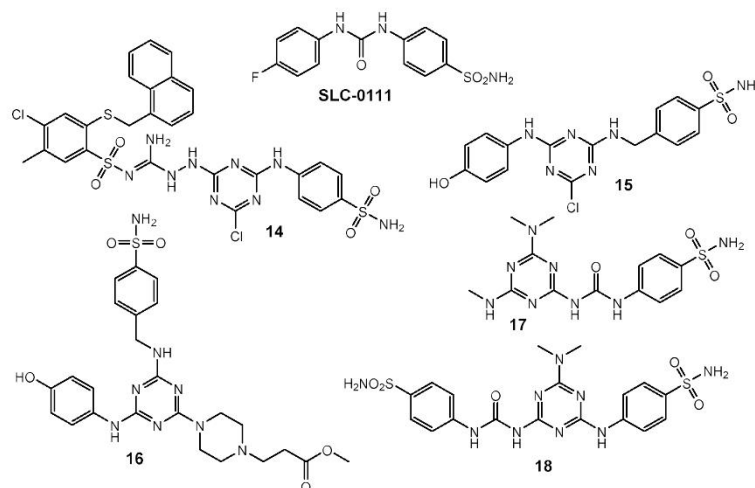


**Figure 4.** Structure of CA inhibitors.

#### 2.5. Epidermal Growth Factor Receptor Inhibitors

The role of the epidermal growth factor receptor (EGFR) in the pathogenesis process is an important topic of scientific research. As a result, it was discovered that mutations leading to overexpression of EGFR genes (e.g., increased regulation or amplification) are significantly associated with many cancers: lung granuloma (40% of cases), rectal tumors, glioblastoma (50%), and epithelial carcinomas of the head and neck (80–100%) [47,48].

Through the “one pot” reaction, 15 novel monastrol-1,3,5-triazine derivatives were obtained and investigated for anti-cancer properties and cytotoxicity. Derivative **19** substituted by 3-fluorophenylamino groups (Figure 5) presented highest IC<sub>50</sub> against cancer cell lines [HeLa—39.7  $\mu$ M; MCF-7—41.5  $\mu$ M; HL-60 (human pro-myelocytic leukemia cell)—23.1  $\mu$ M; HepG2—31.2]. This compound was nontoxic to normal epithelial cells MCF-12A while at a concentration of 10 nM the inhibition of EGFR-TK by **19** was equal 96.4% [13].

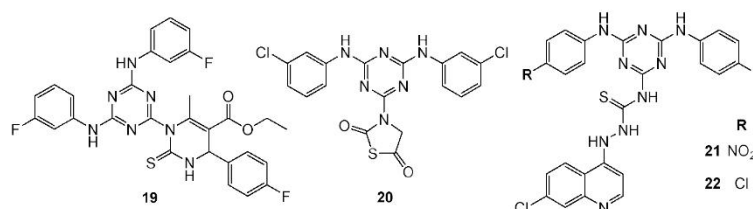


**Figure 5.** Structure of EGFR inhibitors.

Analysis of molecular modelling and Lipinski’s rule of five allowed us to select four compounds that were tested for anti-breast cancer activity. The strongest action with respect to EGFR-TK was observed for 3-(4,6-bis((3-chlorophenyl)amino)-1,3,5-triazin-2-yl)thiazolidine-2,5-dione **20** (Figure 5) (IC<sub>50</sub> = 2.54  $\mu$ M). An in vitro study against MDA-MB-21, BT-474 (breast tumor) and MCF-7 showed an increase of apoptosis rates. In addition, a significant decline expression of  $\beta$ -catenin was noticed in MDA-MB-21 cell lines [14].

Bhat et al. took a closer look at 4-aminoquinoline-1,3,5-triazine derivatives. Compounds **21** (Figure 5) presented IC<sub>50</sub> values of 44.5  $\mu$ M, 52.2  $\mu$ M, 40.3  $\mu$ M, and 56.4  $\mu$ M against HeLa, MCF-7, HL-60, and HepG2. Derivative **22** (Figure 5) showed IC<sub>50</sub> values of

32.4  $\mu\text{M}$ , 32.3  $\mu\text{M}$ , 26.3  $\mu\text{M}$ , and 45.3  $\mu\text{M}$  against HeLa, MCF-7, HL-60, and HepG2. Both molecules did not reveal cytotoxicity to MCF-12A cells. The activity of derivatives **21** and **22** inhibiting EGFR-TK was 96.3% and 90.5%, respectively [15].

### 2.6. Vascular Endothelial Growth Factor

Vascular endothelial growth factor (VEGF) production can be induced in a cell that does not receive enough oxygen [49]. When a cell is deficient in oxygen, it produces hypoxia induced factor (HIF). HIF stimulates the release of VEGF (including the modulation of erythropoiesis). Circulating VEGF then binds to VEGF receptors on endothelial cells, triggering a tyrosine kinase pathway leading to angiogenesis [50]. Expression of angiopoietin-2 in the absence of VEGF leads to endothelial cell death and vascular regression. VEGF acts as the central mediator of tumor angiogenesis, stimulating the growth of new blood vessels from nearby capillaries and allowing tumors to access the oxygen and nutrients they need to grow [51].

Quinazoline-1,3,5-triazine derivatives **23**, **24**, and **25** (Figure 6) demonstrated antitumor activity against HeLa, MCF-7, HL-60, and HepG2 with  $\text{IC}_{50}$  values in range of 6–16  $\mu\text{M}$ . In addition, they were non-toxic against the normal cell line of HFF (human foreskin fibroblasts). Molecular docking results demonstrated the high potency of derivatives **23**, **24** and **25** to bind the hydrophobic pocket of the N-terminal chain in the ATP binding site of VEGFR [52].

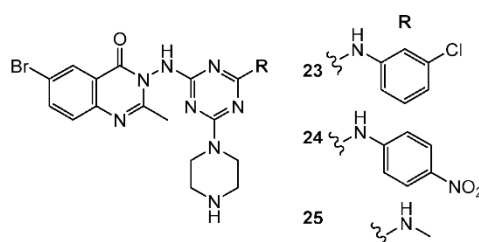


Figure 6. Structure of VEGF inhibitors.

### 2.7. Focal Adhesion Kinase Inhibitors

Focal Adhesion Kinase (FAK) is a 125-kDa cytoplasmic tyrosine kinase. Deregulation of FAK-dependent processes such as cell adhesion, growth, survival, and mobility are a significant component of tumor progression. Overexpression of FAK leads to the inhibition of apoptosis and an increase in the incidence of metastatic tumors [53].

Dao et al. showed that compound **26** (Figure 7) is the strongest FAK inhibitor ( $\text{IC}_{50} = 0.05 \mu\text{M}$ ). Growth inhibitory activity on human glioblastoma (U-87MG), human colon carcinoma (HCT-116), MDA-MB-231, and human prostate cancer (PC-3) by compound **26** obtained the following results 0.42  $\mu\text{M}$ , 0.13  $\mu\text{M}$ , 0.14  $\mu\text{M}$ , and 0.63  $\mu\text{M}$  compared to TAE-226 (0.19  $\mu\text{M}$ , 0.23  $\mu\text{M}$ , 1.9  $\mu\text{M}$ , and 0.26  $\mu\text{M}$ ). Furthermore, compound **26** turned out to fit well into the ATP binding site of the FAK via molecular docking [16].

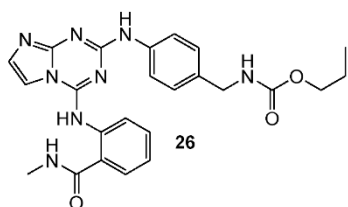
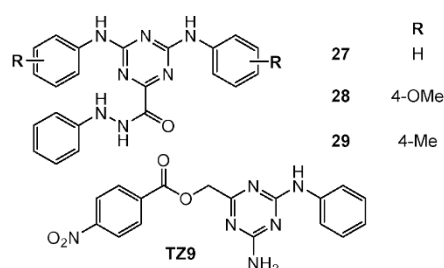


Figure 7. Structure of FAK inhibitor.

### 2.8. Ubiquitin Conjugating Enzyme Inhibitors

RAD6, an E2 ubiquitin-conjugating enzyme, is overexpressed in many cancer cells and is responsible for the positive regulation of  $\beta$ -catenin, its stabilization and activity. *N'*-phenyl-4,6-bis(arylamino)-1,3,5-triazine-2-carbohydrazides derivatives **27–29** (Figure 8) were evaluated for their ability to inhibit Rad6B ubiquitin conjugation in the human cancer cell lines: OV90 (ovarian cancer), H1299 (human non-small cell lung carcinoma), A549, MCF-7, MDA-MB231, and HT-29 (colon cancer). For all of the examined compounds lower than for TZ9  $IC_{50}$  values were obtained (3.3–22  $\mu$ M) (Figure 8) [17].



**Figure 8.** Structure of ubiquitin conjugating enzyme inhibitors.

### 2.9. Primary Anticancer Studies

Compound **30** (Figure 9) obtained via the click chemistry method showed higher potency than doxorubicin. Derivative **30** exhibited an  $IC_{50}$  against MCF-7 and HepG2 cells of 2.95  $\mu$ g/mL and 3.70  $\mu$ g/mL, respectively, and showed no toxic activity against the growth of normal HFB4 cells [18].

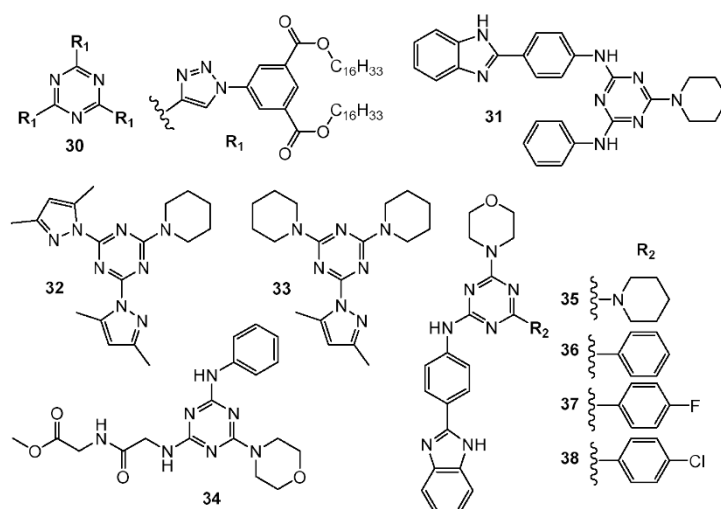


**Figure 9.** Structures of compounds 30–38.

Interesting results have emerged from the comparison of the antitumor properties of the two groups of 1,3,5-triazine derivatives. The groups differed only in one substituent, the first group contained chlorine and the second group contained morpholine. In the second case, a noticeable increase in cytotoxic activities was observed. According to cancer

cell lines MCF-7, MDAMB-231, HT-29, HGC-27 the derivative **31** (Figure 9) proved to be most potent with  $IC_{50}$  values of 4.8  $\mu$ M, 8.3  $\mu$ M, 9.8  $\mu$ M, and 15.1  $\mu$ M [19].

Pyrazolyl-1,3,5-triazine derivatives were tested in vitro against MCF 7, MDA-MB-231, HepG2, LoVo (colorectal carcinoma) and K-562 (leukemia). Compounds **32** and **33** (Figure 9) demonstrated  $IC_{50}$  values within the range of 5 to 9  $\mu$ M. An in vivo test on a zebrafish proved the non-toxicity of compounds **32** and **33** [20].

Trisubstituted s-triazine derivatives containing morpholine/piperidine, anilines, and dipeptides were evaluated for their anticancer activity against MCF-7 and MDA-MB-231. Among the 15 synthesized compounds, analog **34** (Figure 9) elicited the highest inhibitory properties against MCF-7 ( $IC_{50}$  = 0.82  $\mu$ M). Moreover MCF-7 cells were significantly arrested in the G2/M stage. An in vivo studies of **34** in zebrafish presented non-toxic properties [21].

A novel series of triazine-benzimidazole analogs were synthesized and their antiproliferative activity against 60 human cancer cell lines was evaluated. Screening data revealed that triazine substituted with piperidine **35**, phenyl **36**, 4-fluorophenyl **37**, and 4-chlorophenyl **38** (Figure 9) presented the highest inhibiting potency [22].

4-Phenethylthio-2-phenylpyrazolo[1,5-a][1,3,5]triazin-7(6H)-one **39** (Figure 10) was designed and synthesized as a potential anticancer agent. An in vitro evaluation of its antiproliferative activity against A549 and MDA-MB231 confirmed the assumption. The test results were not good enough. On the other hand, modifications of the obtained structure may contribute to the improvement of anti-cancer properties [23].

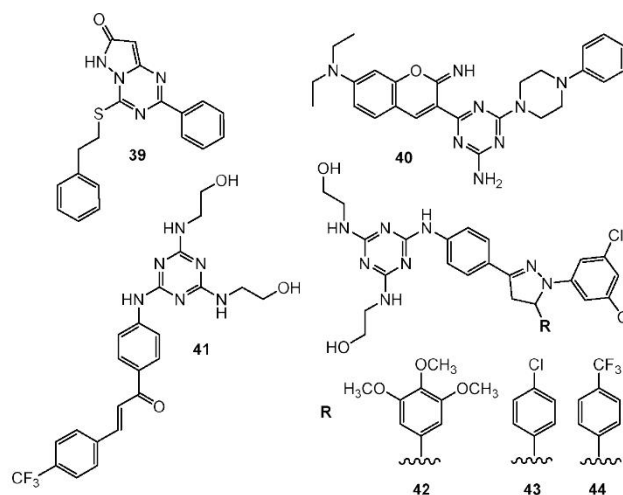


**Figure 10.** Structures of compounds 39–44.

The series of novel hybrid molecules formed from 2,4-diamino-1,3,5-triazine and 2-iminocoumarin were tested toward the human pancreatic cancer cell line DAN-G, human A-427, human non-small cell lung cancer cell line LCLC-103H, human cervical cancer cell line SISO, and human urinary bladder cancer cell line RT-4. Compound **40** (Figure 10) presented the following values  $IC_{50}$ : 2.14  $\mu$ M, 1.51  $\mu$ M, 2.21  $\mu$ M, 2.60  $\mu$ M, and 1.66  $\mu$ M [24].

Moreno et al. designed and synthesized 28 1,3,5-triazine-based 2-pyrazolines. In vitro tests were conducted against 58 different human tumor cell lines. The first stage of research checked mean growth and growth inhibition, and identified four compounds **41–44** (Figure 10) with the lowest value (%). In the next step, the inhibitory activity of compounds **41–44** in terms of  $GI_{50}$  and  $LC_{50}$  was verified, determining the most susceptible carcinoma cell lines [25].



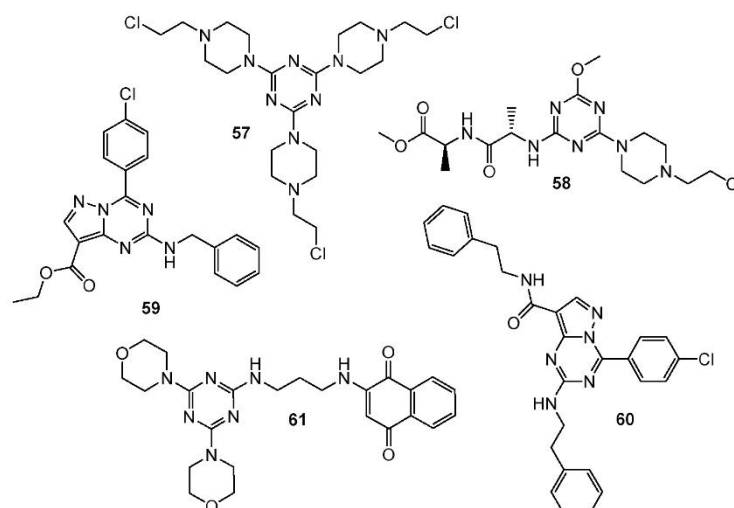


Figure 12. Structures of compounds 57–61.

A total of thirty-four novel pyrazolo[1,5-a][1,3,5]triazine derivatives were screened against 60 cancer cell lines. Results suggested that the most antiproliferative compounds were **59** and **60** (Figure 12). Analog **59** exhibited% inhibition ranging from 40% to 115%, and 82.38% for CDK2, and derivative **60** exhibited% inhibition ranging from 43% to 92%, and 81.96% for CDK2 [34].

Hybrid molecule containing 1,4-naphthoquinone, 1,3,5-triazine and morpholine **61** (Figure 12) turned out to be strongly complexed with PI3K $\gamma$  and AMPK (5' AMP-activated protein kinase) during docking studies. Analog **61** had an IC<sub>50</sub> value of approximately 25  $\mu$ M when exposed to the SKMEL-103 (N-RAS mutated) cell line. A Western blot determined the decreased expression of both PI3K $\gamma$  and AMPK [35].

Screening studies of 2-(dichloromethyl)pyrazolo[1,5-a][1,3,5]triazines **62–66** (Figure 13) showed potential anticancer properties against non-small cell lung cancers, colon cancers, renal cancer, etc. [36].

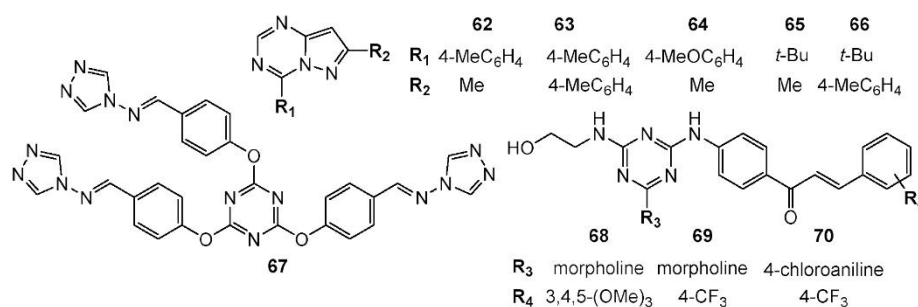


Figure 13. Structures of compounds 61–70.

Prepared 4-amino-1,2,4-triazole Schiff base derivative **67** (Figure 13) was verified as an antitumor agent. The IC<sub>50</sub> value of **67** was equal to 144.1  $\mu$ g/mL for A549 and 195.6  $\mu$ g/mL for the human hepatoma cell line (Bel7402) [37].

From the series of novel chalcone- and pyrazoline-based 1,3,5-triazines derivatives, compounds 68–70 (Figure 13) demonstrated the best potent in vitro anticancer activity with GI<sub>50</sub> values significantly lower than reference drug 5-FU. Chalcone 68 showed GI<sub>50</sub> values in the range of 0.422–3.05 µM, with the SR cell line (leukemia, GI<sub>50</sub> = 0.422 µM) being the most sensitive strain. Compound 69 exhibited GI<sub>50</sub> values in the range of 1.25–8.66 µM, with the MCF7 (GI<sub>50</sub> = 1.25 µM) being the most sensitive strain, while compound 70 showed GI<sub>50</sub> values in the range of 1.48–14.9 µM, being especially effective against HCT-116 with GI<sub>50</sub> = 1.48 µM. The best cytotoxicity value was shown by compound 69 against UO-31 (renal cancer, LC<sub>50</sub> = 5.08 µM) [38].

### 3. Search Strategy and Selection Criteria

The aim of this study was to collect knowledge and data on the synthesized novel 1,3,5-triazine derivatives, their effects on cancer cells, and to identify enzymes as potential targets for these substances. To carry out the study, the following databases were searched: PubMed (NCBI), Web of Science, and Scopus, using the following key words: 1,3,5-triazine, s-triazine, anticancer, antitumor, and enzyme inhibitor. We examined original articles and case studies published between 2015 and 2021. The results of the study include the compounds from papers with the highest activity.

### 4. Conclusions

The “hybrid” approach incorporating a triazine framework ensures an improved profile against the target biological pathways pertaining to infectious parasites, microbes, and conditions such as cancer and neurodegeneration. The multi-targeting approach of the hybrid compounds ensures an effective overcoming of the key regulatory pathways contributing to complications such as drug resistance. This review presents a comprehensive discussion on the candidature of the 1,3,5-triazine scaffold for a rational development of the hybrid molecules by conjugation with bioactive pharmacophoric moieties. The basis of superior efficacy of 1,3,5-triazine based hybrid molecules by considering their interactions with the cellular targets has also been discussed in a succinct manner. The literature revealed that s-triazine derivatives possess diverse anticancer potential, easy synthetic routes for synthesis, and have attracted researchers for development of new chemotherapeutic agents. Extensive research is required on the 1,3,5-triazine moiety to find novel analogs suitable for clinical applications in cancer treatment.

**Author Contributions:** Conceptualization, D.M. and D.D.; writing—original draft preparation, D.M.; review and editing, D.M. and D.D.; supervision, D.D. All authors have read and agreed to the published version of the manuscript.

**Funding:** Publication was written during doctoral studies under the project No POWR.03.02.00-00-1051/16 co-funded from European Union funds, PO WER 2014–2020.

**Institutional Review Board Statement:** Not applicable.

**Informed Consent Statement:** Not applicable.

**Data Availability Statement:** Not applicable.

**Conflicts of Interest:** Authors declare no conflict of interest.

### References

1. WHO, Regional Office for Europe. *World Cancer Report: Cancer Research for Cancer Development*; IARC: Lyon, France, 2020.
2. Pathak, A.; Tanwar, S.; Kumar, V.; Banarjee, B.D. Present and Future Prospect of Small Molecule & Related Targeted Therapy Against Human Cancer. *Vivechan Int. J. Res.* **2018**, *9*, 36–49. [[PubMed](#)]
3. Pogorelčnik, B.; Janežič, M.; Sosič, I.; Gobec, S.; Solmajer, T.; Perdih, A. 4,6-Substituted-1,3,5-Triazin-2(1H)-Ones as Monocyclic Catalytic Inhibitors of Human DNA Topoisomerase II $\alpha$  Targeting the ATP Binding Site. *Bioorg. Med. Chem.* **2015**, *23*, 4218–4229. [[CrossRef](#)] [[PubMed](#)]

4. Zhang, B.; Zhang, Q.; Xiao, Z.; Sun, X.; Yang, Z.; Gu, Q.; Liu, Z.; Xie, T.; Jin, Q.; Zheng, P.; et al. Design, Synthesis and Biological Evaluation of Substituted 2-(Thiophen-2-Yl)-1,3,5-Triazine Derivatives as Potential Dual PI3K $\alpha$ /MTOR Inhibitors. *Bioorg. Chem.* **2020**, *95*, 103525. [[CrossRef](#)] [[PubMed](#)]
5. Hu, J.; Zhang, Y.; Tang, N.; Lu, Y.; Guo, P.; Huang, Z. Discovery of Novel 1,3,5-Triazine Derivatives as Potent Inhibitor of Cervical Cancer via Dual Inhibition of PI3K/MTOR. *Bioorg. Med. Chem.* **2021**, *32*, 115997. [[CrossRef](#)] [[PubMed](#)]
6. Singla, P.; Luxami, V.; Paul, K. Synthesis, in Vitro Antitumor Activity, Dihydrofolate Reductase Inhibition, DNA Intercalation and Structure–Activity Relationship Studies of 1,3,5-Triazine Analogues. *Bioorg. Med. Chem. Lett.* **2016**, *26*, 518–523. [[CrossRef](#)] [[PubMed](#)]
7. Zhou, X.; Lin, K.; Ma, X.; Chui, W.-K.; Zhou, W. Design, Synthesis, Docking Studies and Biological Evaluation of Novel Dihydro-1,3,5-Triazines as Human DHFR Inhibitors. *Eur. J. Med. Chem.* **2017**, *125*, 1279–1288. [[CrossRef](#)] [[PubMed](#)]
8. Ng, H.-L.; Ma, X.; Chew, E.-H.; Chui, W.-K. Design, Synthesis, and Biological Evaluation of Coupled Bioactive Scaffolds as Potential Anticancer Agents for Dual Targeting of Dihydrofolate Reductase and Thioredoxin Reductase. *J. Med. Chem.* **2017**, *60*, 1734–1745. [[CrossRef](#)] [[PubMed](#)]
9. Żołnowska, B.; Stawiński, J.; Szafranski, K.; Angeli, A.; Supuran, C.T.; Kawiak, A.; Wieczór, M.; Zielińska, J.; Bączek, T.; Bartoszewski, S. Novel 2-(2-Arylmethylthio-4-Chloro-5-Methylbenzenesulfonyl)-1-(1,3,5-Triazin-2-Ylamino) Guanidine Derivatives: Inhibition of Human Carbonic Anhydrase Cytosolic Isozymes I and II and the Transmembrane Tumor-Associated Isozymes IX and XII, Anticancer Activity, and Molecular Modeling Studies. *Eur. J. Med. Chem.* **2018**, *143*, 1931–1941. [[CrossRef](#)] [[PubMed](#)]
10. Havránková, E.; Csöllei, J.; Vullo, D.; Garaj, V.; Pazdera, P.; Supuran, C.T. Novel Sulfonamide Incorporating Piperazine, Aminoalcohol and 1,3,5-Triazine Structural Motifs with Carbonic Anhydrase I, II and IX Inhibitory Action. *Bioorg. Chem.* **2018**, *77*, 25–37. [[CrossRef](#)] [[PubMed](#)]
11. Lolak, N.; Akocak, S.; Bua, S.; Supuran, C.T. Design, Synthesis and Biological Evaluation of Novel Ureido Benzenesulfonamides Incorporating 1,3,5-Triazine Moieties as Potent Carbonic Anhydrase IX Inhibitors. *Bioorg. Chem.* **2019**, *82*, 117–122. [[CrossRef](#)] [[PubMed](#)]
12. Lolak, N.; Akocak, S.; Bua, S.; Sanku, R.K.K.; Supuran, C.T. Discovery of New Ureido Benzenesulfonamides Incorporating 1,3,5-Triazine Moieties as Carbonic Anhydrase I, II, IX and XII Inhibitors. *Bioorg. Med. Chem.* **2019**, *27*, 1588–1594. [[CrossRef](#)] [[PubMed](#)]
13. Srivastava, J.K.; Pillai, G.G.; Bhat, H.R.; Verma, A.; Singh, U.P. Design and Discovery of Novel Monastrol-1,3,5-Triazines as Potent Anti-Breast Cancer Agent via Attenuating Epidermal Growth Factor Receptor Tyrosine Kinase. *Sci. Rep.* **2017**, *7*, 5851. [[CrossRef](#)] [[PubMed](#)]
14. Yan, W.; Zhao, Y.; He, J. Anti-breast Cancer Activity of Selected 1,3,5-triazines via Modulation of EGFR-TK. *Mol. Med. Rep.* **2018**, *18*, 4175–4184. [[CrossRef](#)]
15. Bhat, H.R.; Masih, A.; Shakya, A.; Ghosh, S.K.; Singh, U.P. Design, Synthesis, Anticancer, Antibacterial, and Antifungal Evaluation of 4-aminoquinoline-1,3,5-triazine Derivatives. *J. Heterocycl. Chem.* **2020**, *57*, 390–399. [[CrossRef](#)]
16. Dao, P.; Smith, N.; Tomkiewicz-Raulet, C.; Yen-Pon, E.; Camacho-Artacho, M.; Lietha, D.; Herbeuval, J.-P.; Coumoul, X.; Garbay, C.; Chen, H. Design, Synthesis, and Evaluation of Novel Imidazo[1,2-a][1,3,5] Triazines and Their Derivatives as Focal Adhesion Kinase Inhibitors with Antitumor Activity. *J. Med. Chem.* **2015**, *58*, 237–251. [[CrossRef](#)] [[PubMed](#)]
17. Kothayer, H.; Spencer, S.M.; Tripathi, K.; Westwell, A.D.; Palle, K. Synthesis and in Vitro Anticancer Evaluation of Some 4,6-Diamino-1,3,5-Triazine-2-Carbohydrazides as Rad6 Ubiquitin Conjugating Enzyme Inhibitors. *Bioorg. Med. Chem. Lett.* **2016**, *26*, 2030–2034. [[CrossRef](#)] [[PubMed](#)]
18. El Malah, T.; Nour, H.F.; Nayl, A.A.; Elkhashab, R.A.; Abdel-Megeid, F.M.E.; Ali, M.M. Anticancer Evaluation of Tris (Triazolyl)Triazine Derivatives Generated via Click Chemistry. *Aust. J. Chem.* **2016**, *69*, 905. [[CrossRef](#)]
19. Kumar, G.J.; Kumar, S.N.; Thummuri, D.; Adari, L.B.S.; Naidu, V.G.M.; Srinivas, K.; Rao, V.J. Synthesis and Characterization of New S-Triazine Bearing Benzimidazole and Benzothiazole Derivatives as Anticancer Agents. *Med. Chem. Res.* **2015**, *24*, 3991–4001. [[CrossRef](#)]
20. Farooq, M.; Sharma, A.; Almarhoon, Z.; Al-Dhfyhan, A.; El-Faham, A.; Taha, N.A.; Wadaan, M.A.M.; de la Torre, B.G.; Albericio, F. Design and Synthesis of Mono- and Di-Pyrazolyl-s-Triazine Derivatives, Their Anticancer Profile in Human Cancer Cell Lines, and in Vivo Toxicity in Zebrafish Embryos. *Bioorg. Chem.* **2019**, *87*, 457–464. [[CrossRef](#)]
21. Malebari, A.M.; Abd Alhameed, R.; Almarhoon, Z.; Farooq, M.; Wadaan, M.A.M.; Sharma, A.; de la Torre, B.G.; Albericio, F.; El-Faham, A. The Antiproliferative and Apoptotic Effect of a Novel Synthesized S-Triazine Dipeptide Series, and Toxicity Screening in Zebrafish Embryos. *Molecules* **2021**, *26*, 1170. [[CrossRef](#)]
22. Singla, P.; Luxami, V.; Paul, K. Synthesis and in Vitro Evaluation of Novel Triazine Analogues as Anticancer Agents and Their Interaction Studies with Bovine Serum Albumin. *Eur. J. Med. Chem.* **2016**, *117*, 59–69. [[CrossRef](#)]
23. Smolnikov, S.; Gorgopina, E.; Lezhnyova, V.; Ong, G.; Chui, W.-K.; Dolzhenko, A. 4-Phenethylthio-2-Phenylpyrazolo[1,5-a][1,3,5]Triazin-7(6H)-One. *Molbank* **2017**, *2017*, M970. [[CrossRef](#)]
24. Makowska, A.; Sączewski, F.; Bednarski, P.; Sączewski, J.; Balewski, Ł. Hybrid Molecules Composed of 2,4-Diamino-1,3,5-Triazines and 2-Imino-Coumarins and Coumarins. Synthesis and Cytotoxic Properties. *Molecules* **2018**, *23*, 1616. [[CrossRef](#)] [[PubMed](#)]
25. Moreno, L.; Quiroga, J.; Abonia, R.; Ramírez-Prada, J.; Insuasty, B. Synthesis of New 1,3,5-Triazine-Based 2-Pyrazolines as Potential Anticancer Agents. *Molecules* **2018**, *23*, 1956. [[CrossRef](#)]

26. Wang, X.; Yi, Y.; Lv, Q.; Zhang, J.; Wu, K.; Wu, W.; Zhang, W. Novel 1,3,5-Triazine Derivatives Exert Potent Anti-Cervical Cancer Effects by Modulating Bax, Bcl2 and Caspases Expression. *Chem. Biol. Drug Des.* **2018**, *91*, 728–734. [[CrossRef](#)]
27. Zacharie, B.; Abbott, S.D.; Duceppe, J.; Gagnon, L.; Grouix, B.; Geerts, L.; Gervais, L.; Sarra-Bournet, F.; Perron, V.; Wilb, N.; et al. Design and Synthesis of New 1,3,5-Trisubstituted Triazines for the Treatment of Cancer and Inflammation. *ChemistryOpen* **2018**, *7*, 737–749. [[CrossRef](#)] [[PubMed](#)]
28. Junaïd, A.; Lim, F.P.L.; Tiekink, E.R.T.; Dolzhenko, A.V. New One-Pot Synthesis of 1,3,5-Triazines: Three-Component Condensation, Dimroth Rearrangement, and Dehydrogenative Aromatization. *ACS Comb. Sci.* **2019**, *21*, 548–555. [[CrossRef](#)] [[PubMed](#)]
29. Junaïd, A.; Lim, F.P.L.; Chuah, L.H.; Dolzhenko, A.V. 6, N 2 -Diaryl-1,3,5-Triazine-2,4-Diamines: Synthesis, Antiproliferative Activity and 3D-QSAR Modeling. *RSC Adv.* **2020**, *10*, 12135–12144. [[CrossRef](#)]
30. Junaïd, A.; Lim, F.P.L.; Tiekink, E.R.T.; Dolzhenko, A.V. Design, Synthesis, and Biological Evaluation of New 6, N 2 -Diaryl-1,3,5-Triazine-2,4-Diamines as Anticancer Agents Selectively Targeting Triple Negative Breast Cancer Cells. *RSC Adv.* **2020**, *10*, 25517–25528. [[CrossRef](#)]
31. Pathak, P.; Naumovich, V.; Grishina, M.; Shukla, P.K.; Verma, A.; Potemkin, V. Quinazoline Based 1,3,5-triazine Derivatives as Cancer Inhibitors by Impeding the Phosphorylated RET Tyrosine Kinase Pathway: Design, Synthesis, Docking, and QSAR Study. *Arch. Pharm.* **2019**, *352*, 1900053. [[CrossRef](#)]
32. Krętownski, R.; Drozdowska, D.; Kolesińska, B.; Kamiński, Z.; Frączyk, J.; Cechowska-Pasko, M. The Cellular Effects of Novel Triazine Nitrogen Mustards in Glioblastoma LBC3, LN-18 and LN-229 Cell Lines. *Investig. New Drugs* **2019**, *37*, 984–993. [[CrossRef](#)] [[PubMed](#)]
33. Wróbel, A.; Kolesińska, B.; Frączyk, J.; Kamiński, Z.J.; Tankiewicz-Kwedlo, A.; Hermanowicz, J.; Czarnomysy, R.; Maliszewski, D.; Drozdowska, D. Synthesis and Cellular Effects of Novel 1,3,5-Triazine Derivatives in DLD and Ht-29 Human Colon Cancer Cell Lines. *Investig. New Drugs* **2020**, *38*, 990–1002. [[CrossRef](#)]
34. Oudah, K.H.; Najm, M.A.A.; Samir, N.; Serya, R.A.T.; Abouzid, K.A.M. Design, Synthesis and Molecular Docking of Novel Pyrazolo[1,5-a][1,3,5]Triazine Derivatives as CDK2 Inhibitors. *Bioorg. Chem.* **2019**, *92*, 103239. [[CrossRef](#)]
35. Fiorot, R.; Westphal, R.; Lemos, B.; Romagna, R.; Gonçalves, P.; Fernandes, M.; Ferreira, C.; Taranto, A.; Greco, S. Synthesis, Molecular Modelling and Anticancer Activities of New Molecular Hybrids Containing 1,4-Naphthoquinone, 7-Chloroquinoline, 1,3,5-Triazine and Morpholine Cores as PI3K and AMPK Inhibitors in the Metastatic Melanoma Cells. *J. Braz. Chem. Soc.* **2019**, *30*, 1860–1873. [[CrossRef](#)]
36. Velihina, Y.S.; Pil'ov, S.G.; Zybrev, V.S.; Moskvina, V.S.; Shablykina, O.V.; Brovarets, V.S. 2-(Dichloromethyl)Pyrazolo[1,5-a][1,3,5]Triazines: Synthesis and Anticancer Activity. *Biopolym. Cell* **2020**, *36*, 60–73. [[CrossRef](#)]
37. Jiang, G.; Chang, Q.; Liang, D.; Zhang, Y.; Meng, Y.; Yi, Q. Preparation and Antitumor Effects of 4-Amino-1,2,4-Triazole Schiff Base Derivative. *J. Int. Med. Res.* **2020**, *48*, 030006052090387. [[CrossRef](#)] [[PubMed](#)]
38. Moreno, L.M.; Quiroga, J.; Abonia, R.; Lauria, A.; Martorana, A.; Insuastry, H.; Insuastry, B. Synthesis, Biological Evaluation, and in Silico Studies of Novel Chalcone- and Pyrazoline-Based 1,3,5-Triazines as Potential Anticancer Agents. *RSC Adv.* **2020**, *10*, 34114–34129. [[CrossRef](#)]
39. Champoux, J.J. DNA Topoisomerases: Structure, Function, and Mechanism. *Annu. Rev. Biochem.* **2001**, *70*, 369–413. [[CrossRef](#)]
40. Maheshwari, S.; Miller, M.S.; O'Meally, R.; Cole, R.N.; Amzel, L.M.; Gabelli, S.B. Kinetic and Structural Analyses Reveal Residues in Phosphoinositide 3-Kinase  $\alpha$  That Are Critical for Catalysis and Substrate Recognition. *J. Biol. Chem.* **2017**, *292*, 13541–13550. [[CrossRef](#)] [[PubMed](#)]
41. Hua, H.; Kong, Q.; Zhang, H.; Wang, J.; Luo, T.; Jiang, Y. Targeting MTOR for Cancer Therapy. *J. Hematol. Oncol.* **2019**, *12*, 71. [[CrossRef](#)] [[PubMed](#)]
42. Tarantelli, C.; Lupia, A.; Stathis, A.; Bertoni, F. Is There a Role for Dual PI3K/MTOR Inhibitors for Patients Affected with Lymphoma? *Int. J. Mol. Sci.* **2020**, *21*, 1060. [[CrossRef](#)]
43. Osborne, M.J.; Schnell, J.; Benkovic, S.J.; Dyson, H.J.; Wright, P.E. Backbone Dynamics in Dihydrofolate Reductase Complexes: Role of Loop Flexibility in the Catalytic Mechanism. *Biochemistry* **2001**, *40*, 9846–9859. [[CrossRef](#)] [[PubMed](#)]
44. Wróbel, A.; Drozdowska, D. Recent Design and Structure-Activity Relationship Studies on the Modifications of DHFR Inhibitors as Anticancer Agents. *Curr. Med. Chem.* **2021**, *28*, 910–939. [[CrossRef](#)]
45. Singla, P.; Luxami, V.; Paul, K. Triazine-Benzimidazole Hybrids: Anticancer Activity, DNA Interaction and Dihydrofolate Reductase Inhibitors. *Bioorg. Med. Chem.* **2015**, *23*, 1691–1700. [[CrossRef](#)] [[PubMed](#)]
46. Supuran, C.T.; Scozzafava, A.; Casini, A. Carbonic Anhydrase Inhibitors. *Med. Res. Rev.* **2003**, *23*, 146–189. [[CrossRef](#)]
47. Walker, F.; Abramowitz, L.; Benabderrahmane, D.; Duval, X.; Descatoire, V.; Héning, D.; Lehy, T.; Aparicio, T. Growth Factor Receptor Expression in Anal Squamous Lesions: Modifications Associated with Oncogenic Human Papillomavirus and Human Immunodeficiency Virus. *Hum. Pathol.* **2009**, *40*, 1517–1527. [[CrossRef](#)] [[PubMed](#)]
48. Kumar, V.; Abbas, A.K.; Aster, J.C.; Robbins, S.L. *Robbins Basic Pathology*, 9th ed.; Saunders: Philadelphia, PA, USA, 2013.
49. Palmer, B.F.; Clegg, D.J. Oxygen Sensing and Metabolic Homeostasis. *Mol. Cell. Endocrinol.* **2014**, *397*, 51–58. [[CrossRef](#)]
50. Karkkainen, M.J.; Petrova, T.V. Vascular Endothelial Growth Factor Receptors in the Regulation of Angiogenesis and Lymphangiogenesis. *Oncogene* **2000**, *19*, 5598–5605. [[CrossRef](#)] [[PubMed](#)]

51. Muller, Y.A.; Li, B.; Christinger, H.W.; Wells, J.A.; Cunningham, B.C.; de Vos, A.M. Vascular Endothelial Growth Factor: Crystal Structure and Functional Mapping of the Kinase Domain Receptor Binding Site. *Proc. Natl. Acad. Sci. USA* **1997**, *94*, 7192–7197. [[CrossRef](#)] [[PubMed](#)]
52. Pathak, P.; Shukla, P.K.; Kumar, V.; Kumar, A.; Verma, A. Quinazoline Clubbed 1,3,5-Triazine Derivatives as VEGFR2 Kinase Inhibitors: Design, Synthesis, Docking, in Vitro Cytotoxicity and in Ovo Antiangiogenic Activity. *Inflammopharmacology* **2018**, *26*, 1441–1453. [[CrossRef](#)] [[PubMed](#)]
53. Mehlen, P.; Puisieux, A. Metastasis: A Question of Life or Death. *Nat. Rev. Cancer* **2006**, *6*, 449–458. [[CrossRef](#)] [[PubMed](#)]